NASA/TM–2013-217976

# Generalized Predictive Control of Dynamic Systems with Rigid-Body Modes

*Raymond G. Kvaternik*
*Langley Research Center, Hampton, Virginia*

April 2013

## NASA STI Program . . . in Profile

Since its founding, NASA has been dedicated to the advancement of aeronautics and space science. The NASA scientific and technical information (STI) program plays a key part in helping NASA maintain this important role.

The NASA STI program operates under the auspices of the Agency Chief Information Officer. It collects, organizes, provides for archiving, and disseminates NASA's STI. The NASA STI program provides access to the NASA Aeronautics and Space Database and its public interface, the NASA Technical Report Server, thus providing one of the largest collections of aeronautical and space science STI in the world. Results are published in both non-NASA channels and by NASA in the NASA STI Report Series, which includes the following report types:

- TECHNICAL PUBLICATION. Reports of completed research or a major significant phase of research that present the results of NASA Programs and include extensive data or theoretical analysis. Includes compilations of significant scientific and technical data and information deemed to be of continuing reference value. NASA counterpart of peer-reviewed formal professional papers, but having less stringent limitations on manuscript length and extent of graphic presentations.

- TECHNICAL MEMORANDUM. Scientific and technical findings that are preliminary or of specialized interest, e.g., quick release reports, working papers, and bibliographies that contain minimal annotation. Does not contain extensive analysis.

- CONTRACTOR REPORT. Scientific and technical findings by NASA-sponsored contractors and grantees.

- CONFERENCE PUBLICATION. Collected papers from scientific and technical conferences, symposia, seminars, or other meetings sponsored or co-sponsored by NASA.

- SPECIAL PUBLICATION. Scientific, technical, or historical information from NASA programs, projects, and missions, often concerned with subjects having substantial public interest.

- TECHNICAL TRANSLATION. English-language translations of foreign scientific and technical material pertinent to NASA's mission.

Specialized services also include organizing and publishing research results, distributing specialized research announcements and feeds, providing information desk and personal search support, and enabling data exchange services.

For more information about the NASA STI program, see the following:

- Access the NASA STI program home page at *http://www.sti.nasa.gov*

- E-mail your question to help@sti.nasa.gov

- Fax your question to the NASA STI Information Desk at 443-757-5803

- Phone the NASA STI Information Desk at 443-757-5802

- Write to:
  STI Information Desk
  NASA Center for AeroSpace Information
  7115 Standard Drive
  Hanover, MD 21076-1320

NASA/TM–2013-217976

# Generalized Predictive Control of Dynamic Systems with Rigid-Body Modes

*Raymond G. Kvaternik*
*Langley Research Center, Hampton, Virginia*

National Aeronautics and
Space Administration

Langley Research Center
Hampton, Virginia 23681-2199

April 2013

Available from:

NASA Center for AeroSpace Information
7115 Standard Drive
Hanover, MD 21076-1320
443-757-5802

# Table of Contents

## Abstract

*The results of numerical simulations aimed at assessing the applicability and effectiveness of Generalized Predictive Control (GPC) for active control of dynamic systems having rigid-body modes are presented. GPC is a linear, time-invariant, multi-input/multi-output predictive control method that uses an AutoRegressive with eXternal input (ARX) model to characterize the system and to design the controller. The equations underlying the method are presented and discussed, including system identification, calculation of control law matrices, and calculation of the commands applied to the control effectors. Although the method can accommodate both embedded (implicit) and explicit feedforward paths for incorporation of disturbance effects, only the case of embedded feedforward in which the disturbances acting on the system are assumed to be unknown is considered here. Representative results from numerical simulations using mathematical models of both a free-free three-degree-of-freedom mass-spring-dashpot system and the XV-15 tiltrotor research aircraft operating in the airplane mode of flight are presented. Both regulator (zero target response) and tracking (nonzero target response) problems were studied. Results obtained from these simulations have been decidedly positive. In particular, in the cases calling for zero system response in the presence of external disturbances, the closed-loop simulations showed reductions of nearly 100% for most of the examples. In the tracking examples where the system is commanded to follow a specified path, the GPC controllers were able to produce the desired system responses, even in the presence of external disturbances.*


## Nomenclature

| | |
|---|---|
| ARX | AutoRegressive with eXternal input |
| $d$ | disturbance |
| $f_s$ | sampling frequency |
| GPC | Generalized Predictive Control |
| $h_p$, $h_c$ | prediction and control horizons |
| $k$ | integer denoting discrete time index |
| $\ell$ | number of time points/samples used for system identification |
| $m$ | number of outputs |
| OMP | observer Markov parameters |
| $p$ | order of ARX model |

| | |
|---|---|
| $r$ | number of inputs |
| $r_c$ | number of control inputs |
| $r_d$ | number of disturbance inputs |
| SID | System IDentification |
| $\mathcal{T}, \mathcal{A}, \mathcal{B}$ | coefficient matrices in multi-step output prediction equation |
| $u_c$ | control input |
| $u_d$ | disturbance input |
| $u_c(k)$ | control input at time index $k$ |
| $u(k), y(k)$ | vectors of inputs and outputs at $k^{\text{th}}$ time index |
| $u(k\text{-}j), y(k\text{-}j)$ | vectors of past inputs and outputs at $(k\text{-}j)^{\text{th}}$ time index; $j < k$ |
| $u(k+j), y(k+j)$ | vectors of future inputs and outputs at $(k+j)^{\text{th}}$ time index; $j \geq 0$ |
| $\bar{Y}$ | matrix of observer Markov parameters |
| $\alpha^c, \beta^c, \chi^c$ | control law gain matrices |
| $\alpha_i, \beta_i$ | observer Markov parameters/coefficient matrices of ARX equation |
| $a_1, b_1$ | longitudinal and lateral tip-path-plane flapping angles |
| $\beta$ | sideslip angle |
| $u, v, w$ | perturbation linear velocities |
| $x, y, z$ | perturbation linear displacements |
| $p, q, r$ | perturbation angular velocities |
| $\varphi, \theta, \psi$ | perturbation angular displacements |
| $\Delta t$ | sampling time ($1/ f_s$) |

## Introduction

In 2003, the Aeroelasticity Branch and the Army Research Laboratory's Vehicle Technology Directorate at NASA Langley Research Center, in collaboration with Bell Helicopter Textron Inc, completed a series of experimental evaluations of a predictive control technique known as Generalized Predictive Control (GPC) (ref. 1) to assess its potential for actively controlling the swashplate of tiltrotor aircraft to enhance aeroelastic stability in both helicopter and airplane modes of flight. The studies employed a 1/5-scale, semi-span aeroelastic model of the V-22 that had been refurbished to serve as a tiltrotor research test bed for use in the Langley Transonic Dynamics Tunnel (TDT). The results of the exploratory experimental investigations conducted with this model are reported in references 2-5. The GPC-based algorithm employed was highly effective in increasing the stability of the critical (least stable) mode for all of the configurations and conditions tested. GPC was later employed to evaluate its potential for active gust load alleviation of fixed-wing aircraft using conventional wing control surfaces. This investigation used data from a TDT test of a large semi-span wing model of an active wing design being studied by Northrop Grumman. The results of this active gust load alleviation investigation are presented in reference 6. The applications of GPC noted above were to systems that contained no rigid-body modes. However, many systems that might be considered likely candidates for GPC-based active control have motions that include rigid-body or near rigid-body behavior. For this reason, it was decided to apply the GPC methodology developed in the aforementioned studies to some representative systems exhibiting such modes and to evaluate the method's ability for actively controlling those types of systems.

The purpose of this report is to present the results of some recent numerical simulations obtained from an application of the programs developed for the earlier GPC investigations to systems with rigid-body and near rigid-body modes. First, a qualitative description of the basic features of GPC is given. Then, key equations underlying the method as applied in the present investigation are presented and discussed, including system identification, formation of the multi-step output prediction equation, calculation of control law matrices, and calculation of the commands applied to the control effectors. These discussions are based on the broader treatment given in reference 6 but tailored to the requirements of the present application. Comments on selection of control model parameters and treatment of external disturbances are then presented. Representative results from two types of numerical simulations of closed-loop behavior are presented next. The first set of simulations was made using a three-degree-of-freedom mathematical model of a free-free mass-spring-dashpot system. The second set of simulations was made using a state-space math model of the rigid-body dynamics of the XV-15 tiltrotor research aircraft. Both models were subjected to a variety of user-defined external disturbances and user-defined target responses intended to demonstrate the ability of GPC to handle both regulation and tracking problems for systems with rigid-body modes and to illustrate the robustness of GPC to aggressive changes in simulated operating environment.

## Basic Features of GPC

Predictive control refers to a strategy wherein the decision for the current control action is based on minimization of a quadratic performance index that involves a prediction of the

system's controlled response at some number of time steps into the future. A variety of predictive controllers have been proposed (ref. 7). Among these, Generalized Predictive Control, which was introduced in 1987 (ref. 8), has received considerable attention by the controls community. GPC is a linear, time-invariant, multi-input/multi-output predictive control method that uses an AutoRegressive with eXternal input (ARX) model (i.e., a linear difference equation) to describe the input-output relationship of a system. The coefficient matrices of the ARX equation are determined by appropriate system identification techniques. Such a model gives the current output as a weighted linear combination of the current input and past inputs and outputs. The input-output equation is used to form a multi-step output prediction equation over a finite prediction horizon. An expression for the control to be imposed at the next time step is obtained by minimizing the deviation of the predicted controlled system outputs from the desired (or target) outputs, subject to a penalty on control effort. A version of the GPC procedure was developed at NASA Langley Research Center in 1997 for both efficient computation and treatment of unknown disturbances by Dr. Jer-Nan Juang and his team. Their work resulted in a suite of MATLAB (ref. 9) m-files that were collected into a predictive control toolbox that can be used by researchers for GPC studies. A summary of the salient aspects of the theory underlying their development may be found in references 1 and 10-19, among others.

The essential features of the GPC-based control system used in the present studies are depicted in figure 1. The system has $r_c$ control inputs $u_c$, $m$ measured outputs $y$, and is subject to external disturbances $d$. Measurement noise (not shown) can also be present. There are two fundamental steps involved in GPC: identification of the system; and use of the identified model to design the controller. Any system identification technique that returns an ARX model for the system may be used. System identification is done "on-line" in the presence of the disturbances acting on the system. If the disturbances are unknown, their effects are automatically accounted for (at least approximately) and embedded in the ARX model that is identified. This approach leads to a feedback controller with an embedded (or implicit) feedforward path and is the type of controller designed and used in the present investigation. It should be noted, however, that if any of the disturbances acting on the system are measurable, that data can be used in an explicit feedforward path simultaneously with the feedback data to enhance closed-loop performance, as was investigated in reference 6. In either case, a random excitation $u_{id}$ is applied initially with $u_c$ equal to zero to identify the open-loop system. Dither is also added to the closed-loop control input $u_c$ if it is necessary to re-identify the open-loop system while operating in the closed-loop mode.

## Key Equations Underlying Present Application of GPC

The key equations underlying the implementation of GPC used in the present application are summarized and discussed below. The form of the ARX model that is identified is given first. Then, the system identification procedure that provides the coefficient matrices in the ARX equation is summarized. The manner of extending this (the ARX) one-step output prediction equation to obtain the multi-step output prediction equation that is used for designing the controller is then described. Finally, the control law itself is derived.

## ARX Model

The relationship between the input and output discrete time histories of a linear, time invariant, multi-input/multi-output (MIMO) system subject to unknown or unmeasurable disturbances can be described by an ARX model (linear difference equation) that has the form

$$y(k) = \alpha_1 y(k\text{-}1) + \alpha_2 y(k\text{-}2) + \cdots + \alpha_p y(k\text{-}p) + \beta_0 u(k) + \beta_1 u(k\text{-}1) + \cdots + \beta_p u(k\text{-}p) \tag{1}$$

This equation states that the current output $y(k)$ at time index $k$ is given as a weighted sum of the $p$ past sets of output values $y(k\text{-}1),\ldots, y(k\text{-}p)$ and the current and $p$ past sets of input values $u(k)$, $u(k\text{-}1),\ldots, u(k\text{-}p)$. The integer $p$ is called the order of the ARX model. The coefficient matrices $\alpha_i$ and $\beta_i$ are referred to as observer Markov parameters (OMP) or ARX parameters and are the quantities to be determined by the identification algorithm. Closed-loop performance will be enhanced by performing the system identification in the presence of the external disturbances acting on the system, thereby ensuring that disturbance information will be incorporated in the identified model. As mentioned earlier, the OMP may be determined by any identification technique that returns an ARX model of the system. The approach used here is described below.

## System Identification Procedure

System identification (SID) deals with the problem of estimating a dynamical math model of a system using measured input-output data. The goal of SID is to determine the OMP of the ARX model using the measured input-output data stream. System identification in the presence of the operational disturbances acting on the system is the first of the two major computational steps of the GPC method. The number of inputs is $r$ and the number of outputs is $m$. To initiate the identification process, the open-loop system is excited with band-limited white noise. These independent random excitations are applied at the $r$ inputs simultaneously and the $m$ responses are measured or calculated, as appropriate, at $\ell$ equally-spaced time points. The resulting input and output time histories $u(k)$ and $y(k)$ are then used to form the data matrices $\bar{y}$ and $\bar{V}$ in the equation

$$\bar{y} = \bar{Y}\bar{V} \tag{2}$$

where

$$\underset{m\times\ell}{\bar{y}} = \left[ y(0)\ \ y(1)\ \ y(2)\cdots y(p)\cdots y(\ell-1) \right] \tag{3}$$

and

$$\bar{V} = \underset{[r+(r+m)p]\ \times \ell}{\begin{bmatrix} u(0) & u(1) & u(2) & \cdots & u(p) & \cdots & u(\ell-1) \\ & v(0) & v(1) & \cdots & v(p-1) & \cdots & v(\ell-2) \\ & & v(0) & \cdots & v(p-2) & \cdots & v(\ell-3) \\ & & & \ddots & \vdots & \vdots & \vdots \\ & & & & v(0) & \cdots & v(\ell-p-1) \end{bmatrix}} \tag{4}$$

Equations 3 and 4 follow from writing the equations for a discrete-time state-space observer model of a linear time-invariant system at a sequence of time indices $k$ = 0, 1, 2, …, ($\ell$-1) and then arranging them into a matrix form (ref. 11). Equations 3 and 4 are valid under the assumption that the system is initially at rest. For nonzero unknown initial conditions, the first $p$ columns of $\bar{y}$ and $\bar{V}$ must be deleted to eliminate the effect of the initial conditions on the measured data (ref. 11). The vector $v(k)$ appearing in the data matrix $\bar{V}$ is formed from the vectors $u(k)$ and $y(k)$ according to

$$\underset{(r+m)\times 1}{v(k)} = \begin{Bmatrix} u(k) \\ y(k) \end{Bmatrix} \tag{5}$$

The order of the ARX model, $p$, and the number of data points, $\ell$, used for identification are specified by the user. Some guidelines for their selection are given later. The sizes of key vectors and matrices are noted here and throughout the report as appropriate to facilitate computational considerations related to computer implementation.

In forming the matrices given in equations 4 and 5, it has been assumed that a deadbeat observer has been added to the system (ref. 18). This addition is purely implicit as its action is introduced by the assembling and processing of the input/output data in the manner shown above. It is through this expedient that the matrix $\bar{V}$ is reduced to a size amenable for practical numerical computation of its pseudo-inverse. The system identification process yields observer Markov parameters rather than system Markov parameters because of the inclusion of the observer. A complete discussion of these aspects of the development may be found in references 11 and 18.

In equation 2, $\bar{Y}$ is the matrix of observer Markov parameters that is identified and has the form

$$\underset{m\times[r+(r+m)p]}{\bar{Y}} = \begin{bmatrix} \beta_0 & \beta_1 & \alpha_1 & \beta_2 & \alpha_2 & \beta_3 & \alpha_3 & \cdots & \beta_p & \alpha_p \end{bmatrix} \tag{6}$$

The solution for $\bar{Y}$ is obtained by solving equation 2 for $\bar{Y}$ according to

$$\overline{Y} = \overline{\mathrm{y}}\,\overline{V}^{\dagger} = \overline{\mathrm{y}}\,\overline{V}^{T}\left[\overline{V}\,\overline{V}^{T}\right]^{-1} \tag{7}$$

where † denotes the pseudo-inverse. If the product $\overline{V}\,\overline{V}^{T}$ is a well-conditioned matrix of reasonable size, the ordinary inverse can be taken as shown. Otherwise, a pseudo-inverse must be used.

## Multi-Step Output Prediction Equation

The one-step output prediction equation given in equation 1 is the starting point for deriving the multi-step output prediction equation that is used for designing the GPC controller. Using equation 1, the output at time index $k+j$ may be written in the form

$$\begin{aligned} y(k+j) = {} & \alpha_1^{(j)} y(k\text{-}1) + \alpha_2^{(j)} y(k\text{-}2) + \cdots + \alpha_p^{(j)} y(k\text{-}p) \\ & + \beta_o u(k+j) + \beta_0^{(1)} u(k+j-1) + \cdots + \beta_o^{(j)} u(k) + \beta_1^{(j)} u(k\text{-}1) + \beta_2^{(j)} u(k-2) + \cdots + \beta_p^{(j)} u(k\text{-}p) \end{aligned} \tag{8}$$

where the coefficient matrices are given by recursive expressions involving the matrices $\alpha_i$ and $\beta_i$ appearing in the ARX equation (ref. 10). The system identification process described earlier provides the matrices $\alpha_i$ and $\beta_i$. Equation 8 shows that the output $y(k+j)$ at time index $k+j$ may be estimated by using $p$ sets of the previous output and input measurements, $y(k\text{-}1),\ldots, y(k\text{-}p)$ and $u(k\text{-}1),\ldots,u(k\text{-}p)$, and the unknown current and future inputs $u(k)$, $u(k+1),\ldots,u(k+j)$. The GPC algorithm is based on system output predictions over a finite horizon $h_p$ known as the prediction horizon. To predict future outputs, some assumption needs to be made about future control inputs. In determining the future control inputs for GPC, it is assumed that control is applied over a finite horizon $h_c$ known as the control horizon that is equal to or less than the prediction horizon. Beyond the control horizon the control input is assumed to be zero. Letting $j$ in equation 8 range over the set of values $j$ = 1, 2, …, $h_p$-1, the resulting equations can be assembled into a multi-step output prediction equation having the compact form

$$\underset{h_p m\times 1}{y_{h_p}(k)} = \underset{h_p m\times h_c r_c}{\mathcal{T}}\ \underset{h_c r_c\times 1}{u_{h_c}(k)} + \underset{h_p m\times pm}{\mathcal{A}}\ \underset{pm\times 1}{y_p(k-p)} + \underset{h_p m\times pr_c}{\mathcal{B}}\ \underset{pr_c\times 1}{u_p(k-p)} \tag{9}$$

The coefficient matrices $\mathcal{T}$, $\mathcal{A}$, and $\mathcal{B}$ are formed from combinations of the observer Markov parameters $\alpha_i$ and $\beta_i$. The quantity $y_{hp}(k)$ denotes a vector containing $h_p$ sets of outputs $y(k)$, $y(k+1)$, …, $y(k+h_p\text{-}1)$, whereas $u_{hc}(k)$ is the vector containing $h_c$ sets of control inputs $u(k)$, $u(k+1)$, …, $u(k+h_c\text{-}1)$ yet to be determined. The quantities $u_p(k\text{-}p)$ and $y_p(k\text{-}p)$ denote vectors containing the previous $p$ sets of control inputs and outputs, respectively. The expanded form of this multi-step output prediction equation for the case in which $h_c = h_p$ is shown in equation 10.

$$\boxed{\beta_0^{(q)} = \beta_1^{(q-1)} + \alpha_1^{(q-1)}\beta_0}$$

$$\begin{Bmatrix} y(k) \\ y(k+1) \\ \vdots \\ y(k+q-1) \\ y(k+q) \\ \vdots \\ y(k+h_p-1) \end{Bmatrix} = \begin{bmatrix} \beta_o & & & & & & \\ \beta_o^{(1)} & \beta_o & & & & & \\ \vdots & \vdots & \ddots & & & & \\ \beta_o^{(q-1)} & \beta_o^{(q-2)} & \cdots & \beta_o & & & \\ \beta_o^{(q)} & \beta_o^{(q-1)} & \cdots & \beta_o^{(1)} & \beta_o & & \\ \vdots & \vdots & \ddots & \vdots & \vdots & \ddots & \\ \beta_o^{(h_p-1)} & \beta_o^{(h_p-2)} & \cdots & \beta_o^{(h_p-q)} & \beta_o^{(h_p-q-1)} & \cdots & \beta_o \end{bmatrix} \begin{Bmatrix} u(k) \\ u(k+1) \\ \vdots \\ u(k+q-1) \\ u(k+q) \\ \vdots \\ u(k+h_c-1) \end{Bmatrix} \qquad h_c = h_p$$

$$\boxed{\alpha_{p-1}^{(q)} = \alpha_p^{(q-1)} + \alpha_1^{(q-1)}\alpha_{p-1}} \qquad \boxed{\beta_{p-1}^{(q)} = \beta_p^{(q-1)} + \alpha_1^{(q-1)}\beta_{p-1}}$$

$$+ \begin{bmatrix} \alpha_1 & \alpha_2 & \cdots & \alpha_{p-1} & \alpha_p \\ \alpha_1^{(1)} & \alpha_2^{(1)} & \cdots & \alpha_{p-1}^{(1)} & \alpha_p^{(1)} \\ \vdots & \vdots & \ddots & \vdots & \vdots \\ \alpha_1^{(q-1)} & \alpha_2^{(q-1)} & \cdots & \alpha_{p-1}^{(q-1)} & \alpha_p^{(q-1)} \\ \alpha_1^{(q)} & \alpha_2^{(q)} & \cdots & \alpha_{p-1}^{(q)} & \alpha_p^{(q)} \\ \vdots & \vdots & \ddots & \vdots & \vdots \\ \alpha_1^{(h_p-1)} & \alpha_2^{(h_p-1)} & \cdots & \alpha_{p-1}^{(h_p-1)} & \alpha_p^{(h_p-1)} \end{bmatrix} \begin{Bmatrix} y(k-1) \\ y(k-2) \\ \vdots \\ y(k-p+1) \\ y(k-p) \end{Bmatrix} + \begin{bmatrix} \beta_1 & \beta_2 & \cdots & \beta_{p-1} & \beta_p \\ \beta_1^{(1)} & \beta_2^{(1)} & \cdots & \beta_{p-1}^{(1)} & \beta_p^{(1)} \\ \vdots & \vdots & \ddots & \vdots & \vdots \\ \beta_1^{(q-1)} & \beta_2^{(q-1)} & \cdots & \beta_{p-1}^{(q-1)} & \beta_p^{(q-1)} \\ \beta_1^{(q)} & \beta_2^{(q)} & \cdots & \beta_{p-1}^{(q)} & \beta_p^{(q)} \\ \vdots & \vdots & \ddots & \vdots & \vdots \\ \beta_1^{(h_p-1)} & \beta_2^{(h_p-1)} & \cdots & \beta_{p-1}^{(h_p-1)} & \beta_p^{(h_p-1)} \end{bmatrix} \begin{Bmatrix} u(k-1) \\ u(k-2) \\ \vdots \\ u(k-p+1) \\ u(k-p) \end{Bmatrix}$$

(10)

The observer Markov parameters $\alpha_i$ and $\beta_i$ resulting from system identification are used to form the first block row in each of the coefficient matrices $\mathcal{T}$, $\mathcal{A}$, and $\mathcal{B}$ in equation 9. These terms are colored red in equation 10. The terms in the remaining block rows are computed using the recursive relations indicated in the boxes above the coefficient matrices in equation 10 (ref. 10). All terms in equation 10 are known, except for the $h_c$ sets of commands and the $h_p$ sets of predicted responses. The goal of the GPC control algorithm is to determine the set of commands $u(k)$, $u(k+1)$, …, $u(k+h_c-1)$ that are required to achieve a predicted response $y(k)$, $y(k+1)$, …, $y(k+h_p-1)$ that is as near as possible to a desired or target response $y_T(k)$, $y_T(k+1)$, …, $y_T(k+h_p-1)$. It should be noted that the system Markov parameters, which are commonly used as the basis for identifying discrete-time state-space models of linear dynamical systems, form the first block column in the matrix $\mathcal{T}$; the remaining block columns in that matrix are formed from subsets of these parameters. The sequence of system Markov parameters is the pulse response of a system and is unique for a given linear system. Note that equation 10 assumes that $h_c = h_p$, in which case the matrix $\mathcal{T}$ has $h_p$ block rows and $h_p$ block columns. However, $h_c$ can be less than $h_p$, in which case one would retain only the first $h_c$ block columns of $\mathcal{T}$. The matrices $\mathcal{A}$ and $\mathcal{B}$ both have $h_p$ block rows and $p$ block columns.

## Derivation of Control Law

The predictive control law is obtained by minimizing the deviation of the predicted controlled response (as computed from the multi-step output prediction equation) from a desired response over a prediction horizon $h_p$. To this end, one first defines an error function that is the difference between the desired or target response $y_T(k)$ and the predicted response $y_{hp}(k)$:

$$\begin{aligned}\varepsilon &= y_T(k) - y_{h_p}(k) \\ &= y_T(k) - \mathcal{T} u_{h_c}(k) - \mathcal{A} y_p(k-p) - \mathcal{B} u_p(k-p)\end{aligned} \tag{11}$$

A performance index $J$ quadratic in the error and the unknown controls is then formed:

$$J = \varepsilon^T Q \varepsilon + u_{h_c}^T R\, u_{h_c} \tag{12}$$

Two weighting matrices are included in the performance index: $R$ (symmetric and positive definite) is used to weight the control effort and stabilize the closed-loop system; $Q$ (symmetric and positive semi-definite) is used to weight the relative importance of the differences between the target and predicted responses. Typically, $R$ and $Q$ are assumed to be diagonal with $R$ having the same value $w_c$ along its diagonal and $Q$ having the same value $w_r$ along its diagonal. Minimizing $J$ with respect to $u_{hc}(k)$ and then solving for $u_{hc}(k)$ gives

$$\underset{h_c r_c \times 1}{u_{h_c}(k)} = -\Big( \underset{h_c r_c \times h_p m}{(\mathcal{T}^T Q \mathcal{T} + R)^{\dagger} \mathcal{T}^T Q} \Big) \Big( -y_T(k) + \mathcal{A} y_p(k-p) + \mathcal{B} u_p(k-p) \Big) \tag{13}$$

as the control sequence to be applied to the system over the next $h_c$ time steps $k$, $k$+1, …, $k$+$h_c$-1. However, only the first $r_c$ values corresponding to the first or current time step $k$

$$\underset{r_c \times 1}{u_c(k)} = -\chi^c y_T(k) + \alpha^c y_p(k-p) + \beta^c u_p(k-p) \tag{14}$$

are applied to the $r_c$ control inputs, the remainder are discarded, and a new control sequence is calculated at the next time step. Equation 14 is the desired control law equation. The target response $y_T(k)$ is zero for a regulator problem and non-zero for a tracking problem. The coefficient matrices $\chi^c$, $\alpha^c$, and $\beta^c$ are the control law gain matrices and have sizes $r_c \times mh_p$, $r_c \times pm$, and $r_c \times pr_c$, respectively. The effects of the unknown disturbances are embedded in the coefficient matrices $\mathcal{A}$ and $\mathcal{B}$ (and thus $\alpha^c$ and $\beta^c$) but at the price of increasing the order of the ARX model that must be identified. Note that the matrix $\mathcal{T}$ is unaffected by the disturbances as it is defined solely in terms of the system's Markov parameters, which are unique for a given linear system.

It should be noted that the quantity $\left((\mathcal{T}^T Q \mathcal{T} + R)^\dagger \mathcal{T}^T Q\right)$ in equation 13 has to be evaluated only once if the system does not change after the initial identification and the weights matrices $Q$ and $R$ are not changed. Also, the OMP (and thus the matrices $\mathcal{A}$ and $\mathcal{B}$ and hence $\alpha^c$ and $\beta^c$) can be re-identified efficiently at each time step (e.g., via recursive least squares) if deemed necessary because of rapidly changing external disturbances, as was demonstrated in the studies of reference 6. The availability of the latter option provides the enabling capability for implementing a real-time, fully-adaptive computational procedure for GPC.

## Selection of Control Model Parameters

As in most control systems, there are parameters that must be selected to ensure that there is a proper balance among controller performance, system stability, controller stability, and actuator saturation. The influential parameters of interest for GPC are: the order of the ARX model $p$, the prediction horizon $h_p$, the control horizon $h_c$, and the control weights $w_c$

An expression for estimating the order $p$ of the ARX model that is the product of the system identification process is given by $pm \geq n_s + n_d$, where $m$ is the number of outputs, $n_s$ is the number of system states, and $n_d$ is the number of disturbance states. The number of system states is typically chosen to be twice the (estimated) number of significant structural modes in the system; the number of disturbance states is set to twice the (estimated) number of frequencies in the disturbance. For simulated systems such as those studied herein these parameters are easily defined. However, in practice, the number of system states and disturbance states is often either unknown or not known with any certainty. It turns out that simply choosing $p$ to be about five times the estimated number of significant structural modes in a system is a good starting point and is often adequate. Increasing p also alleviates the effects of measurement noise which may be present in the data. Note that the value required for $p$ decreases as $m$ is increased.

The prediction and control horizons are set according to $h_p \geq p$ and $h_c \leq h_p$. The control horizon can be chosen to be less than the prediction horizon resulting in a more stable (lower required control amplitude) but sluggish controller. However, there is no compelling advantage that can be ascribed to such a choice. Based on experience, setting $h_c = h_p = p$ is a good initial choice and usually provides satisfactory results.

As mentioned earlier, weighting matrices $R$ and $Q$ are used to weight the control effort and to weight the relative importance of the differences between the target and predicted responses, respectively. With $h_c = h_p = p$ set as above, the relative values of the weighting matrices play the major role in the tuning process. Therefore, the weighting matrix $Q$ is usually set to an identity matrix. The control weight matrix $R$ then becomes the only one needed to be tuned to produce an acceptable solution. Reducing $w_c$ increases controller performance but will increase the magnitude of the required control inputs, which may saturate the actuators or drive the control system unstable. Increasing $w_c$ reduces control effort but increases the time required for the controller to quell the response or produce the desired maneuver. A reasonable set of starting values is 1.0, which can then be adjusted down or up as required.

The parameters $\ell$ and $\Delta t$ are important signal processing parameters and not control parameters per se. However, they are included here because their values do have a strong influence on the design and hence performance of the controller. The integer $\ell$ denotes the number of data points in the time histories used in the GPC calculations. Its value is determined by the need to have a data record long enough to capture about 5-10 cycles of the lowest frequency mode in the measured response time histories used for SID and controller design. It should be noted that the value chosen depends on the sample time $\Delta t$ (which is the reciprocal of the sampling frequency used to discretize continuous-time data) since the smaller the value of $\Delta t$ the longer the data record that is needed. Some guidelines for choosing the sampling frequency are given in reference 6.

## Comment on Treatment of External Disturbances

In most cases, the external disturbances acting on a system are unknown. In such situations the best that can be done is to identify the system in the presence of the disturbances so as to include their effects in the OMP of the identified ARX model. The control law obtained using the OMP with the embedded disturbance information is then used to compute the control inputs. As mentioned earlier, this situation represents the case of feedback with embedded or implicit feedforward and is the procedure that was employed successfully in the GPC-based active controls testing of the tiltrotor model mentioned earlier. If any of the external disturbances acting on the system can be measured an explicit feedforward loop can be employed in combination with the feedback loop to enhance closed-loop performance. In fact, embedded feedforward and explicit feedforward can be used simultaneously if the disturbances acting on a system contain a combination of known/measurable and unknown/unmeasurable components. This situation was addressed extensively in reference 6. However, the present study assumes that all the external disturbances are unknown and derives a feedback controller with embedded feedforward.

## Results and Discussion

Results from two types of closed-loop simulations are presented. The first uses a mathematical model of a free-free, three-degree-of-freedom mass-spring-dashpot system subject to user-specified disturbance forces and user-specified target response time histories. The other uses a state-space math model of the rigid-body dynamics of the XV-15 tiltrotor research aircraft operating in the airplane mode of flight. The intent of these simulations is to demonstrate the effectiveness of a GPC-based active control system to both quell the response to a disturbance (the regulator problem) and to produce a desired or target response (the tracking problem) either with or without a disturbance.

### Comment on Codes Used for Simulations

Two MATLAB programs were used for the studies that provided the numerical results for this report. One is a version of the three-degree-of-freedom (3-DOF) mass-spring-dashpot system that was used to develop the GPC software system for the tiltrotor model testing but modified to include the coding needed for calculating the additional terms associated with a non-zero target response. This program treats a simple dynamic system with user-defined properties

and user-defined external disturbances and target responses and thus lends itself to easy modification to explore a variety of what-if questions. The other program is also a version of the aforementioned 3-DOF code but modified to use an existing rigid-body state-space model of the XV-15 tiltrotor research aircraft rather than the mass-spring-dashpot system. Because this model was developed for a specific flight condition and cannot be modified by the user, the model was used as-received. However, the model did allow for the imposition of user-defined disturbances and target responses.

## Numerical Simulations Using 3-DOF Math Model

The 3-DOF mass-spring-dashpot system used in these simulations is depicted in figure 2 and the corresponding equations of motion are summarized in Appendix A. The model has three masses, two springs, and two dashpots. Disturbance forces $ud_1$, $ud_2$, and $ud_3$ and control forces $uc_1$, $uc_2$, and $uc_3$ act on masses $m_1$, $m_2$, and $m_3$, respectively. The degrees of freedom $x_1$, $x_2$, and $x_3$ are the absolute displacements of the corresponding masses. For the simulations, the masses were set equal to 1 lb-sec$^2$/in, the spring rates to 1 lb/in, and the damping coefficients to 0.0 lb/in/sec. Zero damping was assumed to preclude inherent dissipative forces acting on the system, thereby providing a more demanding dynamic environment for the controller. As indicated in table 1, the resulting state matrix yields the following eigenvalues for the system: 0±0i, 0±1.0i, and 0±1.7321i. These in turn yield natural frequencies of 0.0, 0.15915, and 0.27566 Hz and corresponding damping ratios of 0.0, 0.0, and 0.0 for the three natural modes of the system. Disturbances, control forces, and responses (displacements, velocities, or accelerations) can be specified and selected in a variety of combinations (see Appendix A). However, unless noted otherwise, for the results to be presented here, control forces were applied at masses 1, 2, and 3 ($r_c$ = 3), disturbances were imposed at masses 1, 2, and 3 ($r_d$ = 3), and displacements were measured at masses 1, 2, and 3 ($m$ = 3). Target responses (both zero and non-zero) were specified for all three masses. Several different types of disturbances and target responses were devised and imposed on the system to provide a challenging control task for GPC.

### Simulation Conditions and Parameter Settings

Based on the signal processing guidelines given in reference 6, as well as extensive previous experience with the 3-DOF system, the sampling frequency $f_s$ was set to 20 Hz (so that $\triangle t$=0.05 sec) and the number of data points $\ell$ of input/output data was set to 600, unless noted otherwise. The control horizon $h_c$ was set equal to the prediction horizon $h_p$ and $h_p$ was set equal to the order of the ARX model $p$. The use of feedback with embedded feedforward requires $p$ as computed by the disturbance-free relationship $pm \geq n_s$ to be increased to provide the additional computational degrees of freedom needed to ensure that the effects of the unknown disturbances are embedded in the observer Markov parameters that are computed during system identification. To this end, the value of $p$ so-computed was increased to 12. The response weights $w_r$ were set to 1.0 and the control weights $w_c$ were set to 0.0005. Previous experience with the model indicates that the selected values are all reasonable but not optimal. No attempt was made to "optimize" (i.e., tune) the parameters $p$, $h_c$, $h_p$, and $w_c$ to the nuances of the system to the different disturbances and target responses to elicit the best possible closed-

loop behavior. In the closed-loop simulations, the loop was closed (controller turned on) after 50 time points (2.5 sec).

The MATLAB function *c2d.m* was used to convert the continuous-time state-space model of the 3-DOF system (Appendix A) to discrete-time using $\triangle t = 0.05$ as set above. The resulting discrete-time model was then used in the MATLAB function *dlsim.m* to generate the random time histories needed to identify the ARX model and design the controller as described earlier in the report. The function *dlsim.m* was also used to compute the open-loop time histories for those examples in which disturbances act on the system.

Results are presented below for feedback with embedded feedforward, in which all the disturbances acting on the system are assumed to be unknown while performing the SID and controller design. Both regulator and tracking examples are presented. It should be noted that the time index $k$ is used on the time axes of the results figures rather than actual time $t$. While either variable can be used in plotting time histories because they are related according to $t = k\,\Delta t$, $k = 0, 1, 2, \ldots, \ell\text{-}1$, time index is used here. It should also be noted that the number of examples presented is rather large. This is intentional and is intended to provide a sufficiently diverse collection of results from which to better judge the efficacy of GPC in the subject application.

**Results for Regulation and Tracking of 3-DOF System**

Representative results illustrating the ability of GPC to either suppress disturbance-induced responses of the 3-DOF system (the regulator problem) or to cause the system to follow a desired target response (the tracking problem) are presented in this section. For convenience of discussion below, the disturbances are sometimes denoted as ud1, ud2, and ud3, the control inputs by uc1, uc2, and uc3, and the target responses by yt1, yt2, and yt3.

***Regulator Examples*:** Figures 3 through 11 show comparisons of open- and closed-loop displacement responses of the 3-DOF model to a variety of external disturbances. These examples are presented in composite figures consisting of two rows of two figures each. The upper left figure shows the disturbances acting on the system; the upper right shows the open-loop responses of the system; the lower left shows the control forces applied to the system; and the lower right shows the closed-loop responses of the system.

In figure 3 there are three sinusoidal disturbance forces acting on the system: usin1=2cos(2πft) on mass 1, usin2=1sin(2πft) on mass 2, and usin3=3sin(2πft + π/3) on mass 3, where f=0.27566 Hz, the third natural frequency of the system. The open-loop responses are diverging oscillations because the excitations are at a natural frequency of the system. A linear drift associated with the rigid-body degree of freedom of the system is also evident in each of the responses. All the control inputs are oscillatory, as expected. The large amplitude spikes appearing in the control force time histories at and slightly after time index 50 always occur when turning on the controller abruptly as done in the present simulations. It should be pointed out that the accommodation of such spikes by MATLAB when plotting the results oftentimes compresses the remainder of those time histories to a level that makes them difficult to distinguish and to read their values on the vertical axis. For this reason, those control time

histories that have been judged remiss in this regard have been preemptively hand adjusted before inclusion in this report. While figure 3 shows both the unadjusted and adjusted control subplots, all subsequent figures will show only the most appropriate subplot but not both. As can be seen, the open-loop responses are essentially suppressed immediately after closing the loop.

The disturbances in figure 4 consist of both sinusoidal and constant forces. A one-pound sinusoidal force usin2=1sin($2\pi$ft), with f=0.27566 Hz, acts on mass 2 and constant forces of two and three pounds act on masses 1 and 3, respectively (Note that constant forces may be viewed as zero-frequency cosine forces, which provide excitation at the zero natural frequency of the system). Because the rigid-body displacements induced by the two constant forces acting on the system dominate its response, the overall open-loop motion is seen to be primarily exponentially diverging with negligible oscillatory behavior. The control forces consist of a combination of oscillatory and constant forces consistent with the character of the disturbances. Again, the open-loop responses are essentially driven to zero immediately after closing the loop.

Constant forces act on all three masses of the system in figure 5: two pounds on mass 1, one pound on mass 2, and three pounds on mass 3. The resulting open-loop responses are exponentially diverging motions of the masses. The computed control forces are all constant in this case, as should be expected for a system disturbed solely by constant forces. Again, the open-loop responses are driven to zero almost instantly after closing the loop.

In figure 6 all three masses are subjected to random excitations. Rigid-body motion dominates the open-loop responses, which are driven to negligibly small values promptly after imposition of control.

Figure 7 has the same sinusoidal disturbances as in figure 3 but with frequencies different from the natural frequencies of the system. The force usin1 with f=0.1 Hz acts on mass 1, usin2 with f=0.2 Hz acts on mass 2, and usin3 with f=0.3 Hz acts on mass 3. The open-loop oscillatory responses again all have a linear drift, as they did in figure 3. Suppression of the open-loop responses occurs almost instantly after engaging the controller.

In figure 8 ud1 is a one-minus-cosine function (1-cosine) over the entire time interval, ud2=usin2 with f=0.27566 Hz, and ud3 is a single “saw-tooth” pulse (a narrow trapezoid) in an otherwise zero time history. The open-loop response is primarily a linearly diverging displacement beyond a time index of about 300. Here, the closed-loop responses are small but not zero.

The disturbances in figure 9 are all 1-cosine functions. The disturbance acting on mass 2 extends over the entire time interval while the disturbances acting on masses 1 and 3 extend over different sub time intervals. Note that the open-loop responses diverge exponentially very rapidly in this case but are easily suppressed by the controller.

Figure 10 has ud1=usin1 with f=0.27566 Hz, ud2=u1step (a step function with a single step), and ud3=usin2.*usin3 (.* is MATLAB notation denoting an element-by-element product of usin2 and usin3). The control input at mass 2 has a small overshoot in amplitude at time index

225 where the up step occurs in disturbance ud2. Closed-loop responses are quite small but not zero.

In figure 11 ud1=usin1, ud2=usin2+u1step, and ud3=usin3+2(1-cosine), with f=0.27566 Hz. The open-loop responses of the masses are again dominated by the rigid-body freedom of the system but the calculated control input time histories are able to subdue the disturbance-induced responses.

***Tracking Examples*:** Figures 12 through 22 show comparisons of target and achieved displacement responses of the 3-DOF system for a variety of imposed target responses with no disturbances acting on the system. Figures 23 through 26 provide comparisons of target and achieved responses to several sets of target responses while the system is subjected to a variety of disturbances.

The results for the tracking simulations without disturbances acting on the system are presented in composite figures consisting of two rows of two figures each. The upper left figure shows the control forces applied to the system; the upper right figure shows a comparison of the target and achieved responses for mass 1; the lower left figure shows a comparison of the target and achieved responses for mass 2; and the lower right figure shows a comparison of the target and achieved responses for mass 3.

In the example shown in figure 12 a sinusoidal target response is assigned to each mass: yt1=2sin(2πft) with f=0.1 Hz, yt2=1cos(2πft) with f=0.2 Hz, and yt3=5sin(2πft+π/4) with f=0.3 Hz. Closed-loop responses (achieved responses) are basically identical to the specified target responses.

In figure 13 the target response yt1 for mass 1 is a single saw-tooth wave (a narrow trapezoid) in an otherwise null time history while yt2 and yt3 are the same mass 2 and mass 3 targets as in figure 12. The required control inputs (particularly of mass 1) are more active in the vicinity of time index 200 here than in figure 12 to accommodate the pulse-like character of the saw-tooth target. Closed-loop (achieved) responses are in excellent agreement with the target responses.

In figure 14 yt1 is a single-step step function, yt2 is a one-minus-cosine function, and yt3 is a random function. As might be expected, the required control inputs here are very active because of the random tracking requirement for mass 3. Tracking is very good except for some very minor differences at the corners of the step target and at some of the peaks and troughs of the random target. It should be noted that the control input for mass 1 contains two spikes centered at time index 225 where the response jumps in value from 0 to +5. These are simply a nuance of the manner in which the tracking input data are introduced and processed in the present implementation when a vertical (infinite slope) step discontinuity is encountered. These may or may not be as evident as seen here depending on the magnitude of the discontinuity.

The spiking of control inputs to satisfy tracking requirements as exhibited in figure 14 can be eliminated or at least reduced if problematic target shapes containing vertical step-function portions are passed through a moving-average filter to provide smooth non-vertical

transitions between any jumps appearing in those shapes. The resulting shapes also more closely represent realizable target inputs. To illustrate this, the step target of mass 1 was passed through a 20-point moving average filter (using MATLAB function *filtfilt.m*). The resulting filtered target is compared to the original unfiltered target in figure 15. Note that the averaging action of the filter has resulted in a narrow, smoothly varying, non-vertical transition between the two horizontal portions of the step function. The example of figure 14 was then rerun using the filtered step target of figure 15 giving the results shown in figure 16. The large-amplitude spikes in the uc1 control input are now much reduced and are no larger than the other control inputs. Tracking is now excellent.

Figure 17 has yt1=a 0.5 Hz sinusoid with exponentially increasing amplitude, yt2=a 0.5 Hz sinusoid with exponentially decreasing amplitude, and yt3=a three-step step function. Note that large control inputs are required to enforce the diverging target of mass 1 and that there are only small spikes in the controls associated with the vertical discontinuities in the target response of mass 3. Tracking is very good.

Figure 18 has yt1=a two-step step function, yt2=a shifted 0.5 Hz sinusoid with exponentially decreasing amplitude, and yt3=a random function. Tracking is excellent but the required control inputs for masses 2 and 3 are quite large. The spiking in uc1 due to the vertical discontinuities in the target for mass 1 is not remarkable here as the spikes are no larger than the other control inputs.

In figure 19 yt1= sum of an exponentially diverging sinusoid with increasing frequency and a single-step step function, yt2=sum of a 1-cosine function and an up-down-up sequence of a three-toothed saw-tooth waveform, and yt3=sum of an exponentially converging sinusoid with increasing frequency, a random function, and a negative saw-tooth function. Spiking of uc1 occurs at time index 225 where there is a vertical step change in the target response. Tracking is excellent but requires some rather large control inputs.

The examples in figures 20-22 are for an extended data stream of 1500 time points. Each 1500-point target response is composed of three consecutive but different 500-point segments. Large amplitude spikes occur in the control inputs at times where there are sizable vertical step changes in the target response time histories. The spikes can, however, be reduced considerably if the target responses are filtered before being imposed on the system (recall the discussion of figures 14-16). The tracking in figures 20-22 is excellent.

The results for the tracking simulations with disturbances acting on the system are presented in composite figures consisting of three rows of two figures each. The upper left figure shows the disturbances acting on the system; the upper right figure shows the open-loop responses of the system; the center left figure shows the control forces applied to the masses of the system; the center right figure shows a comparison of the target and achieved responses for mass 1; the lower left figure shows a comparison of the target and achieved responses for mass 2; and the lower right figure shows a comparison of the target and achieved responses for mass 3.

Figure 23 has the same disturbances as the regulator example in figure 10 and the same targets as the tracking-without-disturbances example in figure 14. The spike in the magnitude of

uc1 at time index 225 occurs because of the up step in the target response of mass 1 at that time index. Tracking of masses 1 and 3 is very good but that of mass 2 is fair at best. Note that the control inputs in figure 23 are different both in character and amplitude than those in figures 10 and 14 because of the need to simultaneously quell disturbances and enforce target responses in the present case.

In the example of figure 24 spikes in uc3 occur at time indices corresponding to the up and down steps in the mass 3 target at time indices of 300 and 482, respectively. Tracking of the targets for masses 1 and 3 is excellent but the enforcement of the random target for mass 2 is only fair.

The targets in figure 25 are 0.27566 Hz sinusoids with amplitudes of 2, 1, and 5, respectively. The calculated control inputs are all primarily sinusoidal with only hints of the 1-cosine and saw-tooth disturbances reflected in them. Tracking is excellent. Comparing the present control time histories with those of the regulator example of figure 8 with the same disturbances suggests that the amplitudes of the required control inputs is dictated primarily by the presence of non-zero targets.

Figure 26 has the same disturbances as figure 24. The small spike in uc1 at time index 225 is due to the up step in the mass 1 target. There is also a small spike in uc2 at time index 300 arising from the down step in the ud2 disturbance at that time index. Tracking of masses 1 and 3 is good but the 1-cosine achieved response of mass 2 is only fair because of the disturbance down step in ud2 at time index 300.

***Summary of Observations*:** Taken as a whole, the 3-DOF simulations indicate that the GPC-based controllers functioned well whether they were employed as regulators or trackers. When used in the regulation mode, they (the GPC controllers) were able to significantly reduce or quell system open-loop responses under a variety of imposed disturbance conditions and to do so immediately after closing the loop. The maximum values of the disturbance forces imposed on all but one of the 3-DOF system examples in figures 3-11 varied from one to ten pounds. For these examples the maximum values of the computed control forces also varied from about one to ten pounds. In the one example in which the disturbance was 50 pounds, the maximum control force was also 50 pounds. These results suggest that in regulation problems where both the control inputs and the imposed disturbances are forces, the computed control forces are of the same order of magnitude as the disturbances.

When used to meet a tracking requirement, the GPC controllers were able to produce the commanded responses, even in the presence of disturbances acting on the system, and to do so promptly after closing the loop. Based on the results presented in figures 12-26, the tracking problem is much more demanding than the regulator problem. That is, the control inputs required for satisfactory tracking are typically larger than those needed for adequate regulation. Also, large amplitude spikes can occur in the calculated control inputs when the target response time histories have vertical step discontinuities or offsets within them. However, such control spikes can be precluded or at least significantly reduced simply by filtering problematic targets to smooth out any such discontinuities. The spiking notwithstanding, the values calculated for the

control forces in the tracking examples are all reasonable when considered from the perspective of the magnitude and complexity of the imposed target responses.

## Numerical Simulations Using State-Space Model of XV-15 Tiltrotor Aircraft

The XV-15 tiltrotor aircraft used in this simulation is shown flying in the airplane mode in figure 27. An existing linearized state-space model defining the rigid-body flight dynamics of the XV-15 flying at 150 knots in level flight at sea level altitude was used for the present studies. The coordinate system and sign convention for the 12 state variables used to describe the state-space model are depicted in figure 28. The formation of this model is summarized in Appendix B. It should be noted that the mass, damping, and stiffness matrices defining the model are not diagonal, indicating that there is coupling between the longitudinal and lateral/directional equations of motion.

The dynamic characteristics of the XV-15 math model are summarized in table 2. The state matrix of the aircraft yields the following eigenvalues for the longitudinal and lateral/directional modes of the system: -1.4173 ± 2.9364i (short-period mode), -0.44913 ± 1.6058i (Dutch-roll mode), -0.019449 ± 0.18404i (phugoid mode), -0.73883 + 0.0i (roll convergence mode), and -0.15843 + 0.0i (spiral convergence mode). The damped natural frequencies of the oscillatory short-period, Dutch-roll, and phugoid modes are 0.46734 Hz, 0.25556 Hz, and 0.029291 Hz, respectively. The non-oscillatory roll convergence and spiral convergence modes have zero frequency. Damping ratios of the three oscillatory modes are: 0.43469, 0.26936, and 0.10509, respectively. Damping ratios of the non-oscillatory (aperiodic) modes are unity. The modes are thus well damped, indicating that the system is stable.

As mentioned earlier, because this model was developed for a specific flight condition and not amenable to change by the user, the model was used as-received. Thus, for the results to be presented here, there are four pilot control inputs (rotor collective pitch, rotor longitudinal cyclic pitch, rotor lateral cyclic pitch, and pedals) and four measured responses (the perturbation values of aircraft forward velocity, pitch angle, roll angle, and sideslip angle). However, disturbances and target responses can be imposed on the model by the user. There are from one to six possible disturbances that can be imposed (either singly or in combinations up to six) consistent with the six rigid-body degrees of freedom of the aircraft and four target responses consistent with the four measured responses. Thus, $r_c = 4$, $m = 4$, and $r_d$ can be varied from 1 to 6.

### Simulation Conditions and Parameter Settings

Based on the signal processing guidelines given in reference 6, as well as some limited previous experience with the XV-15 model, the sampling frequency $f_s$ was set to 40 Hz ($\triangle t$=0.025 sec) and the number of time points $\ell$ of input/output data was set to 600. The control horizon $h_c$ was set equal to the prediction horizon $h_p$, $h_p$ was set equal to the order of the ARX model $p$, and $p$ was set to 15. The response weights $w_r$ were set to 1.0 and the control weights $w_c$ were set to 0.0005. Again, no attempt was made to "optimize" (i.e., tune) the parameters $p$, $h_c$, $h_p$, and $w_c$ to the idiosyncrasies of the system to elicit the best possible closed-loop

responses. In the simulations, the loop was closed (controller turned on) after 40 time points (1.0 sec).

The MATLAB function *c2d.m* was used to convert the continuous-time state-space model of the XV-15 tiltrotor aircraft (Appendix B) to discrete time using $\triangle t$ =0.025 as set above. The resulting discrete-time state-space model was then used in the MATLAB function *dlsim.m* to generate the random time histories needed to identify the ARX model and design the controller as described earlier in the report. The function *dlsim.m* was also used to compute the open-loop time histories for those examples in which disturbances are present.

Results are presented below for feedback with embedded feedforward, in which all the disturbances acting on the system are assumed to be unknown while performing the SID and controller design. Several different types of disturbances and target responses were devised and imposed on the system to provide a challenging control task for GPC. Both regulator and tracking examples are presented. It should be noted that actual time *t* rather than time index *k* is used on the time axes of the results figures here in contrast to the presentation of the 3-DOF results. This change was motivated by the fact that the XV-15 is a real aircraft with well-documented physical characteristics, many of which involve physical time units. Also, as was done for the 3-DOF system, the number of examples presented for the XV-15 system is also intentionally rather large to better illustrate the robustness of GPC in the subject application.

**Results for Regulation and Tracking of XV-15**

Representative results illustrating the ability of GPC to either quell disturbance-induced responses of the XV-15 (the regulator problem) or to cause the system to follow a desired target response (the tracking problem) are presented in this section. For convenience of discussion below, the (perturbation) force and moment disturbances imposed on the system are denoted by X, Y, Z, RM, PM, and YM and the target responses are denoted by yt1, yt2, yt3, and yt4. X is an axial force (+ forward), Y is a side force (+ right), Z is a vertical force (+ down), RM is a rolling moment (+ right wing down), PM is a pitching moment (+ nose up), and YM is a yawing moment (+ nose right), yt1=forward velocity, yt2=pitch angle, yt3=roll angle, and yt4=sideslip angle. It should be mentioned that no attempt was made at defining disturbances and target responses for the simulations that are consistent with the design operating limits of the subject aircraft. This means that the character and magnitude of some of the imposed disturbances and target responses may be outside the permissible operating environment of the aircraft.

***Regulator Examples:*** Figures 29 through 46 show comparisons of open- and closed-loop responses of the XV-15 to a variety of external disturbances. These results are presented in composite figures consisting of two rows of two figures each. The upper left figure shows the disturbances acting on the system; the upper right figure shows the open-loop responses of the system; the lower left figure shows the control forces applied to the system; and the lower right figure shows the closed-loop responses of the system.

Figures 29-34 display results for a sequence of six cases which differ only in the direction of a single sinusoidal force or moment disturbance imposed on the system at the damped natural frequency of the short-period mode (0.46734 Hz). The disturbances are applied to the aircraft at

its CG in the order X, Z, PM, Y, RM, and YM. Because the subject aircraft is a stable (damped) system there is no divergence of the open-loop responses during oscillatory excitation at a natural frequency as there was for the 3-DOF system. It should be noted that longitudinal disturbances (X, Z, and PM) produce primarily longitudinal responses (forward velocity and pitch angle, $u$ and $\theta$) and lateral disturbances (Y, RM, and YM) produce primarily lateral responses (roll angle and sideslip angle, $\varphi$ and $\beta$). This is so because although there is considerable aerodynamic coupling of the longitudinal and lateral motions in the damping matrix of the XV-15 state-space matrix, there is little coupling in the mass and stiffness matrices. The open-loop responses are suppressed immediately after closing the loop using appropriate control inputs that are well within the control limits of the aircraft. The large amplitude spikes appearing in the control force time histories in the vicinity of one second are a consequence of turning on the controller abruptly in the simulations.

An indication of the response of the system to short-burst excitations is provided in figures 35-36. Figure 35 shows the response to a short sinusoidal disturbance of 2000 lb in the axial (X) direction. The disturbance was formed from a 2400 point (60 sec) time history of a 0.46734 Hz sine wave with the last 2200 points set to zero resulting in a five second disturbance at the short-period mode frequency. The open-loop time history is plotted for 12,000 points (300 sec) to provide a record long enough to allow estimation of the system frequency and damping from the decaying time history. This yields a damped natural frequency of 0.028 Hz and a damping ratio of 0.11, which are characteristic of the low-damped phugoid mode. Open-loop responses are suppressed promptly after engaging the controller. (NOTE: Because the short-period mode is heavily damped compared to the phugoid mode, its response is very short-lived with a duration of only about five seconds and appears as the broad spike at very small time. Thus, only the response of the lightly-damped phugoid mode is prominent in the open-loop response.) In figure 36 the disturbance is a 5000 lb 200 point (5 sec) pulse in the X direction. The data stream used in this case is 24,000 points long (600 sec) for all subplots. Open-loop response time histories yield a damped natural frequency of 0.028 Hz and a damping ratio of 0.11, again indicating excitation of the low-damped phugoid mode. There is immediate quelling of the open-loop responses after closing the loop.

In figure 37 the disturbances are Z, PM, and Y and are given by usin1=2000cos(2πft) with f=0.46734 Hz (the short period frequency), usin2=1000sin(2πft) with f=0.25556 Hz (Dutch roll), and usin3=1500sin(2πft+π/3) with f=0.029291 Hz (phugoid), respectively. Very little control input is required (less than 0.2 inches) in this case. Suppression of the responses occurs immediately after loop closure.

The three disturbances in figure 38 are Z=usin1 with f=0.46734 Hz, PM=usin2 with f=0.25556 Hz, and Y=u1step (a one-step step function). Spiking occurs both in the pedal input and the closed-loop sideslip response angle time histories at the step location of the Y disturbance. Aside from the spiking in the pedal input, all control inputs are again very small (less than 0.2 inches). Of the four closed-loop responses, only sideslip is not fully suppressed.

Figure 39 has the same Z and PM disturbances as figure 38 but the Y disturbance is now u2step, a two-step step function. Spiking occurs in the pedal control input at times corresponding to the steps in the Y disturbance. Again, of the four closed-loop responses only

sideslip is not reduced to zero. The sideslip angle also has a small spike at the location of each of the steps in the Y disturbance.

In figure 40 the disturbances are Z=usin1, PM=usin2, and Y=a random function. Note that the random motion of the pedal dominates the required control inputs, all of which are rather small. The resulting closed-loop responses are all considerably reduced.

Figure 41 represents the case of full longitudinal excitation wherein X, Z, and PM disturbances act on the system. Here, X=usin1, Z=usin2, and PM=u1step. Complete suppression of the open-loop responses occurs immediately after loop closure.

Figure 42 represents the case of full lateral excitation wherein Y, RM, and YM disturbances act on the system. Here, Y=usin1, RM=usin2, and YM=u1step. Again, there is immediate suppression of the open-loop response upon closing the loop.

In figure 43 there is a single disturbance given by PM=usin2+usawtooth2 (a multi-toothed saw-tooth wave) acting on the system. There are three small spikes evident in the longitudinal cyclic control input at locations corresponding to the vertical discontinuities in the pitching moment disturbance. Quelling of the open-loop responses is again seen to occur directly after imposing the controls.

Figure 44 is another example of full longitudinal excitation of the system but with X, Z, and PM now being an upward-pointing pyramid, a downward-pointing pyramid, and usawtooth2, respectively. Slight spiking occurs in the longitudinal cyclic control input at the locations of the three vertical discontinuities in the pitching moment disturbance. Suppression is again immediate.

The example of figure 45 employs a full set of six disturbances (X, Y, Z, RM, PM, and YM). The random control input of the pedal dominates the set of control inputs to quell the random excitation force in the Y direction. Suppression of the open-loop response occurs promptly after closing the loop.

Lateral excitations Y, RM, and YM are imposed in figure 46, where $Y=usin1=2000\cos(2\pi ft)$ with f=0.46734 Hz, $RM=usin2=1000\sin(2\pi ft)$ with f=0.25556 Hz, and $YM=usin3=1500\sin(2\pi ft+\pi/3)$ with f=0.029291 Hz. There is immediate quelling of the open-loop response.

***Tracking Examples:*** Figures 47 through 55 show comparisons of closed-loop (achieved) responses of the XV-15 to a variety of imposed target responses with no disturbances acting on the system. Figures 56 through 68 show comparisons of closed-loop responses of the aircraft to several sets of target responses while being subjected to a variety of disturbances.

The results for the tracking simulations without disturbances are presented in composite figures consisting of three rows. The first row contains one figure which shows a time history of the four control inputs applied to the system; the second row contains two figures which show comparisons of the target and achieved responses for the forward velocity and pitch angle,

respectively; and the third row contains two figures which show comparisons of the target and achieved responses for roll angle and sideslip angle, respectively.

The target responses in figure 47 are all sinusoids: yt1=psin1=20cos(2πft), with f=0.1 Hz, yt2=psin2=10sin(2πft), with f=0.2 Hz, yt3=psin3=15cos(2πft), with f=0.3 Hz, and yt4=psin4=25sin(2πft), with f=0.4 Hz. The required control inputs are all sinusoidal, as expected, and provide excellent tracking of the target responses.

Figures 48-50 compare the performance of the controller for cases in which problematic targets (those having step-type discontinuities in their waveforms) are unfiltered and filtered. In figure 48, yt1 is the product of psin1 and a converging exponential (psin1*expc), yt2 is the product of psin2 and a diverging exponential (psin2*expd), yt3 is a product of a nonuniformly-toothed saw-tooth wave and a converging exponential (psaw*expc), and yt4 is the product of a random function and a diverging exponential (prandom*expd). The three spikes evident in the calculated lateral cyclic control input occur at the time locations of the three vertical offsets (steps) in the roll target time history. The tracking is excellent. Figure 49 is a repeat of figure 48 but with the roll target response yt3 filtered by a 20-point moving average filter (MATLAB function *filtfilt.m*). The three roll control spikes are now gone. Tracking remains excellent. Figure 50 is a repeat of figure 49 but with the sideslip target also filtered. The time histories of the required control inputs are now both considerably smoother as well as slightly smaller.

Figures 51-52 are another comparison of filtered and unfiltered tracking responses but for a different set of target responses. In figure 51 yt1=psin1, yt2=psin1+p2step, yt3=prandom, and yt4=psin4. Large spikes appear in the calculated pedal control inputs at t=1.45 sec and t=6.25 sec due to the vertical steps in the pitch target response. The tracking is very good. Figure 52 is a repeat of figure 51 but with the pitch target response filtered by a 20-point moving average filter. There are now no spikes in the pedal control input. Tracking is excellent.

Figures 53-55 are the final set of comparisons of filtered and unfiltered tracking responses for the case of no disturbances. In figure 53 yt1=p1step-psaw, yt2=(psin1+p2step)/5, yt3=psaw, and yt4=p2step+p1mc, where p1mc is a (1-cosine) function. Large spikes appear in the lateral cyclic and pedal control inputs due to the various infinite-slope vertical steps in all four target responses. Tracking is very good. Figure 54 compares the filtered and unfiltered targets of figure 53. Figure 55 is a repeat of figure 53 but using the filtered targets of figure 54. The control input time history is now smoothly varying with no large amplitude spikes as before. Tracking is now excellent.

The results for the tracking simulations with disturbances acting on the system are presented in composite figures consisting of four rows. The first row has two figures: the first shows the disturbances acting on the system while the second shows the open-loop responses of the system The second row contains one figure which shows a time history of the four control inputs applied to the system; the third row contains two figures which show comparisons of the target and achieved responses for the forward velocity and pitch angle, respectively; and the fourth row contains two figures which show comparisons of the target and achieved responses for roll angle and sideslip angle, respectively.

Figures 56-59 have longitudinal disturbances X=usin1, Z=usin2, and PM=u2step acting on the system. In figure 56 the target responses are yt1=psin1*expc, yt2=psin2*expd, yt3=psaw*expc, and yt4=prandom*expd, the same as in figure 48. The control inputs look the same as those in the no-disturbance case of figure 48 but they are not identical numerically. The small differences are just enough to quell the disturbances in figure 56. Spikes on the lateral cyclic input are due to the three vertical steps in the roll target. There is, however, very good tracking. Figure 57 is a repeat of figure 56 but with a filtered roll target. No spikes are now present in the control inputs. Tracking is excellent. Figure 58 is a repeat of figure 57 but with the sideslip target also filtered. All the control inputs are now both smoothly varying and reduced in magnitude. Tracking remains excellent. Figure 59 is a repeat of figure 58 but with the disturbances increased by a factor of 20. All control inputs are now larger by a factor of about two to accommodate the twenty-fold increase in magnitude of the disturbances. Tracking is still excellent.

Figures 60-62 have lateral disturbances Y, RM, and YM which are identical to those used for X, Z, and PM in figure 56. However, the set of target responses is different. In figure 60 the target responses are yt1=p1step–psaw, yt2=psin1+p2step, yt3=psaw, and yt4=p2step+p1mc. There are large amplitude spikes in the lateral cyclic and pedal control inputs due to the vertical steps in all four target responses. Tracking is very good. Figure 61 shows a comparison of filtered and unfiltered targets for figure 60. Figure 62 is a repeat of figure 60 but with filtered targets. Controls now vary smoothly with time and the spikes no longer appear. Tracking is now excellent.

Figures 63-64 show a comparison of filtered and unfiltered tracking responses for the case in which the six disturbances of figure 45 act on the system. Figure 63 has the same set of targets as in figure 56. Spikes occur in the lateral cyclic control input at the time locations of the vertical steps in the roll target yt3. Tracking is very good. The control inputs are much larger (even without considering the spikes) than in figure 45 because of the tracking requirement imposed in figure 63. Figure 64 is a repeat of figure 63 but with filtered roll and sideslip targets. Controls vary smoothly with time now and have slightly smaller values. Tracking is excellent.

Figure 65 has the same pitch disturbance as in figure 43 and the same filtered targets as in figure 50. Note that all the calculated control inputs are considerably different from those in the regulator example of figure 43 because of the additional tracking requirements imposed in figure 65. However, the present control inputs are very nearly those of the zero-disturbance tracking example in figure 50. Tracking is excellent.

Figure 66 has the same X, Z, and PM disturbances as in figure 44 and the same filtered targets as in figures 50 and 65. Control inputs here are larger than those in figure 44 because of the additional tracking requirements imposed in figure 66 but are essentially the same as those in figures 50 and 65 because the targets are the same (recall earlier 3-DOF system comment that targets tend to drive the character and magnitude of the required control inputs). Tracking is excellent.

Figure 67 has a full complement of six disturbances (same as those in figure 45). The target responses are each composed of various combinations of the simpler target responses used

above in figures 47-66) . Control inputs here are much larger than in figure 45 because of the additional target response requirements. Tracking is excellent.

Figure 68 has sinusoidal lateral excitations Y, RM, and YM as in figure 46. The target responses are again each composed of various combinations of simpler target responses used earlier. Much larger control inputs are needed here than in figure 46 to enforce the additional tracking requirements. Tracking is excellent.

***Summary of Observations*:** Viewed as a whole, the XV-15 simulations indicate that the GPC controllers functioned well whether they were employed as regulators to suppress disturbance-induced system responses or as trackers to cause the system to follow a prescribed response. When used in the regulation mode, they were able to either significantly reduce or quell open-loop responses of the system under a variety of imposed disturbance conditions and did so immediately after closing the loop. The control displacements required to achieve these reductions were all about an inch or less in value and well within the control operating ranges of the subject aircraft.

When used to meet a tracking requirement, the GPC controllers were able to produce the commanded responses, even in the presence of disturbances acting on the system, and to do so promptly after closing the loop. Based on the results presented in figures 29-68, the tracking problem is much more demanding than the regulator problem. That is, the control inputs required for satisfactory tracking are typically (much) larger than those needed for regulation. It was also observed that large amplitude spikes can occur in the calculated control inputs (as they did for the 3-DOF system) when the target response time histories have vertical (infinite-slope) step discontinuities. However, such spikes can be averted simply by filtering suspect problematic targets to reduce the slope of such abrupt transitions. The spiking notwithstanding, the values calculated for the control inputs in the tracking examples, although substantially larger than those required in the regulation examples, appear reasonable considering the complexity and magnitude of most of the prescribed maneuvers. However, because the XV-15 was not designed for aggressive active-control-induced maneuvers, many of those values exceed the operating limits of the controls on the aircraft.

## Concluding Remarks

The results of numerical simulations aimed at assessing and evaluating the effectiveness of a predictive control method known as Generalized Predictive Control (GPC) for active control of systems dominated by rigid-body behavior have been summarized. GPC is a linear, time-invariant, multi-input/multi-output predictive control method that uses an AutoRegressive with eXternal input (ARX) model to describe the input-output relationship of the system. The coefficient matrices of the ARX equation are determined using system identification techniques. The input-output equation is used to form a multi-step output prediction equation over a finite prediction horizon. The control to be imposed at the next time step is determined by minimizing the deviation of the predicted controlled plant responses from the desired (or target) responses, subject to a penalty on control effort. Following a qualitative discussion of the essential features of GPC, the equations underlying the method as applied during the present investigation were

presented and discussed, including system identification, calculation of control law matrices, and calculation of the commands applied to the control effectors.

Representative results from two types of simulations were presented. The first used a three-degree-of-freedom mathematical model of an unrestrained (free-free) mass-spring-dashpot system. The second used a state-space math model of the rigid-body dynamics of the XV-15 tiltrotor research aircraft cruising at 150 knots in the airplane mode of flight. Both models were subjected to a variety of user-defined external disturbances and user-defined target responses intended to demonstrate the robustness of GPC to changing disturbances and target motions. Results obtained from these simulations have been decidedly positive. In particular, in the regulator examples calling for a quelling of the response in the presence of external disturbances, the closed-loop simulations showed reductions of nearly 100% for most of the examples. Furthermore, the control inputs required to achieve these reductions were all small. For example, the rotor and pedal control displacements required to achieve these reductions for the XV-15 were about an inch or less in amplitude and well within the control operating ranges of the aircraft. In the tracking examples wherein the system is commanded to follow a specified path, the GPC controllers were able to produce the desired responses, even in the presence of external disturbances. The control inputs needed to produce the target trajectories were notably larger than those required for regulation but reasonable when viewed from the perspective of the level of complexity and magnitude of the commanded maneuvers.

Based on the results of these studies, it has been demonstrated that GPC is an excellent approach for active control of the rigid-body behavior of dynamic systems.

# Appendix A

## State-Space Model for 3-DOF Mass-Spring-Dashpot System*

The second-order matrix equations of motion for the free-free, 3-degree-of-freedom, mass-spring-dashpot system shown in figure 2 are given by

$$\begin{bmatrix} m_1 & 0 & 0 \\ 0 & m_2 & 0 \\ 0 & 0 & m_3 \end{bmatrix} \begin{Bmatrix} \ddot{x}_1 \\ \ddot{x}_2 \\ \ddot{x}_3 \end{Bmatrix} + \begin{bmatrix} c_2 & -c_2 & 0 \\ -c_2 & c_2 + c_3 & -c_3 \\ 0 & -c_3 & c_3 \end{bmatrix} \begin{Bmatrix} \dot{x}_1 \\ \dot{x}_2 \\ \dot{x}_3 \end{Bmatrix} + \begin{bmatrix} k_2 & -k_2 & 0 \\ -k_2 & k_2 + k_3 & -k_3 \\ 0 & -k_3 & k_3 \end{bmatrix} \begin{Bmatrix} x_1 \\ x_2 \\ x_3 \end{Bmatrix} = \begin{Bmatrix} f_1 \\ f_2 \\ f_3 \end{Bmatrix}$$

$$= \begin{bmatrix} 1 & 0 & 0 & 1 & 0 & 0 \\ 0 & 1 & 0 & 0 & 1 & 0 \\ 0 & 0 & 1 & 0 & 0 & 1 \end{bmatrix} \begin{Bmatrix} ud_1 \\ ud_2 \\ ud_3 \\ uc_1 \\ uc_2 \\ uc_3 \end{Bmatrix} = \begin{bmatrix} [I_{ud}] & [I_{uc}] \end{bmatrix} \begin{Bmatrix} \{ud\} \\ \{uc\} \end{Bmatrix} = [B_2]\{u\} \tag{A1}$$

where the external forces acting on the system are divided into disturbance forces $ud_i$ and control forces $uc_i$ for convenience in controls work. Note that three disturbance forces and three control forces are assumed in equation A1. The matrix $[B_2]$ is an input influence matrix indicating the locations of the input forces $\{u\}$. Equation A1 can be written compactly as

$$[M]\{\ddot{x}\} + [C]\{\dot{x}\} + [K]\{x\} = \{f\} = [B_2]\{u\} \tag{A2}$$

For controls work, equation A2 is usually recast into a set of first-order differential equations known as state equations having the form

$$\{\dot{X}\} = [A_c]\{X\} + [B_c]\{u\} \tag{A3}$$

where the usual reformulation leads to the state matrix $[A_c]$, input influence matrix $[B_c]$, and state vector $\{X\}$ given by

$$[A_c] = \begin{bmatrix} [0] & [I] \\ -[M^{-1}K] & -[M^{-1}C] \end{bmatrix}; \qquad [B_c] = \begin{bmatrix} [0] \\ [M^{-1}B_2] \end{bmatrix}; \qquad \{X\} = \begin{Bmatrix} \{x\} \\ \{\dot{x}\} \end{Bmatrix} \tag{A4}$$

* This is a corrected version of the formulation presented in Appendix B of reference 6.

In control problems, the first-order equations of motion given by equation A3 are augmented with a set of equations relating the outputs or measured quantities $\{y\}$ to the state variables $\{X\}$ and the inputs $\{u\}$ according to

$$\{y\} = [C_c]\{X\} + [D_c]\{u\} \tag{A5}$$

For mechanical systems, outputs are typically related to the dynamic variables of the problem such as $\{x\}, \{\dot{x}\}$, and $\{\ddot{x}\}$ by equations of the form

$$\{y_d\} = [\bar{C}_d]\{x\}, \quad \{y_v\} = [\bar{C}_v]\{\dot{x}\}, \quad \{y_a\} = [\bar{C}_a]\{\ddot{x}\} \tag{A6}$$

where $\bar{C}_d$, $\bar{C}_v$, and $\bar{C}_a$ are output influence matrices for displacement, velocity, and acceleration, respectively, and for the subject three-degree-of-freedom system (assuming 3 displacements, 3 velocities, and 3 accelerations are measured) have the diagonal forms

$$[\bar{C}_d] = \begin{bmatrix} c_{d_1} & & \\ & c_{d_2} & \\ & & c_{d_3} \end{bmatrix}; \quad [\bar{C}_v] = \begin{bmatrix} c_{v_1} & & \\ & c_{v_2} & \\ & & c_{v_3} \end{bmatrix}; \quad [\bar{C}_a] = \begin{bmatrix} c_{a_1} & & \\ & c_{a_2} & \\ & & c_{a_3} \end{bmatrix} \tag{A7}$$

The matrices $\bar{C}_d$, $\bar{C}_v$, and $\bar{C}_a$ in equation A6 describe the relationship between the units of the dynamic variables in the vectors $\{x\}, \{\dot{x}\}, \{\ddot{x}\}$ and the units of the measured quantities in the vectors $\{y_d\}$, $\{y_v\}$, and $\{y_a\}$, respectively. If the measurement quantity has units of displacement, velocity, or acceleration the corresponding diagonal term is unity; otherwise the diagonal term is a conversion factor from the units of the dynamic variable (e.g., acceleration) to the units of the measured quantity (e.g., volts).

If accelerations are measured, the acceleration output equations (the third set of equations given by A6) must be rewritten in terms of the state variables $\{x\}$ and $\{\dot{x}\}$. This is done by solving equation A2 for $\{\ddot{x}\}$ and substituting the result into the third of equations A6. The resulting equations can then be written solely in terms of the state variables $\{x\}$ and $\{\dot{x}\}$ as

$$
\begin{aligned}
\{y_d\} &= \begin{bmatrix} \bar{C}_d & 0 \end{bmatrix} \begin{Bmatrix} x \\ \dot{x} \end{Bmatrix} = \begin{bmatrix} \bar{C}_d & 0 \end{bmatrix} \{X\} \\
\{y_v\} &= \begin{bmatrix} 0 & \bar{C}_v \end{bmatrix} \begin{Bmatrix} x \\ \dot{x} \end{Bmatrix} = \begin{bmatrix} 0 & \bar{C}_v \end{bmatrix} \{X\} \\
\{y_a\} &= \begin{bmatrix} -\bar{C}_a M^{-1} K & -\bar{C}_a M^{-1} C \end{bmatrix} \begin{Bmatrix} x \\ \dot{x} \end{Bmatrix} + \begin{bmatrix} \bar{C}_a M^{-1} B_2 \end{bmatrix} \{u\} \\
&= \begin{bmatrix} -\bar{C}_a M^{-1} K & -\bar{C}_a M^{-1} C \end{bmatrix} \{X\} + \begin{bmatrix} \bar{C}_a M^{-1} B_2 \end{bmatrix} \{u\}
\end{aligned}
\tag{A8}
$$

The output equation (A5) for the general case in which all the displacements, velocities, and accelerations comprise the vector of measured quantities has the form

$$
\{y\} = \begin{Bmatrix} \{y_d\} \\ \{y_v\} \\ \{y_a\} \end{Bmatrix} = \begin{bmatrix} \bar{C}_d & 0 \\ 0 & \bar{C}_v \\ -\bar{C}_a M^{-1} K & -\bar{C}_a M^{-1} C \end{bmatrix} \{X\} + \begin{bmatrix} 0 \\ 0 \\ \bar{C}_a M^{-1} B_2 \end{bmatrix} \{u\} \tag{A9}
$$

which can be written compactly as

$$
\{y\} = [C_c]\{X\} + [D_c]\{u\} \tag{A10}
$$

where $[C_c]$ and $[D_c]$ are the output and direct transmission matrices and are given by

$$
\begin{aligned}
[C_c] &= \begin{bmatrix} \bar{C}_d & 0 \\ 0 & \bar{C}_v \\ -\bar{C}_a M^{-1} K & -\bar{C}_a M^{-1} C \end{bmatrix} \\
[D_c] &= \begin{bmatrix} [0] \\ [0] \\ \begin{bmatrix} \bar{C}_a M^{-1} B_2 \end{bmatrix} \end{bmatrix}
\end{aligned}
\tag{A11}
$$

The output matrix $[C_c]$ depends on the number, type, and location of the sensors used to measure the outputs of interest. The direct transmission matrix $[D_c]$ is zero if accelerations are not included in the output measurements (in which case $\begin{bmatrix} \bar{C}_a \end{bmatrix} = [0]$), or if the accelerations are measured at locations where there are no disturbances or control forces (in which case the corresponding diagonal elements of both $I_{ud}$ and $I_{uc}$ will be zero, the corresponding rows of $[B_2]$ will be null, and the product $\begin{bmatrix} \bar{C}_a M^{-1} B_2 \end{bmatrix}$ will be zero).

Special cases of the general equations given above are easily obtained. For example, the number, type, and combination of input and output quantities can be varied by deleting appropriate rows of the output equation and/or zeroing appropriate diagonal elements in $I_{ud}$, $I_{uc}$, $\overline{C}_d$, $\overline{C}_v$, and $\overline{C}_a$.

# Appendix B

## State-Space Model for XV-15 Tiltrotor Research Aircraft

Figure 27 shows the Bell XV-15 tiltrotor research aircraft flying in airplane mode. This aircraft was designed and built by Bell Helicopter Company during the mid-1970s under a joint NASA/Army contract with the objective of initially serving as a tiltrotor technology demonstrator and then later as a tiltrotor technology research aircraft (ref. 20). The aircraft has a design gross weight of 13,000 lb, carries a crew of two, and has a maximum speed of 300 knots when operating in the airplane mode of flight.

An existing state-space model defining the rigid-body flight dynamics of the XV-15 was used for the present studies. The model was obtained from Bell Helicopter Textron in the 1990s as part of some collaborative studies then underway between Bell and the Aeroelasticity Branch at NASA Langley. When the present GPC investigation was initiated it was with the intention of only using the three-degree-of-freedom math model described in Appendix A. However, it was realized that the subject XV-15 model (which was still in-hand) would be an excellent additional model for the investigation and so it was included as one of the study systems.

Some comments related to manner of obtaining the mass, damping, stiffness, and control effectivity matrices needed for forming the *A* and *B* matrices of the XV-15 state-space equations are in order. These matrices were obtained using a Bell rotorcraft flight simulation program called C81 (ref. 21). The program first seeks the equilibrium or trim solution for a specified flight condition (symmetric level flight at 150 knots in the airplane mode of fight at sea level altitude was used in this instance). This calculation involves numerically solving the nonlinear algebraic equations governing the trim solution of the aircraft for the specified flight condition. The trim solution yields the aircraft's attitude (yaw, pitch, and roll) in space, the longitudinal (fore/aft) and lateral rigid-body flapping angles of the tip-path-plane for each of the two rotors, and the positions of the four pilot controls (rotor collective pitch, rotor longitudinal cyclic pitch, rotor lateral cyclic pitch, and pedals).

There are 11 independent variables that define the trimmed flight condition (three fuselage angles (yaw, pitch, and roll), four pilot controls (collective, longitudinal cyclic, lateral cyclic, and pedals), and the longitudinal and lateral tip-path-plane flapping angles for each of the two rotors). These 11 independent variables must satisfy 10 static equilibrium equations (3 forces and 3 moments at the c.g. of the aircraft and the longitudinal and lateral flapping moments for each of the two rotors. The trim solution is initiated by assuming a fixed value for one of the independent variables (usually fuselage yaw or roll angle); this leads to a set of 10 nonlinear algebraic equations in 10 unknowns. One then makes reasonable guesses for the values of the 10 remaining independent variables and the program iterates on them until all 10 static equilibrium equations are satisfied.

With the trim solution known, the program then obtains the mass, damping, stiffness, and control effectivity matrices that underlie the linear perturbation equations governing the rigid-body behavior of the aircraft about the trim flight condition. This step involves calculating changes in the fuselage and rotor trim forces and moments due to small perturbations in the flight

variables (displacements, velocities, and control inputs). Perturbing (with stick fixed) all the displacement and velocity degrees of freedom in turn leads to the elements of the rigid-body stiffness and damping matrices. Perturbing the linear and angular displacements yields the stiffness matrix. Perturbing the linear and angular velocities gives the damping matrix. The rigid-body mass matrix is formed directly from the known inertial properties of the aircraft. The resulting mass, damping, and stiffness matrices are each of size 10×10.

The control effectivity matrix, which is essentially a partial derivative matrix giving the changes in the forces and moments that act on the airframe and rotors due to perturbation changes in the four pilot controls, is also computed after calculating the trim solution. This computation involves perturbing each of the control inputs in turn, calculating the relevant force or moment, subtracting the trim value of that force or moment, and then dividing by the value of the perturbation. The control effectivity matrix is of size 10×4.

A rigid-body simulation will have 10 rigid-body degrees of freedom (6 from the airframe (x, y, z, θ, ψ, φ) and 4 from the rotors (longitudinal and lateral tip-path-plane flapping ($a_1$ and $b_1$) of each of the two rotors). Because the time constants for the rotor flapping responses are much smaller than the time constants for the rigid-body responses of the airframe, rotor flapping equilibration subsequent to a motion of the airframe can be viewed as essentially instantaneous. Thus, one can assume that tip-path-plane flapping is not an independent state and eliminate the tip-path-plane flapping degrees of freedom from the linear math model by deleting all the rows and columns involving the rotor flapping degrees of freedom in the four governing matrices. This elimination produces 6×6 mass, damping, and stiffness matrices, and a 6×4 control effectivity matrix.

The vector of state variables employed in the state-space model of the XV-15 tiltrotor research aircraft used in the present investigation is given by

$$\{X\} = \lfloor x \quad z \quad \theta \quad y \quad \phi \quad \psi \quad u \quad w \quad q \quad v \quad p \quad r \rfloor^T \tag{B1}$$

The first six state variables are the perturbation displacements and rotations. The last six state variables are the corresponding perturbation linear and angular velocities. The sign convention for these state variables is depicted in figure 28. Note that the rotor longitudinal and lateral tip-path-plane flapping angles $a_1$ and $b_1$ and their first time derivatives are not included in the state vector. This is consistent with the deletion of the rotor flapping equations of motion and all columns dealing with rotor flapping from the full set of linearized equations obtained from C81.

The partial derivative matrix/control effectivity matrix giving the changes in the total forces and moments acting on the aircraft due to perturbation changes in pilot control inputs is given by

$$pdm = \begin{array}{c} \begin{matrix} \text{Collective} & \text{Long Cyclic} & \text{Lat Cyclic} & \text{Pedal} \end{matrix} \\ \begin{bmatrix} 6335. & 75.01 & -40.04 & -101.0 \\ -199.2 & -439.6 & 0.7031 & -12.47 \\ -0.1232E+05 & -0.1011E+05 & 60.41 & 57.13 \\ 0.0000E+00 & 0.0000E+00 & 22.73 & 565.0 \\ 0.9399E-02 & 0.0000E+00 & 8135. & 1953. \\ 0.1958E-03 & 0.0000E+00 & 4028. & 0.1323E+05 \end{bmatrix} \end{array} \begin{array}{l} \\ \text{Change in X force (+fwd)} \\ \text{Change in Z force (+down)} \\ \text{Change in pitching moment} \\ \text{Change in Y force (+right)} \\ \text{Change in rolling moment} \\ \text{Change in yawing moment} \end{array} \quad \text{(B2)}$$

where the meaning of the rows is indicated at the right of the matrix and that of the columns at the top of the matrix. The three rotor controls are defined in terms of inches of stick displacement and the pedal control as inches of pedal displacement. The forces and moments have units of lb and ft-lb, respectively. The sign convention for the stick and pedal movements is as follows: Up collective stick is positive and increases forward thrust. Longitudinal cyclic stick is positive for stick forward and produces a nose-down pitch of the aircraft. Lateral cyclic stick is positive for stick right and produces a right roll. Positive pedal is right pedal forward and produces a nose-right rotation (yaw) of the aircraft.

The structural mass matrix, which is formed directly from the known inertial properties of the aircraft, is

$$mass = \begin{array}{c} \begin{matrix} \dot{u} & \dot{w} & \dot{q} & \dot{v} & \dot{p} & \dot{r} \end{matrix} \\ \begin{bmatrix} 422.4 & 0.00E+00 & 0.0000E+00 & 0.00E+00 & 0.0000E+00 & 0.0000E+00 \\ 0.00E+00 & 424.0 & 0.0000E+00 & 0.00E+00 & 0.0000E+00 & 0.0000E+00 \\ 0.00E+00 & 36.72 & 0.1791E+05 & 0.00E+00 & 0.0000E+00 & 0.0000E+00 \\ 0.00E+00 & 0.00E+00 & 0.0000E+00 & 422.4 & 0.0000E+00 & 0.0000E+00 \\ 0.00E+00 & 0.00E+00 & 0.0000E+00 & 0.00E+00 & 0.4867E+05 & -1234. \\ 0.00E+00 & 0.00E+00 & 0.0000E+00 & 0.00E+00 & -1234. & 0.6025E+05 \end{bmatrix} \end{array} \quad \text{(B3)}$$

where the meaning of the columns is indicated at the top of the matrix and the meaning of the rows is the same as in equation B2.

Perturbing the linear and angular velocity variables as described above yields the damping matrix

$$damp = \begin{array}{c} \begin{matrix} \text{u} & \text{w} & \text{q} & \text{v} & \text{p} & \text{r} \end{matrix} \\ \begin{bmatrix} 12.57 & -68.98 & 0.1272E+05 & 0.0000E+00 & 37.39 & -0.9300E-02 \\ 75.24 & 298.2 & -0.1040E+06 & 0.0000E+00 & -103.4 & 0.0000E+00 \\ -119.0 & 679.6 & 0.2933E+05 & -0.1502E-02 & 1285. & 0.9390E-02 \\ 0.00E+00 & 0.5869E-05 & 0.0000E+00 & 81.32 & -0.1294E+05 & 0.1042E+06 \\ 0.00E+00 & 0.0000E+00 & 0.0000E+00 & 404.4 & 0.2685E+05 & 6932. \\ 0.00E+00 & 0.0000E+00 & -0.1479 & -646.3 & 0.1368E+05 & 0.6277E+05 \end{bmatrix} \end{array}$$

(B4)

while perturbing the linear and angular displacement variables leads to the stiffness matrix

$$stiff = \begin{array}{c} \begin{matrix} \text{x} & \text{z} & \theta & \text{y} & \phi & \psi \end{matrix} \\ \begin{bmatrix} 0.00E+00 & 0.00E+00 & 0.1349E+05 & 0.00E+00 & 0.0000E+00 & 0.00E+00 \\ 0.00E+00 & 0.00E+00 & 1665. & 0.00E+00 & -0.9292E-04 & 0.00E+00 \\ 0.00E+00 & 0.00E+00 & 0.0000E+00 & 0.00E+00 & 0.0000E+00 & 0.00E+00 \\ 0.00E+00 & 0.00E+00 & -0.1147E-04 & 0.00E+00 & -0.1349E+05 & 0.00E+00 \\ 0.00E+00 & 0.00E+00 & 0.0000E+00 & 0.00E+00 & 0.0000E+00 & 0.00E+00 \\ 0.00E+00 & 0.00E+00 & 0.0000E+00 & 0.00E+00 & 0.0000E+00 & 0.00E+00 \end{bmatrix} \end{array} \quad \text{(B5)}$$

Again, the meaning of the columns is indicated at the top of the matrices and the meaning of the rows is the same as in equation B2.

Consistent with the development in Appendix A, the continuous-time state matrix is given by

$$A_c = \begin{bmatrix} [0] & [I] \\ -[mass]^{-1}[stiff] & -[mass]^{-1}[damp] \end{bmatrix} \quad \text{(B6)}$$

and the continuous-time input influence matrix $B_c$ is composed of a disturbance part $B_{disturbance}$ and a control part $B_{control}$

$$B_c = [B_{disturbance} \;\; B_{control}] \quad \text{(B7)}$$

where the control portion of $B_c$ is

$$B_{control} = \begin{bmatrix} [0] \\ [mass]^{-1}[pdm] \end{bmatrix} \quad \text{(B8)}$$

and the disturbance portion of $B_c$ is

$$B_{disturbance} = \begin{bmatrix} [0] \\ [mass]^{-1}[I_{ud}] \end{bmatrix} \tag{B9}$$

The matrix $C_c$ appearing in the output equation portion of the state-space equations is given by

$$C_c = \begin{array}{c} \begin{matrix} x & z & \theta & y & \phi & \psi & u & w & q & v & p & r \end{matrix} \\ \begin{bmatrix} 0 & 0 & 0 & 0 & 0 & 0 & 1 & 0 & 0 & 0 & 0 & 0 \\ 0 & 0 & 57.3 & 0 & 0 & 0 & 0 & 0 & 0 & 0 & 0 & 0 \\ 0 & 0 & 0 & 0 & 57.3 & 0 & 0 & 0 & 0 & 0 & 0 & 0 \\ 0 & 0 & 0 & 0 & 0 & 0 & 0 & 0 & 0 & 57.3/(150*1.689) & 0 & 0 \end{bmatrix} \end{array} \begin{matrix} u \\ \theta \\ \phi \\ \beta \end{matrix} \tag{B10}$$

The four output variables are indicated at the right of the matrix $C_c$. The identity of the columns of $C_c$ is indicated above the matrix and corresponds to the sequence of state variables shown in equation B1. Note that the sideslip angle β has replaced the perturbation velocity *v* as the output variable in the fourth equation by virtue of the division of that equation by (150*1.689), the forward flight velocity in ft/sec.

Because none of the desired output variables are accelerations, the matrix $D_c$ appearing in the output equation is a null matrix.

## References


1. Juang, J.-N., and Eure, K. W.: Predictive Feedback and Feedforward Control for Systems with Unknown Disturbances, NASA/TM-1998-208744, December 1998.

2. Kvaternik, R. G.; Juang, J-N.; and Bennett, R. L.: Exploratory Studies in Generalized Predictive Control for Active Aeroelastic Control of Tiltrotor Aircraft. NASA TM-2000-210552, October 2000.

3. Kvaternik, R. G.; Piatak, D. J.; Nixon, M. W.; Langston, C. W.; Singleton, J. D.; Bennett, R. L.; and Brown, R. K.: An Experimental Evaluation of Generalized Predictive Control for Tiltrotor Aeroelastic Stability Augmentation in Airplane Mode of Flight. *J. Amer. Hel. Soc*., Vol. 27, No. 3, July 2002, pp. 198-208.

4. Nixon, M. W.; Langston, C. W.; Singleton, J. D.; Piatak, D. J.; Kvaternik, R. G.; Corso, L. M.; and Brown, R. K.: Hover Test of a Soft-Inplane Gimballed Tiltrotor Model, *J. Amer. Helicopter Soc.*, Vol. 48, No. 1, Jan 2003, pp. 63-66.

5. Nixon, M. W.; Langston, C. W.; Singleton, J. D.; Piatak, D. J.; Kvaternik, R. G.; Corso, L. M.; and Brown, R.: Aeroelastic Stability of a Four-Bladed Semi-Articulated Soft-Inplane Tiltrotor Model. Presented at the AHS 59th Annual Forum and Technology Display, May 6-8, 2003, Phoenix, Arizona. In American Helicopter Society 59th Annual Forum Proceedings.

6. Kvaternik, R. G.; Eure, K. W.; and Juang, J-N: *Exploratory Studies in Generalized Predictive Control for Active Gust Load Alleviation*. NASA TM-2006-214296, April 2006.

7. Clark, D. W. (Ed): *Advances in Model-Based Predictive Control*. Oxford University Press, New York, 1994.

8. Clarke, D. W.; Mohtadi, C.; and Tuffs, P. S.: Generalized Predictive Control – Parts I and II. *Automatica*, Vol. 23, No. 2, 1987, pp. 137-160.

9. MATLAB Reference Guide. The MathWorks, Inc., Natick, MA, August 1992.

10. Juang, J-N., and Phan, M. Q.: *Identification and Control of Mechanical Systems*. Cambridge University Press, New York, NY, 2001.

11. Juang, J-N.: *Applied System Identification*. Prentice-Hall, Englewood Cliffs, NJ, 1994.

12. Eure, K. W.; and Juang, J.-N.: *Broadband Noise Control Using Predictive Techniques*. NASA TM 110320, January 1997.

13. Juang, J.-N.: *State-Space System Realization with Input- and Output-Data Correlation*. NASA TP 3622, April 1997.

14. Juang, J.-N.; and Phan, M. Q.: *Deadbeat Predictive Controllers*. NASA TM 112862, May 1997.

15. Eure, K. W.: *Adaptive Predictive Feedback Techniques for Vibration Control*. Ph.D. Dissertation, Virginia Polytechnic Institute and State University, May 1998.

16. Phan, M. Q.; and Juang, J.-N.: Predictive Controllers for Feedback Stabilization. *Journal of Guidance, Control, and Dynamics*, Vol. 21, No. 5, Sept.-Oct. 1998, pp. 747-753.

17. Juang, J.-N.; and Eure, K. W.: *Predictive Feedback and Feedforward Control for Systems with Unknown Disturbances*. NASA/TM-1998-208744, December 1998.

18. Phan, M. Q.; Horta, L. G.; Juang, J.-N.; and Longman, R. W.: *Identification of Linear Systems by an Asymptotically Stable Observer*. NASA TP 3164, June 1992.

19. Phan, M. Q.; and Juang, J-N: Predictive Feedback Controllers for Stabilization of Linear Multivariable Systems. *AIAA Guidance, Navigation and Control Conference*, San Diego, CA, July 29-31, 1996.

20. Maisel, M. D.; Giulianetti, D. J.; and Dugan, D. C.: *The History of the XV-15 Tilt Rotor Research Aircraft: From Concept to Flight.* NASA SP-2000-4517, 2000.

21. Davis, J. M.; Bennett, R. L.; and Blankenship, B. L.: *Rotorcraft Flight Simulation with Aeroelastic Rotor and Improved Aerodynamic Representation, Volume I, Engineer's Manual*. USAAMRDL-TR-74-10A, June 1974.

Table 1.- Dynamic Characteristics of 3-DOF Math Model

| Eigenvalues of State Matrix | Natural Frequencies (Hz) |
|---|---|
| 0.0 ± 0.0i | 0.0 |
| 0.0 ± 1.0i | 0.15915 |
| 0.0 ± 1.7321i | 0.27566 |

Table 2.- Dynamic Characteristics of XV-15 Math Model

| Mode | Eigenvalues of State Matrix | Damped Natural Frequencies (Hz) | Damping Ratios (Fraction of critical) |
|---|---|---|---|
| Short period | -1.4173±2.9364i | 0.46734 | 0.43469 |
| Dutch roll | -0.44913±1.6058i | 0.25556 | 0.26936 |
| Phugoid | -0.019449±0.18404i | 0.029291 | 0.10509 |
| Roll convergence | -0.73883±0.0i | 0 | 1 |
| Spiral convergence | -0.15843±0.0i | 0 | 1 |

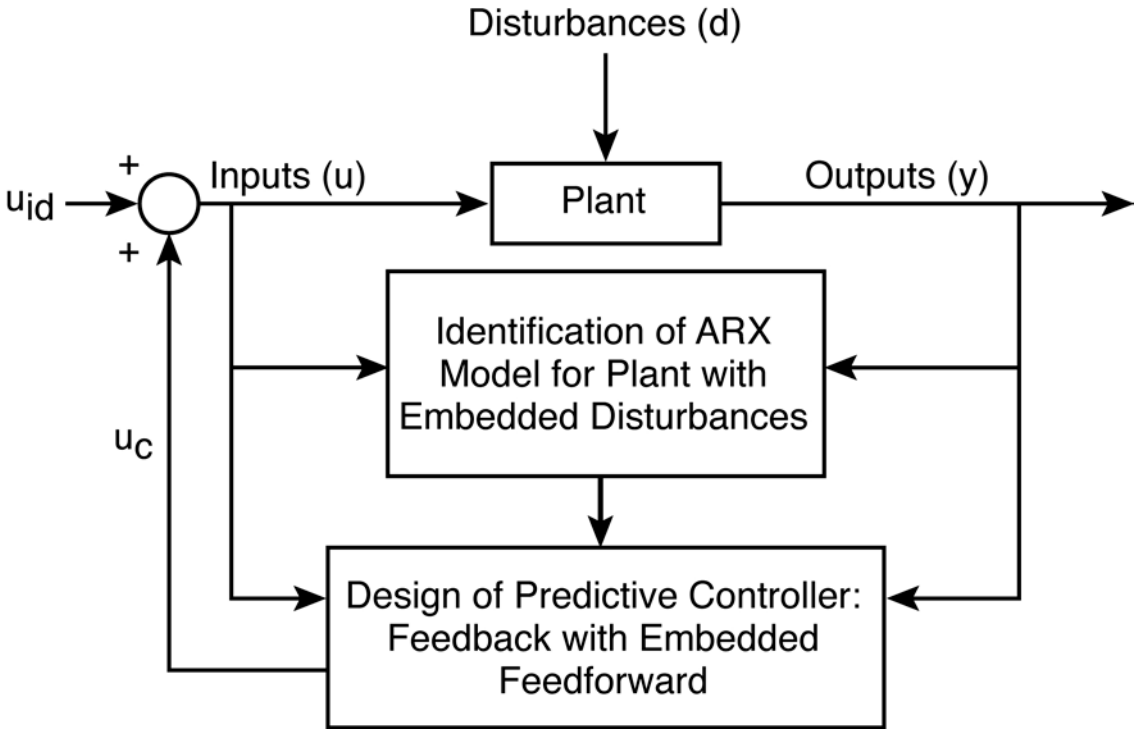


Figure 1.- Block diagram of GPC identification and control procedure.

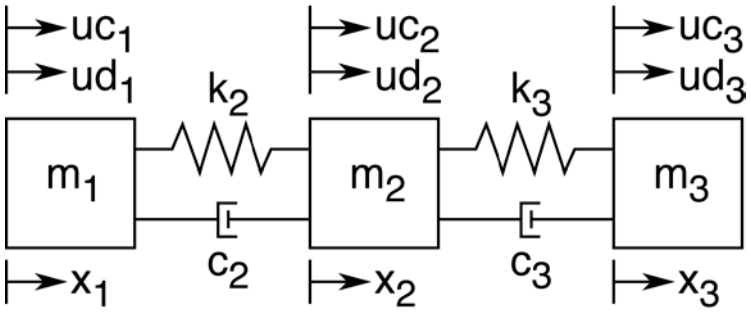


Figure 2.- Unrestrained three-degree-of-freedom mass-spring-dashpot system

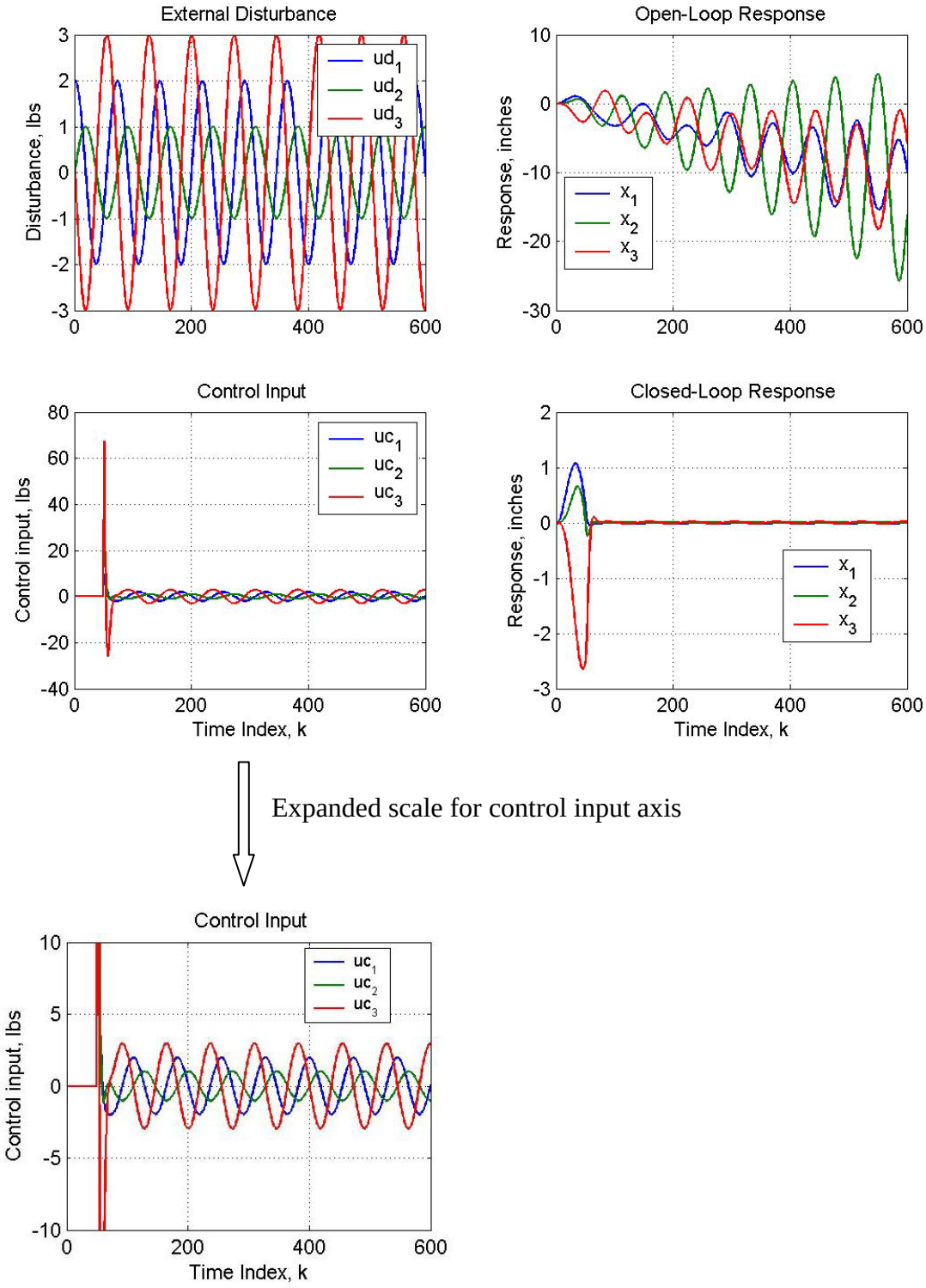


Figure 3.- Regulation of 3-DOF system subjected to three sinusoidal disturbances oscillating at 0.27566 Hz, a system natural frequency.

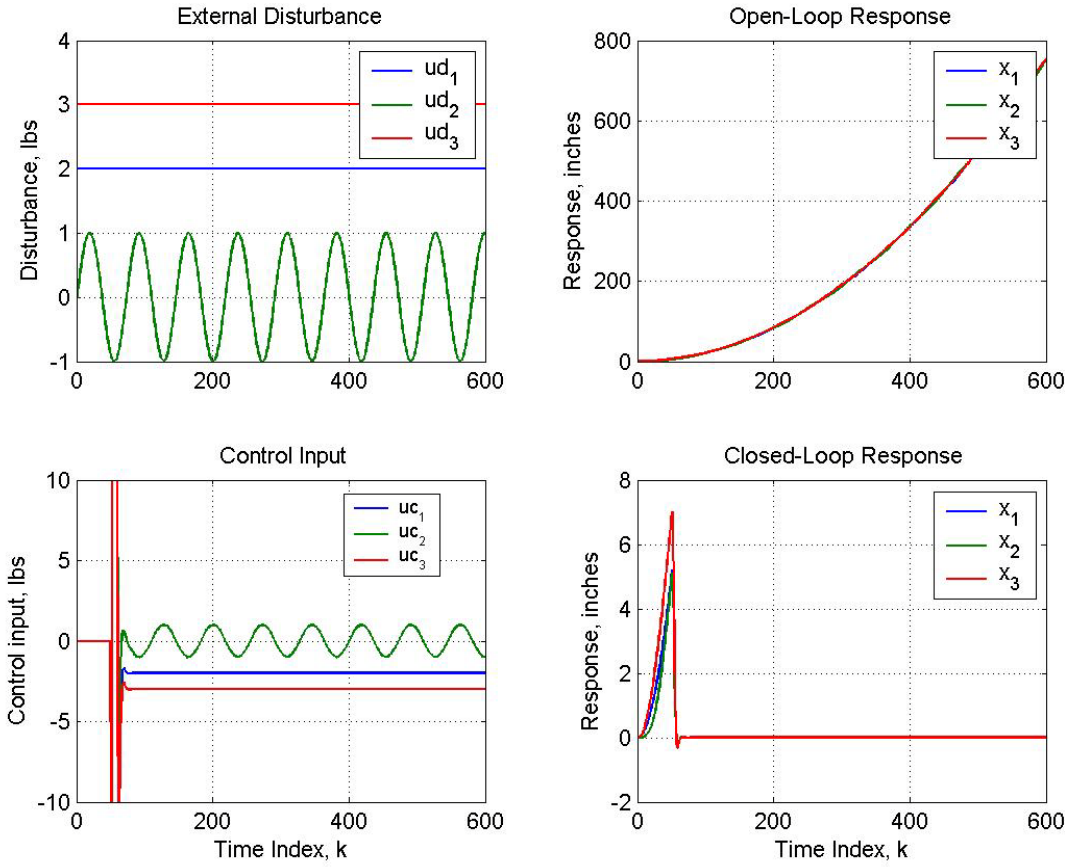


Figure 4.- Regulation of 3-DOF system subjected to a 0.27566 Hz sinusoidal disturbance acting on mass 2 and constant (zero frequency) disturbances acting on masses 1 and 3.

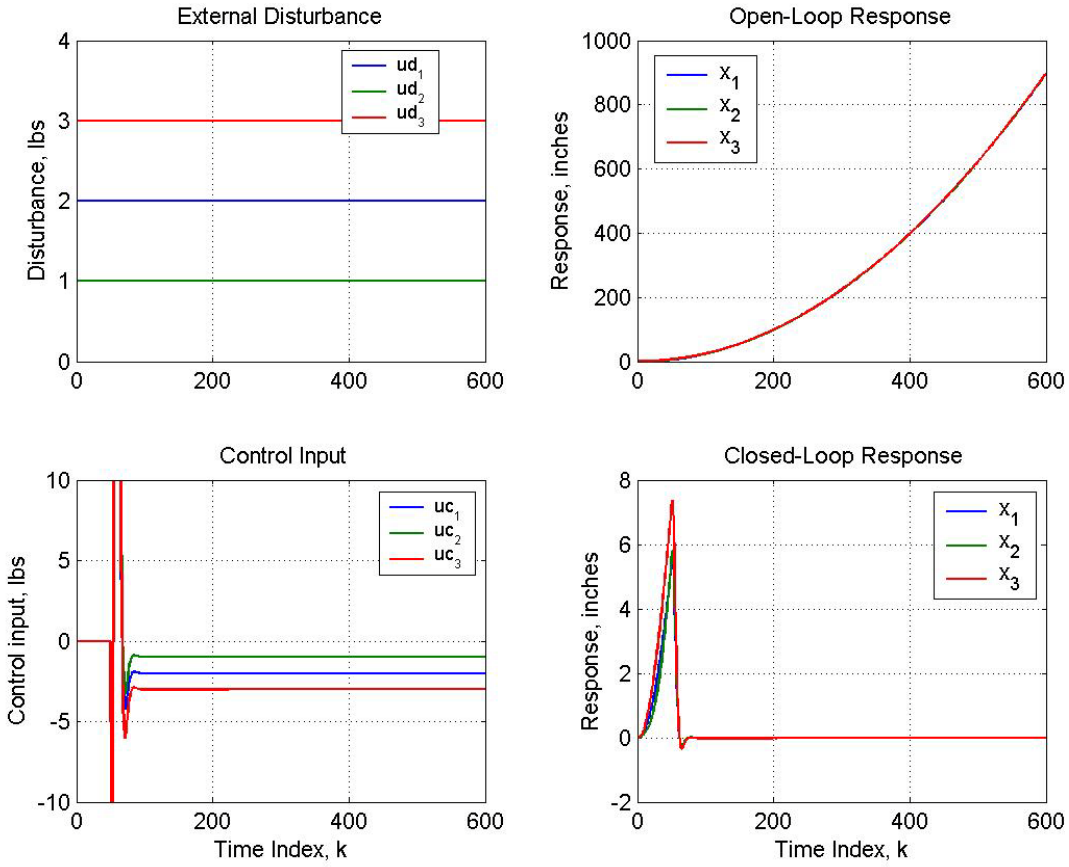


Figure 5.- Regulation of 3-DOF system subjected to a constant disturbance acting on each mass.

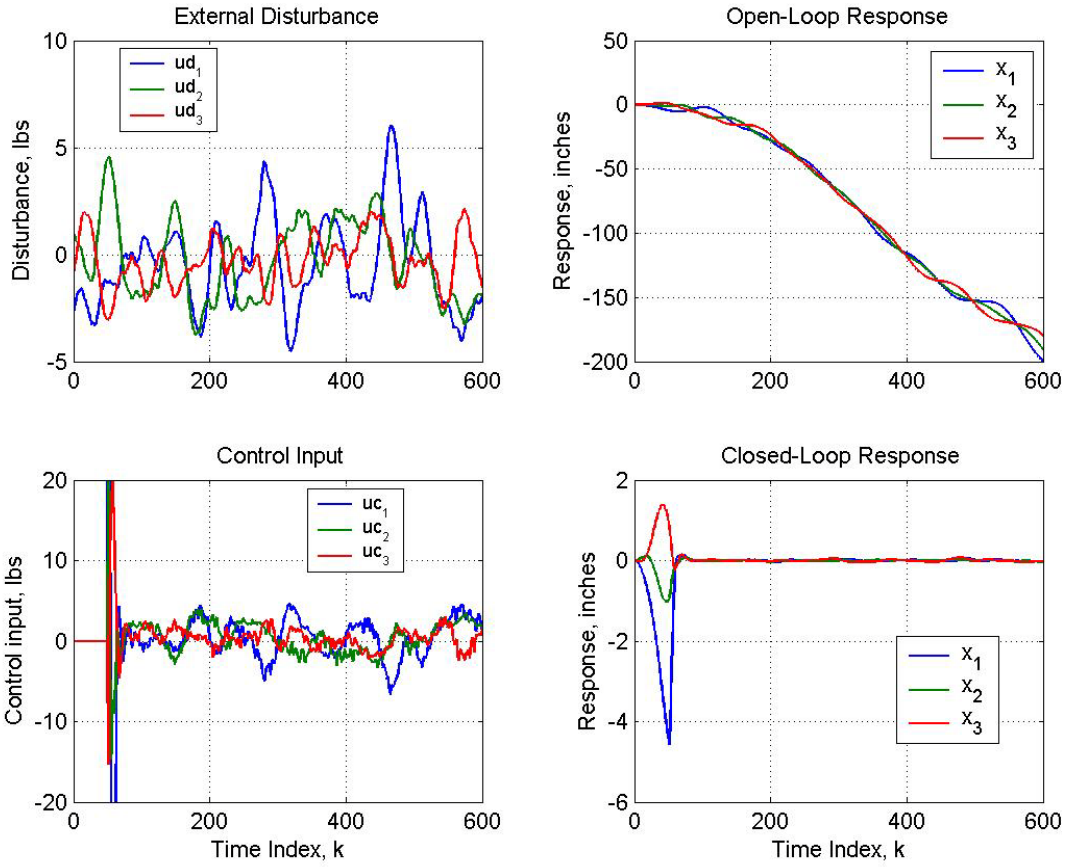


Figure 6.- Regulation of 3-DOF system subjected to a random disturbance acting on each mass.

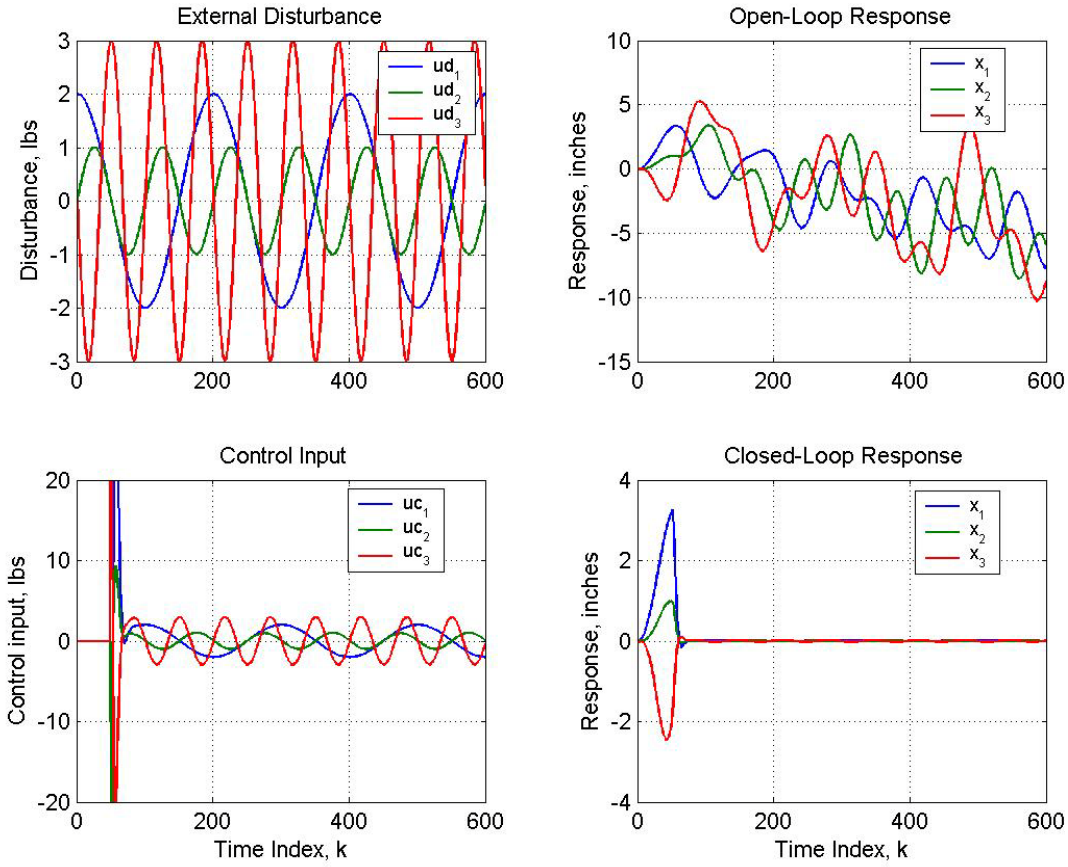


Figure 7.- Regulation of 3-DOF system subjected to sinusoidal disturbances at 0.1, 0.2, and 0.3 Hz.

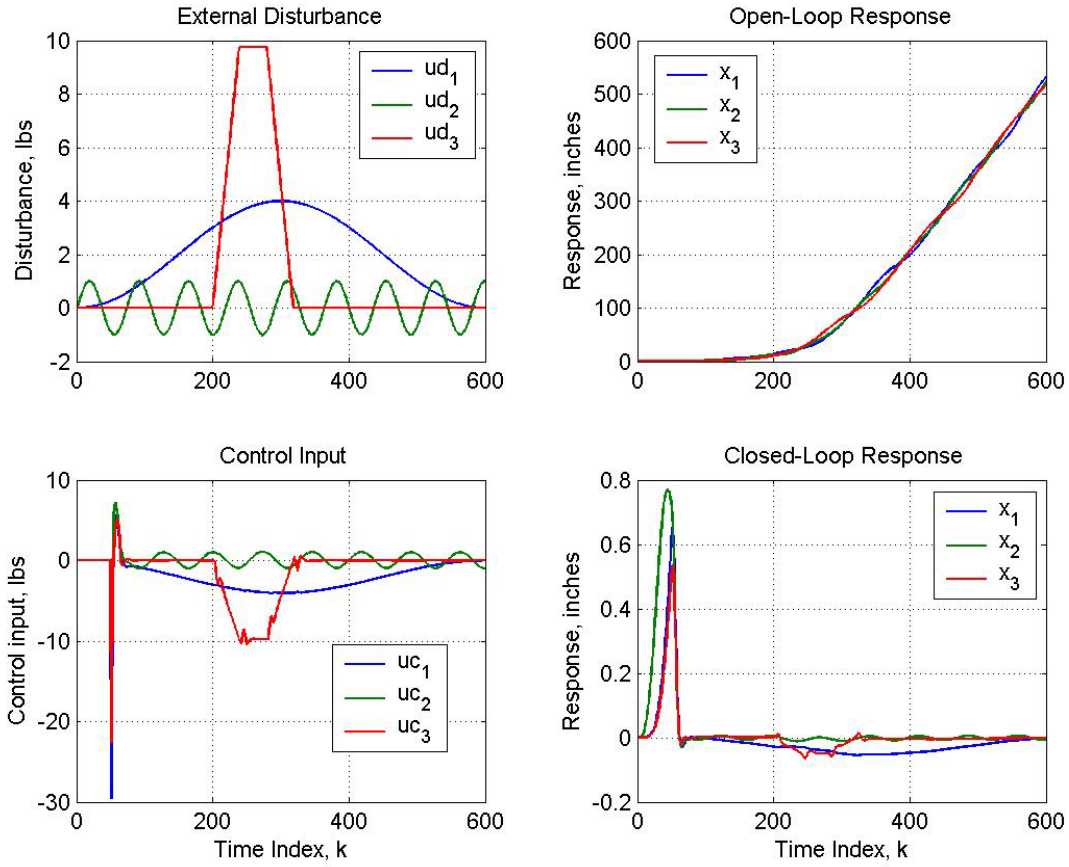


Figure 8.- Regulation of 3-DOF system with disturbances ud1 = a 1-cosine function, ud2 = a 0.27566 Hz sinusoid, and ud3 = a trapezoidal pulse.

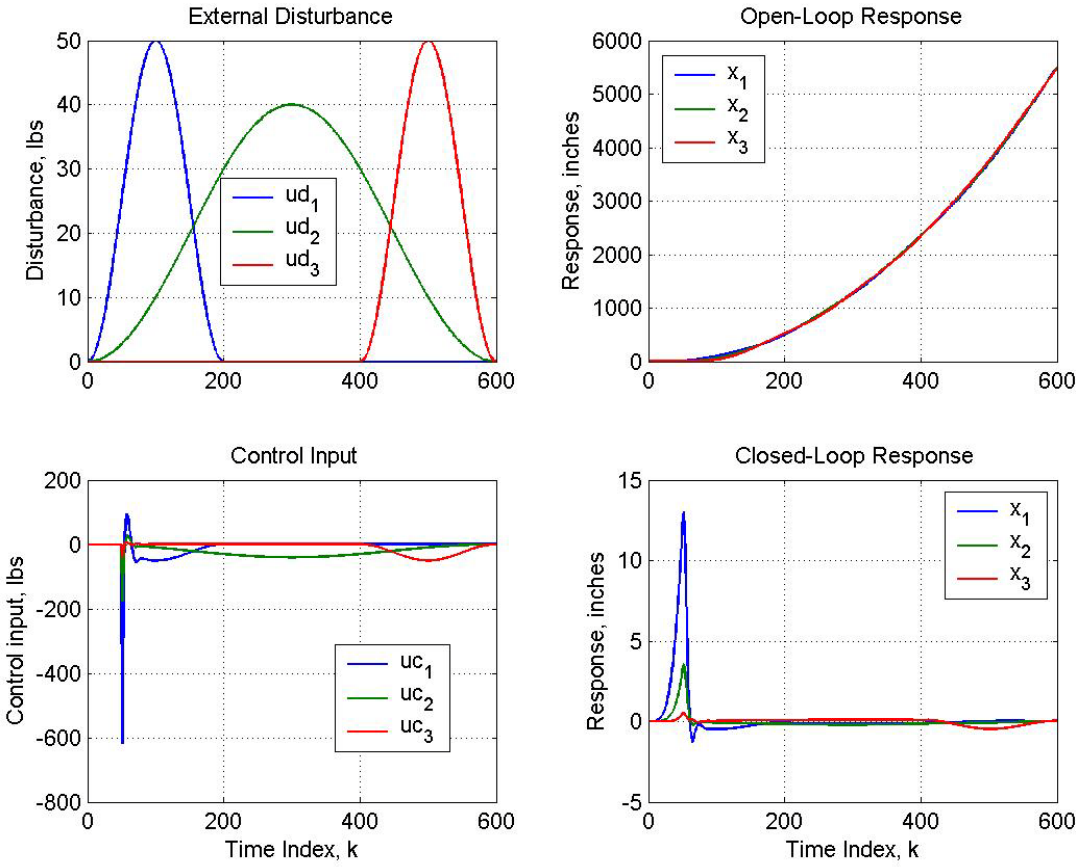


Figure 9.- Regulation of 3-DOF system subjected to 1-cosine function disturbances.

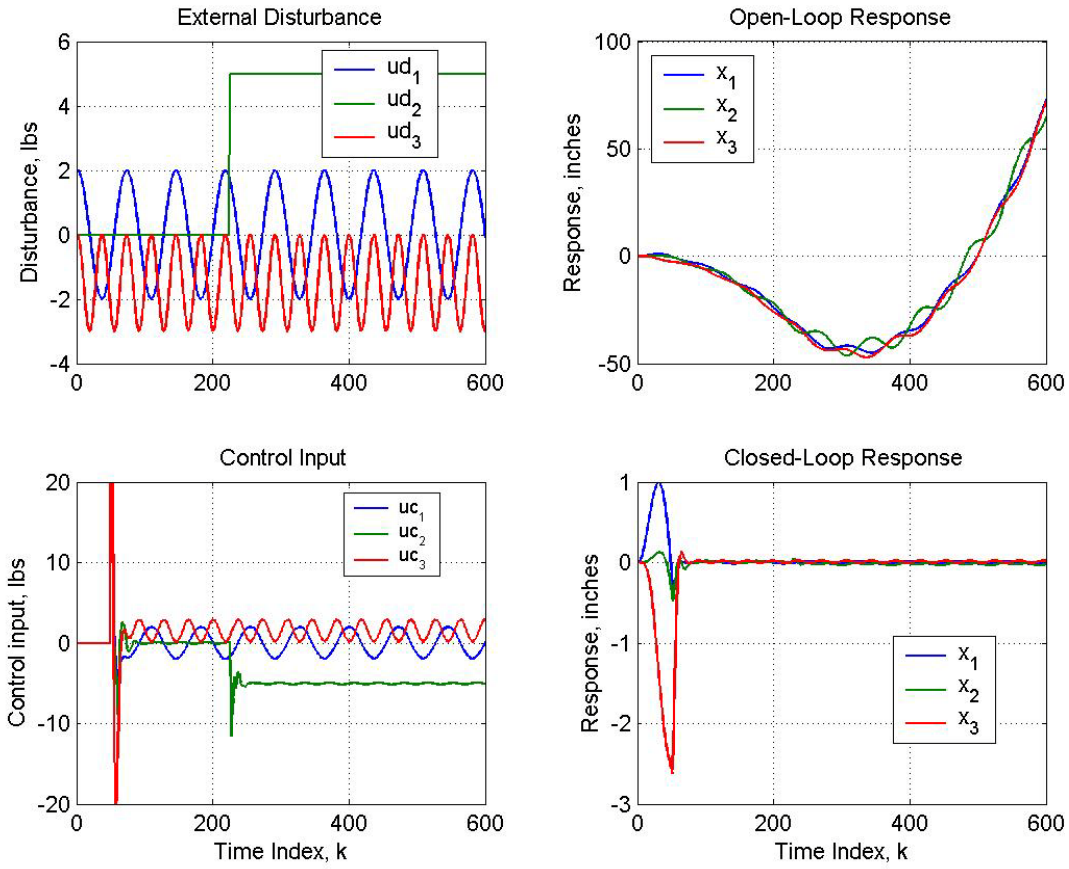


Figure 10.- Regulation of 3-DOF system with ud1 = a 0.27566 Hz sinusoid, ud2 = a step function, and ud3 = an element-by-element product of two 0.27566 Hz sine waves.

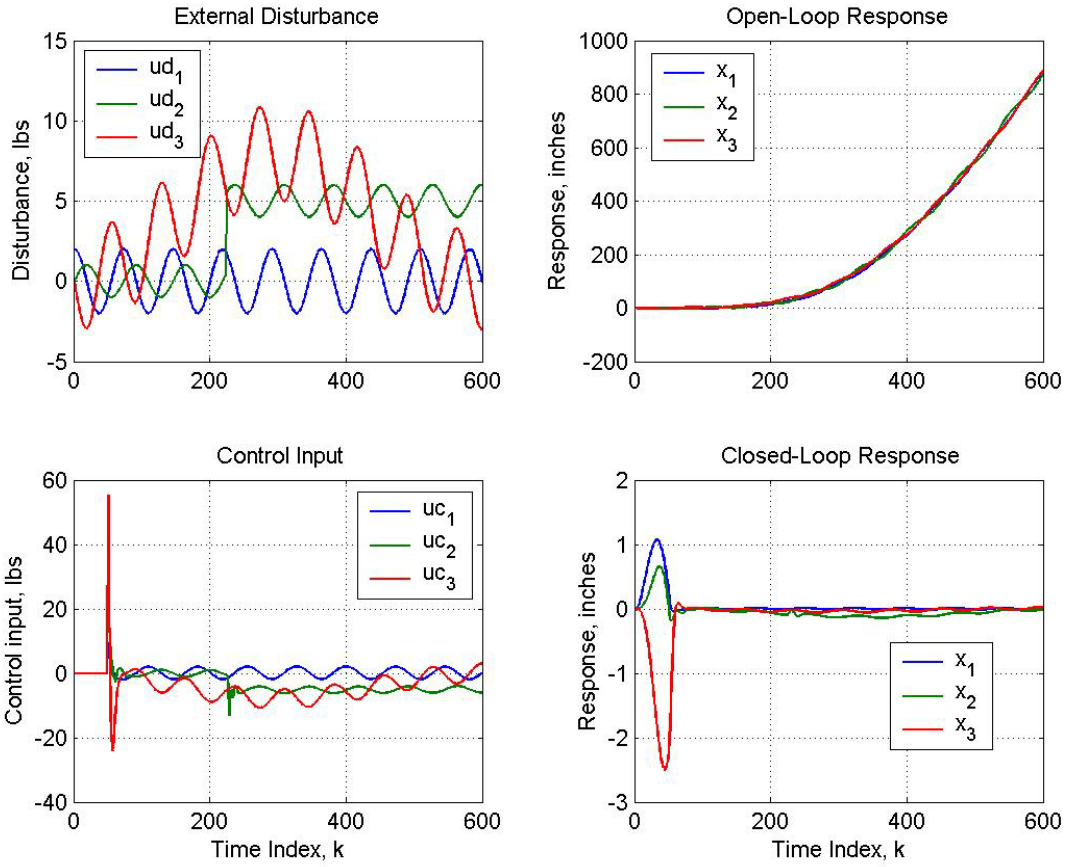


Figure 11.- Regulation of 3-DOF system subjected to three 0.27566 Hz sinusoidal disturbances, two of which are superimposed on 1-cosine and step waveforms.

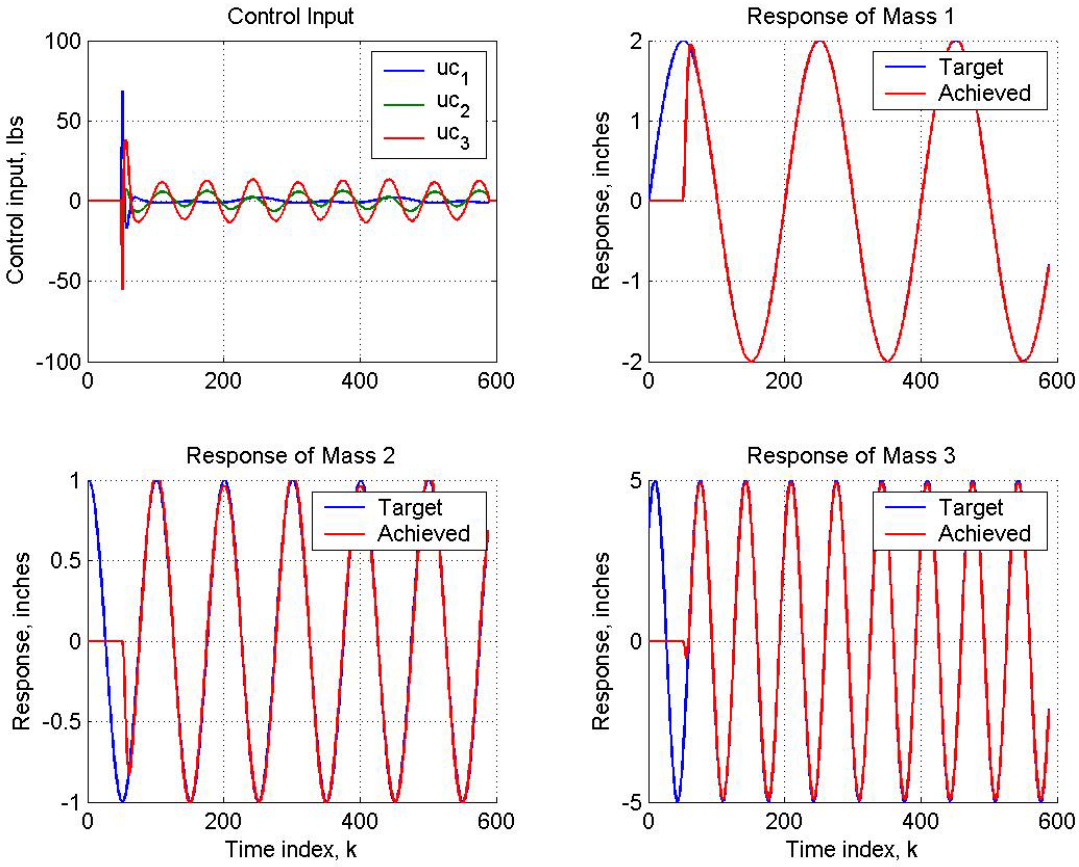


Figure 12.- Tracking of undisturbed 3-DOF system with sinusoidal target responses having frequencies of 0.1, 0.2, and 0.3 Hz.

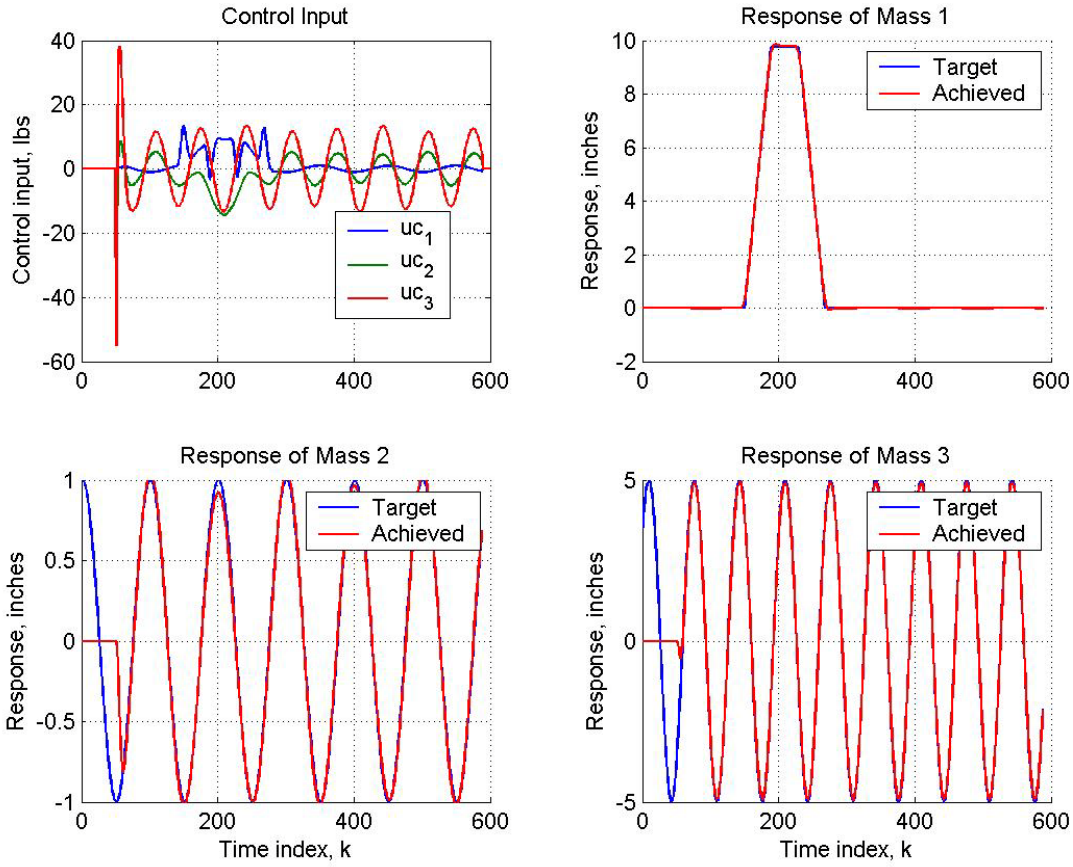


Figure 13.- Tracking of undisturbed 3-DOF system with target responses yt1 = a trapezoidal pulse, yt2 = a 0.2 Hz sinusoid, and yt3 = a 0.3 Hz sinusoid.

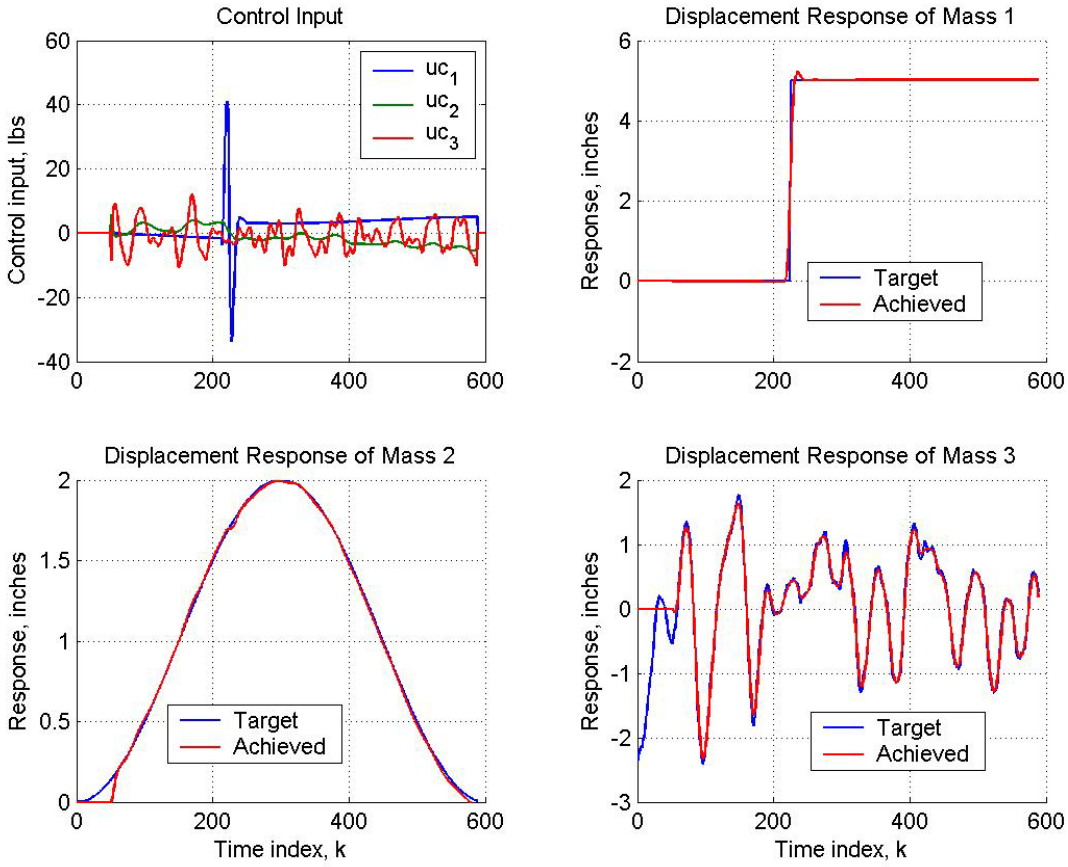


Figure 14.- Tracking of undisturbed 3-DOF system with target responses yt1 = a one-step step function, yt2 = a 1-cosine function, and yt3 = a random function.

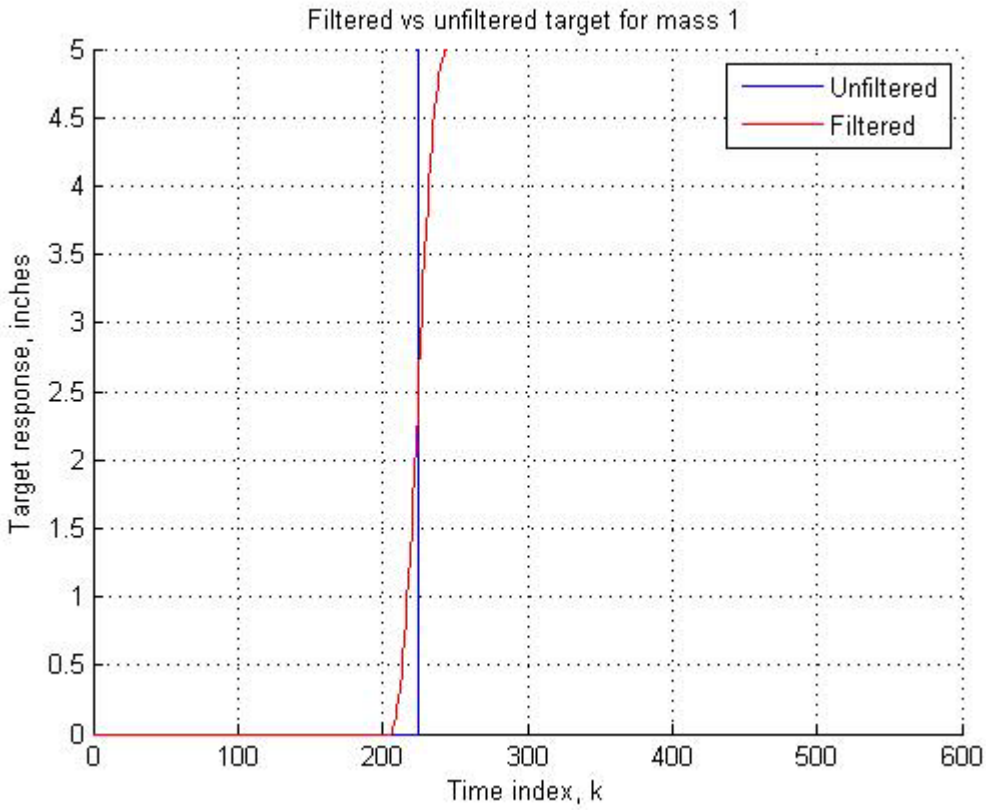


Figure 15.- Comparison of filtered and unfiltered step function targets for mass 1 of undisturbed 3-DOF system.

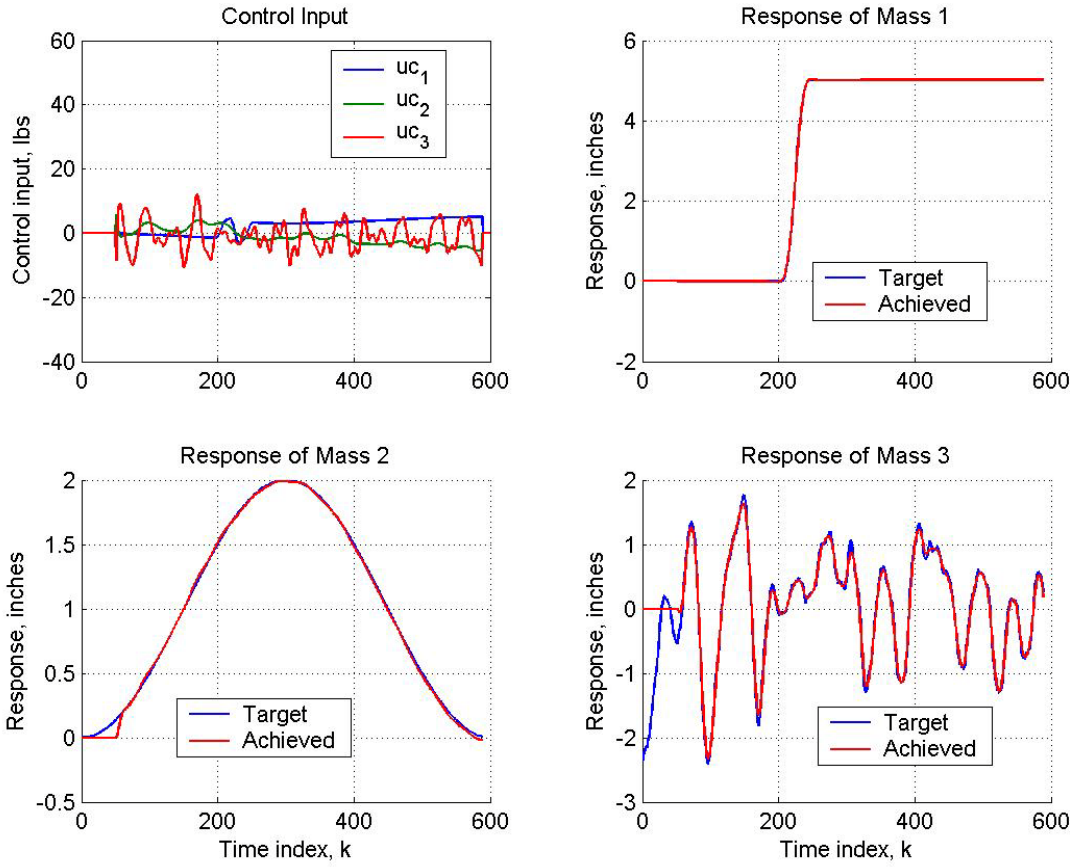


Figure 16.- Tracking of undisturbed 3-DOF system of figure 14 but using the filtered target of figure 15 for mass 1.

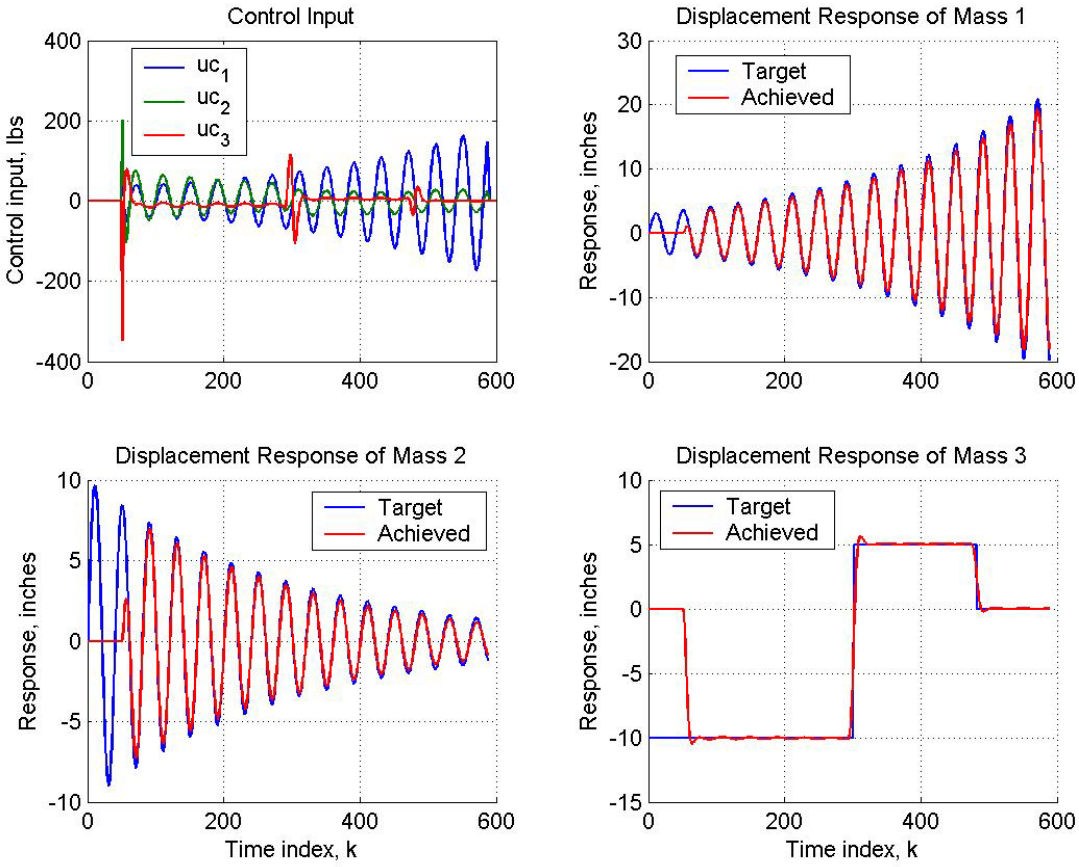


Figure 17.- Tracking of undisturbed 3-DOF system with yt1 = an exponentially diverging 0.5 Hz sinusoid, yt2 = an exponentially converging 0.5 Hz sinusoid, and yt3 = a multi-step step function.

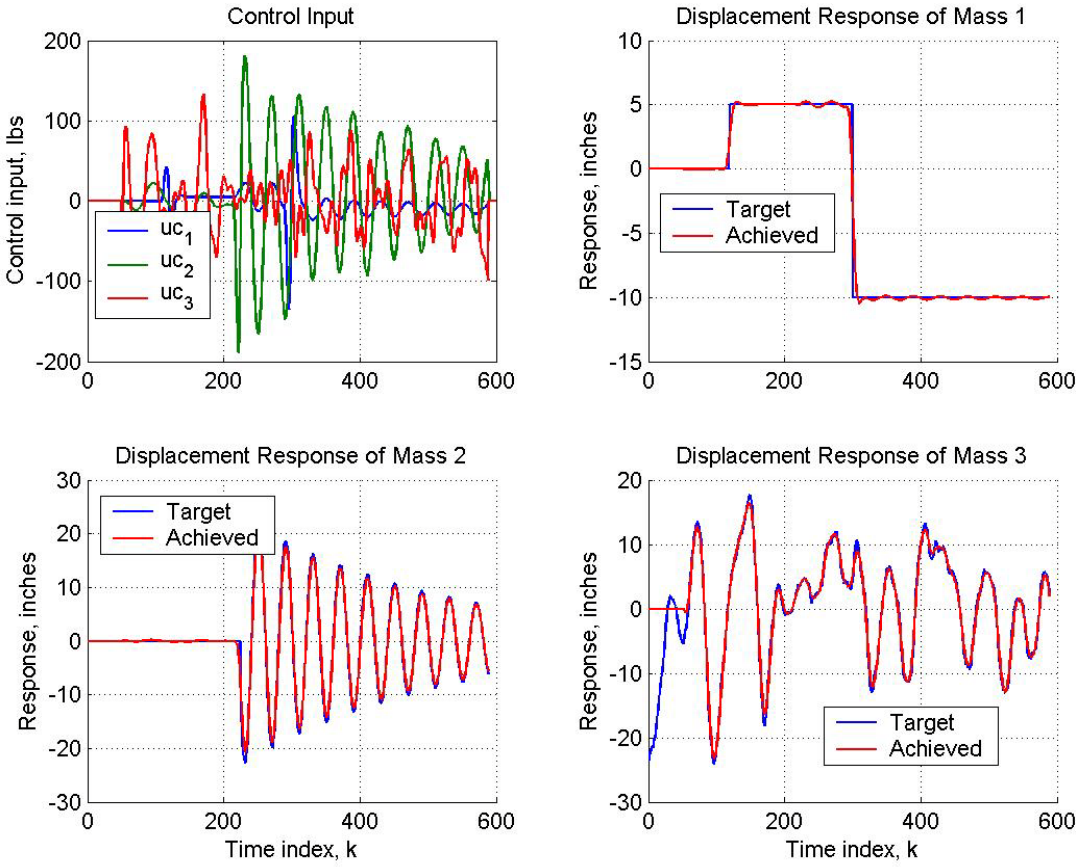


Figure 18.- Tracking of undisturbed 3-DOF system with yt1 = a two-step step function, yt2 = a delayed exponentially converging 0.5 Hz sinusoid, and yt3 = a random function.

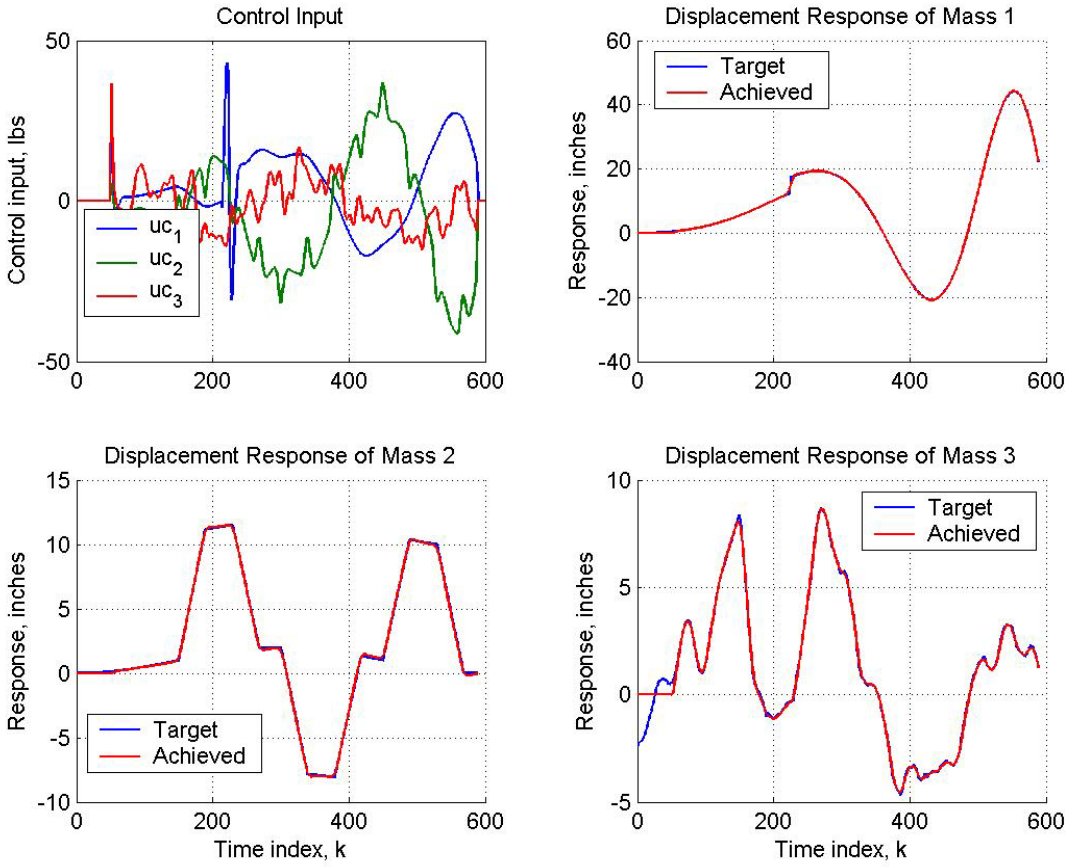


Figure 19.- Tracking of undisturbed 3-DOF system with yt1 = a diverging increasing-frequency sinusoid with a small offset, yt2 = a multi-toothed 1-cosine waveform, and yt3 = a random waveform contaminated by two other waveforms.

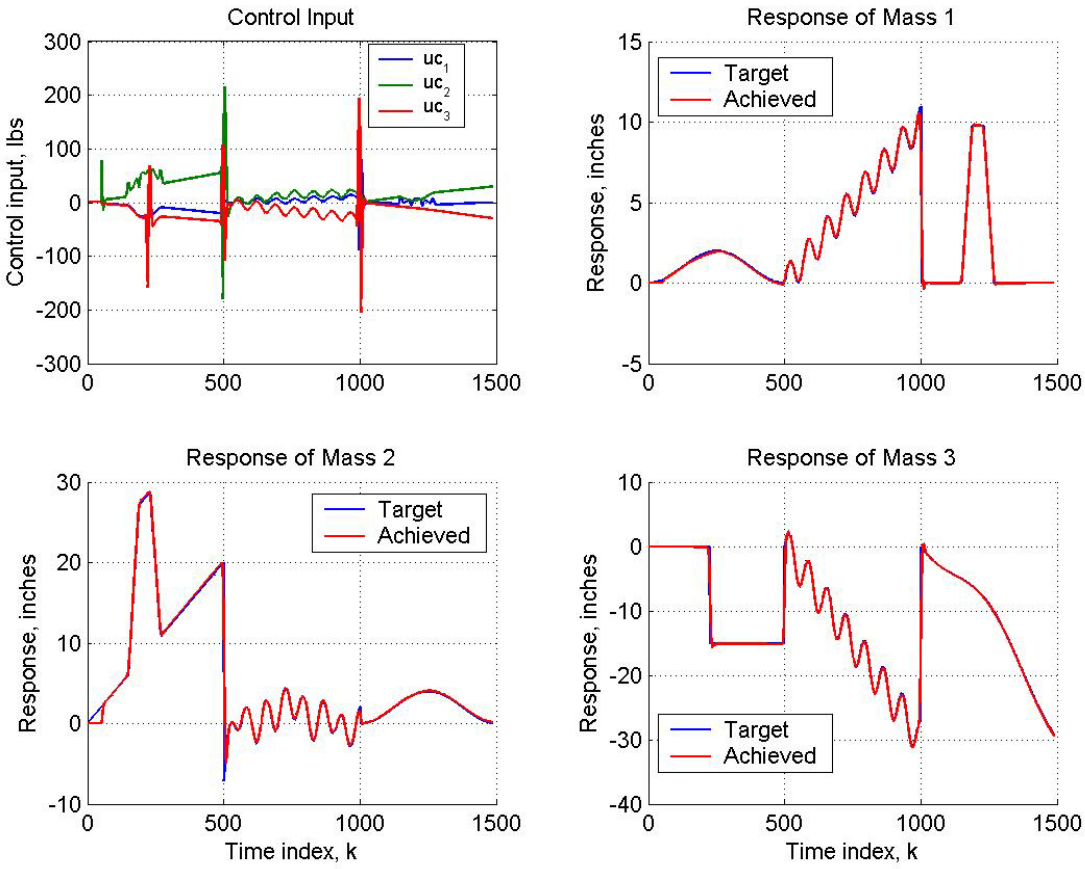


Figure 20.- Tracking of undisturbed 3-DOF system with 1500-point target time histories composed of three 500-point segments having different waveforms.

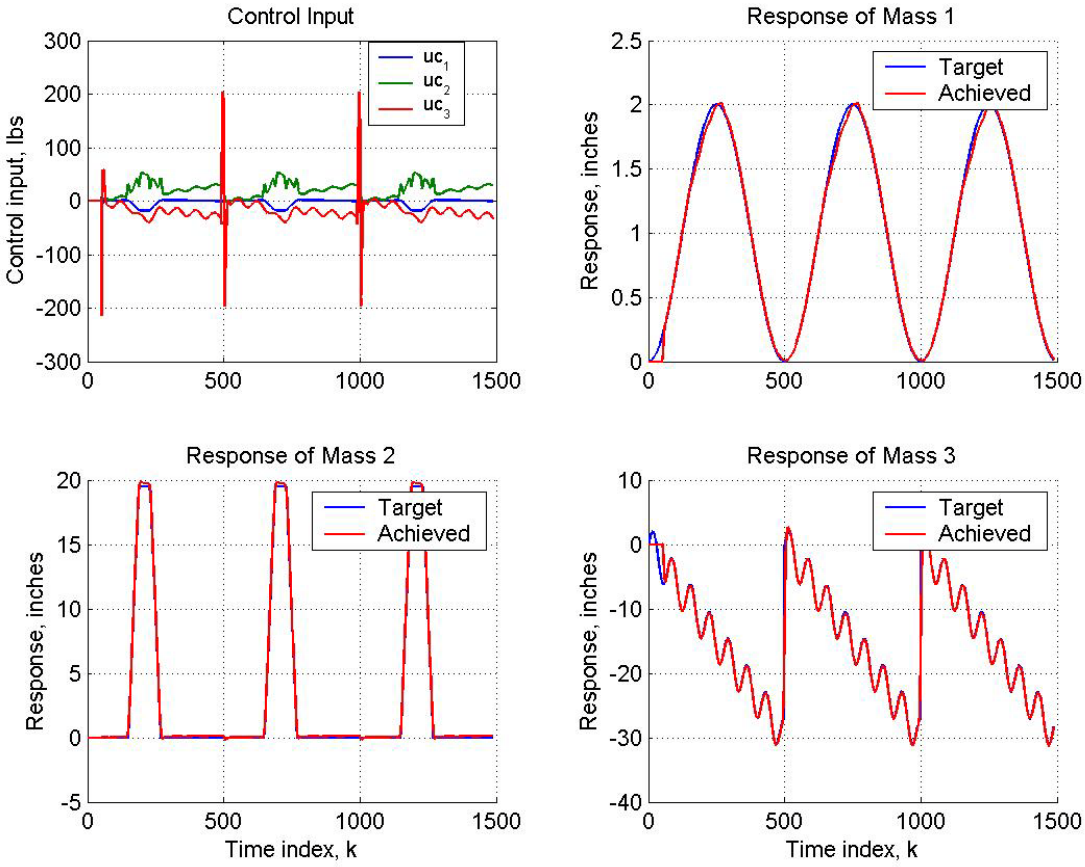


Figure 21.- Tracking of undisturbed 3-DOF system with 1500-point target time histories composed of three 500-point segments having different waveforms.

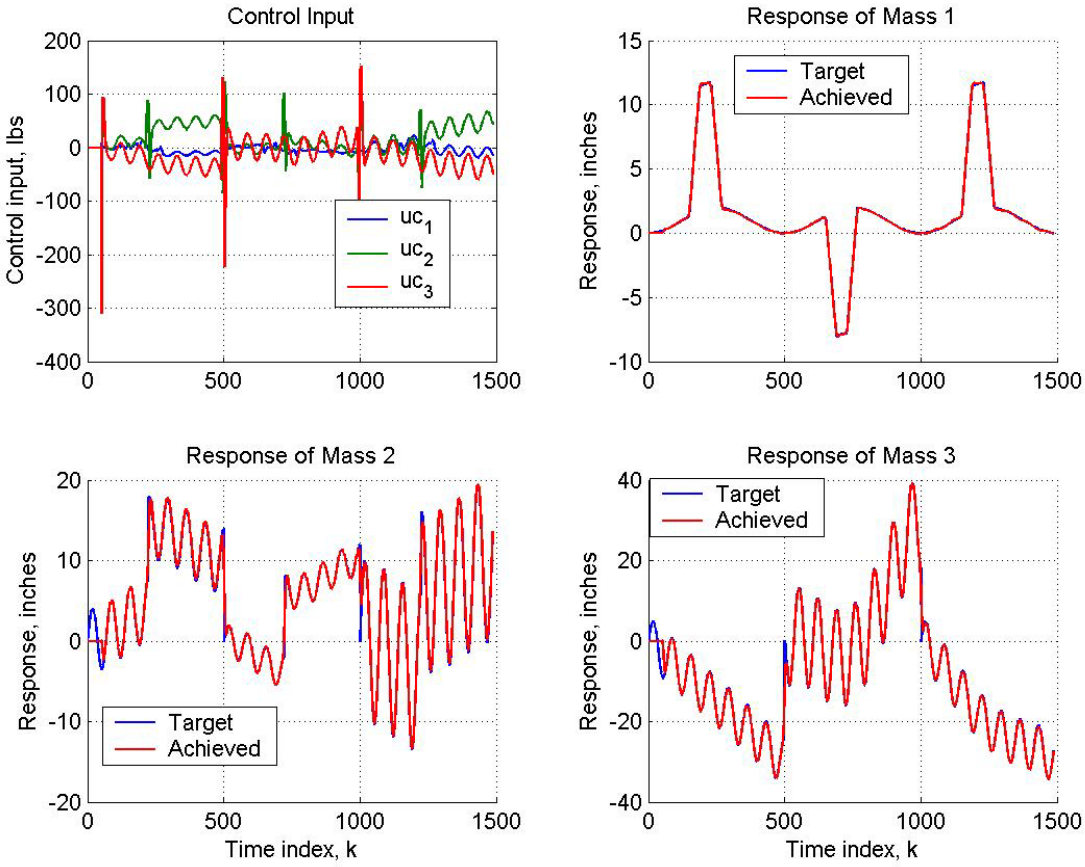


Figure 22.- Tracking of undisturbed 3-DOF system with 1500-point target time histories composed of three 500-point segments having different waveforms.

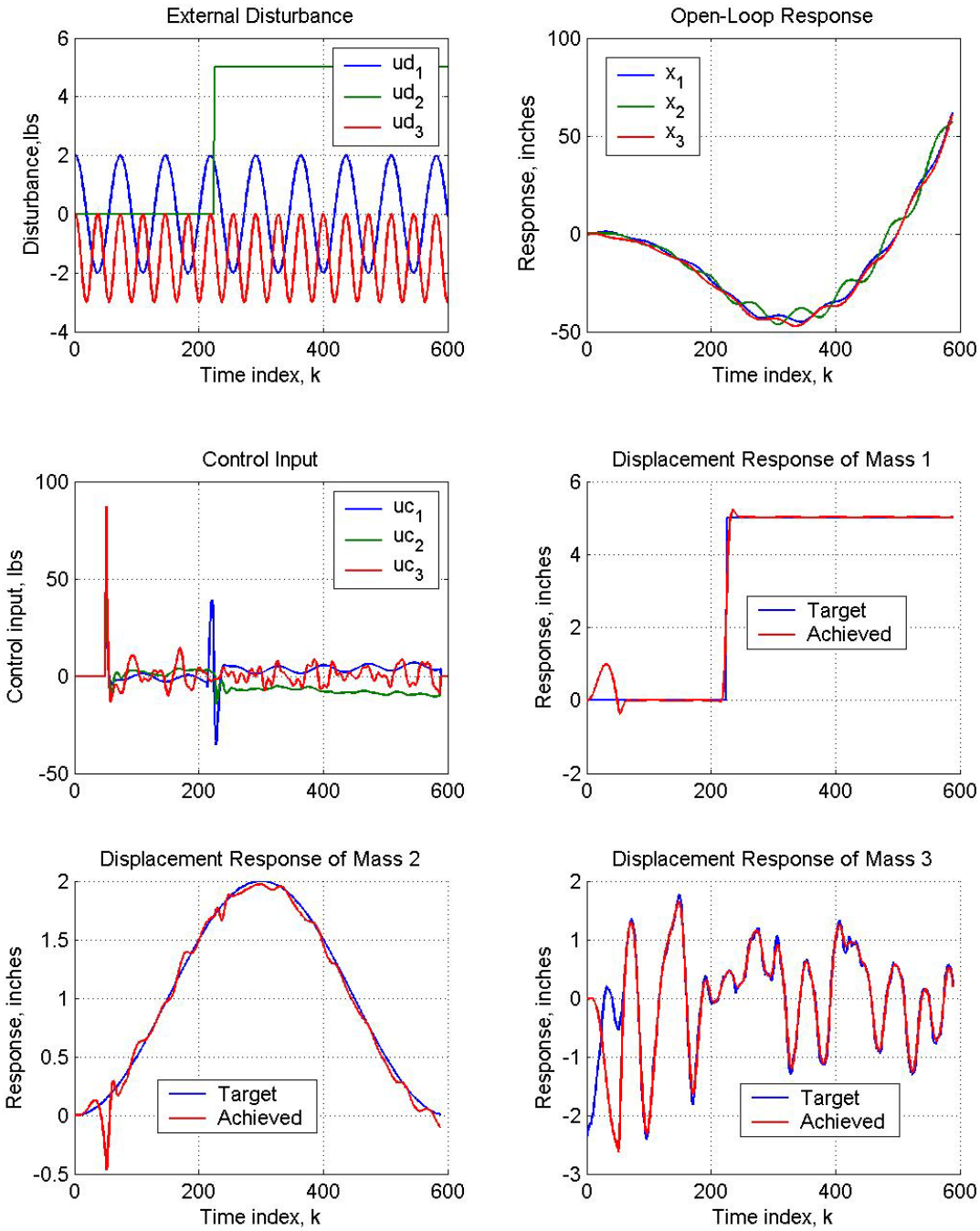


Figure 23.- Tracking of disturbed 3-DOF system wherein a variety of waveforms are used for the disturbances and targets.

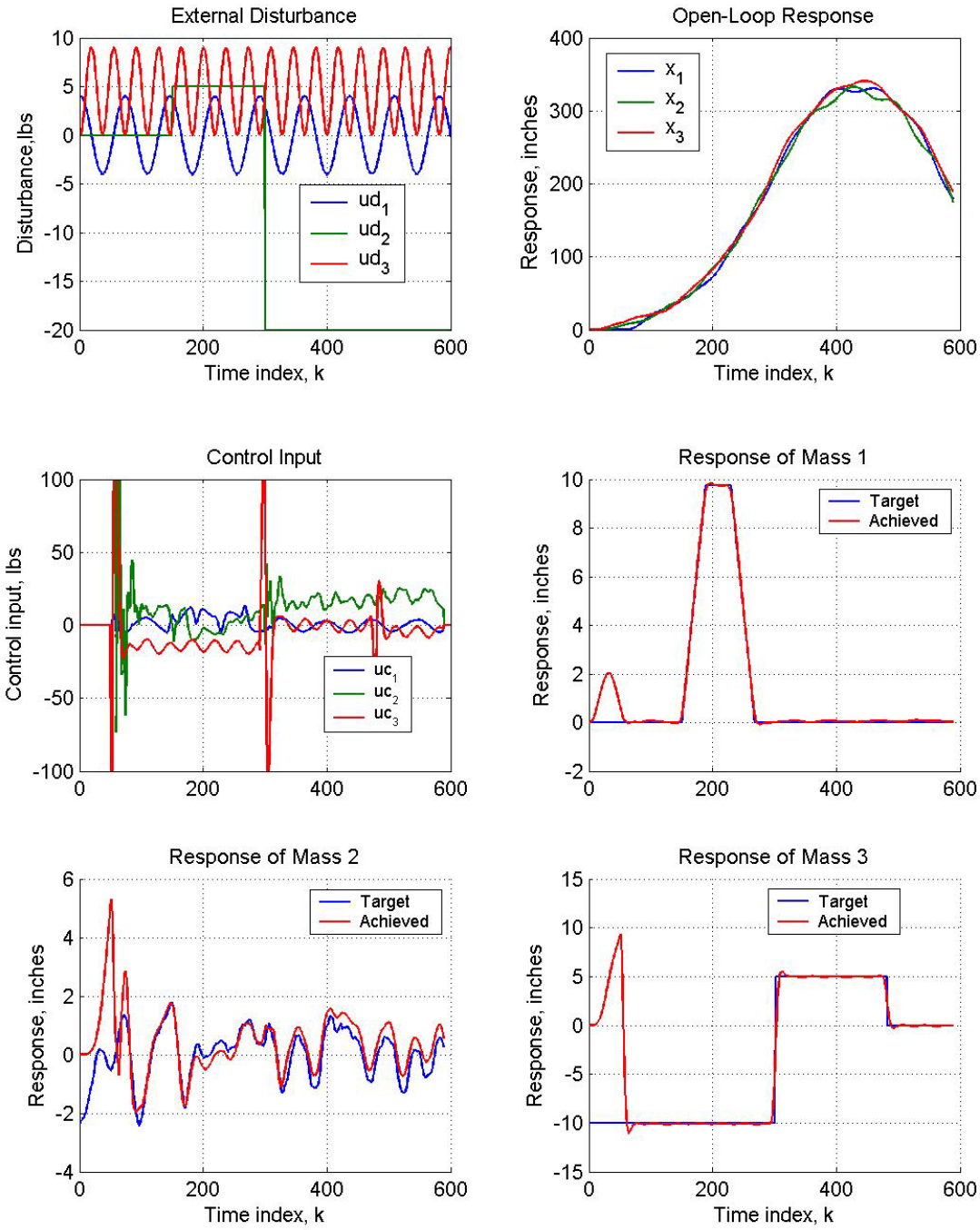


Figure 24.- Tracking of disturbed 3-DOF system in which a variety of waveforms are used for the disturbances and targets.

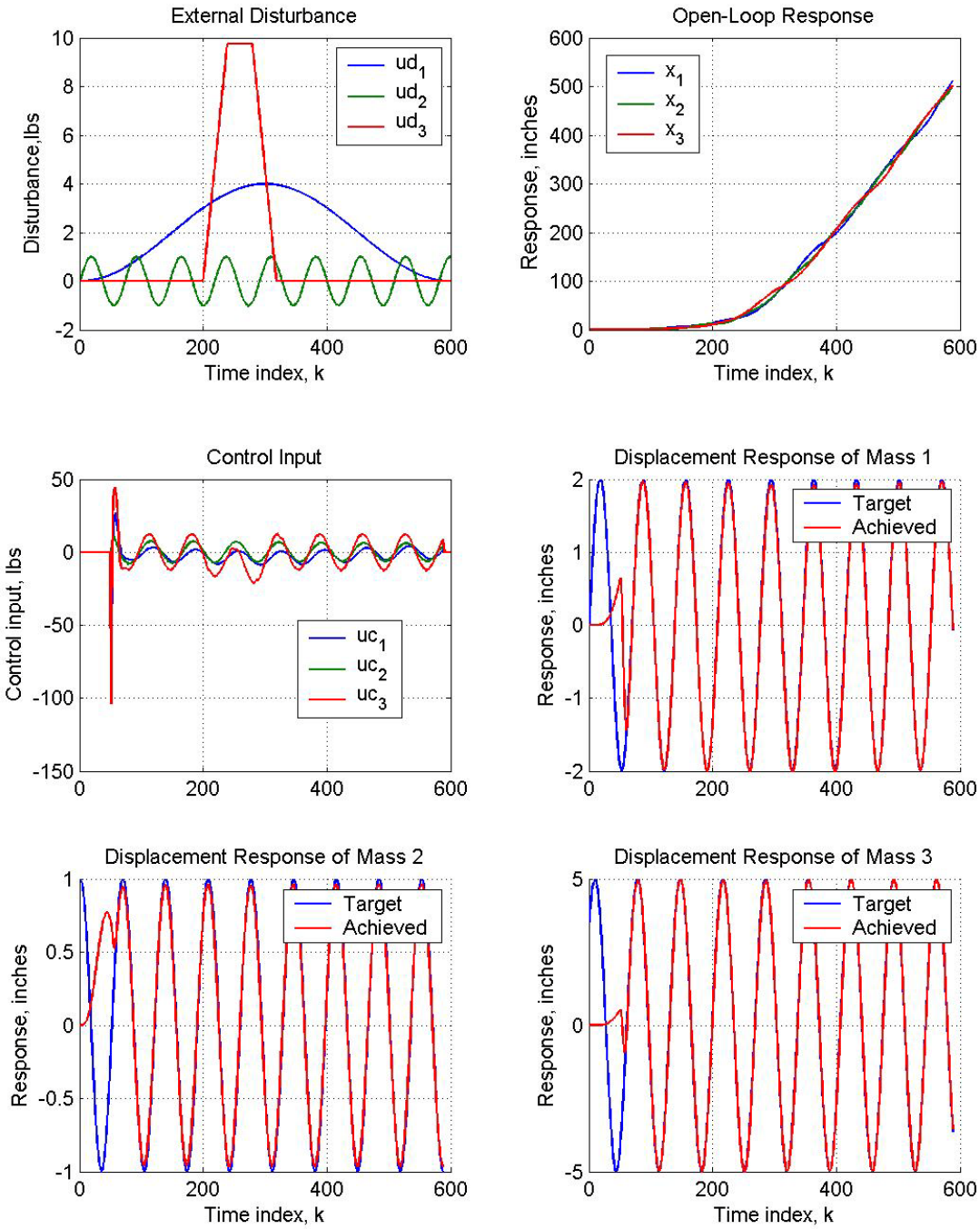


Figure 25.- Tracking of disturbed 3-DOF system where ud1 = a 1-cosine function, ud2 = a 0.27566 Hz sinusoid, ud3 =a trapezoidal pulse, and the targets are 0.27566 Hz sinusoids.

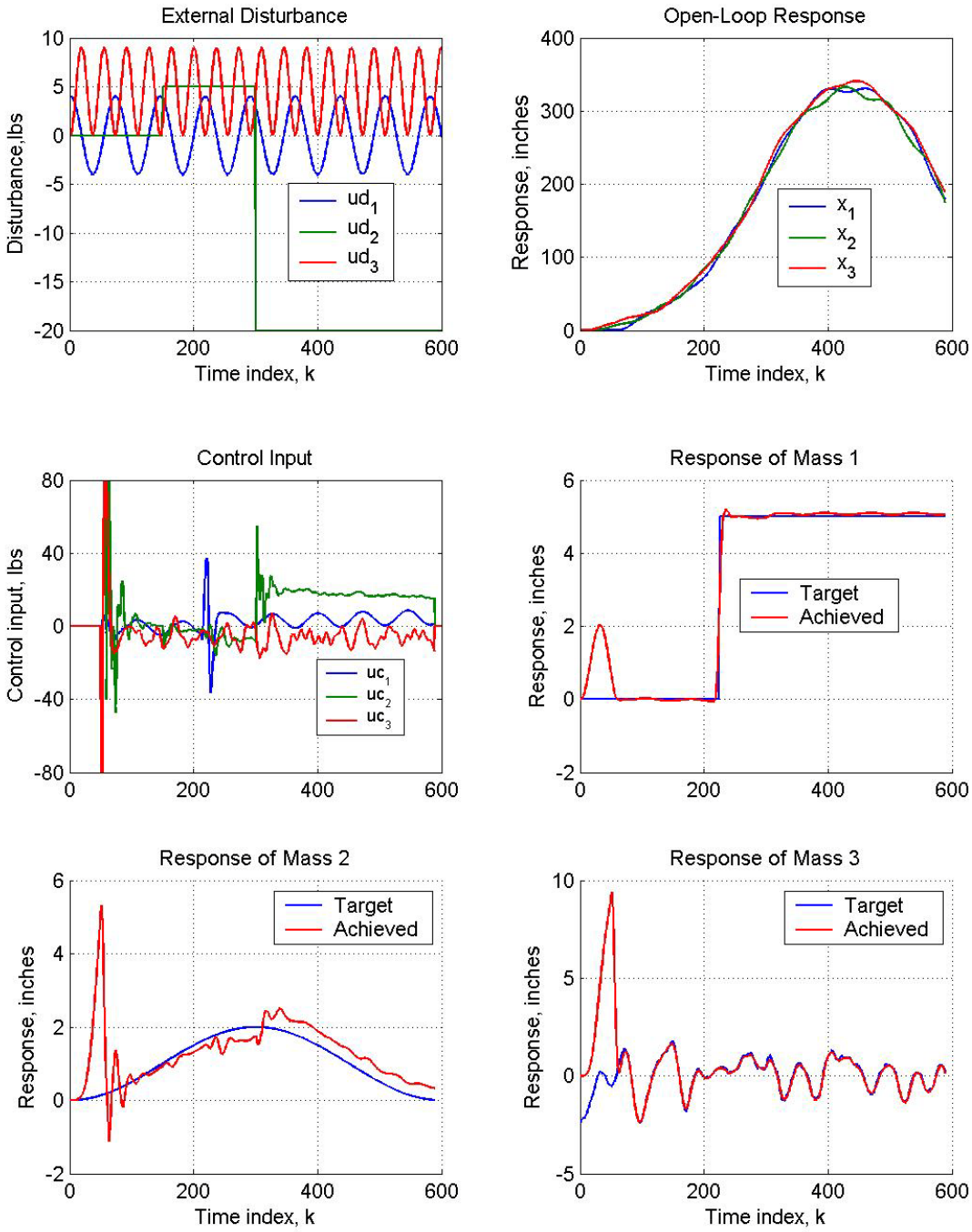


Figure 26.- Tracking of disturbed 3-DOF system in which a variety of waveforms are used for the disturbances and targets.


Figure 27.- XV-15 tiltrotor research aircraft in airplane mode of flight.

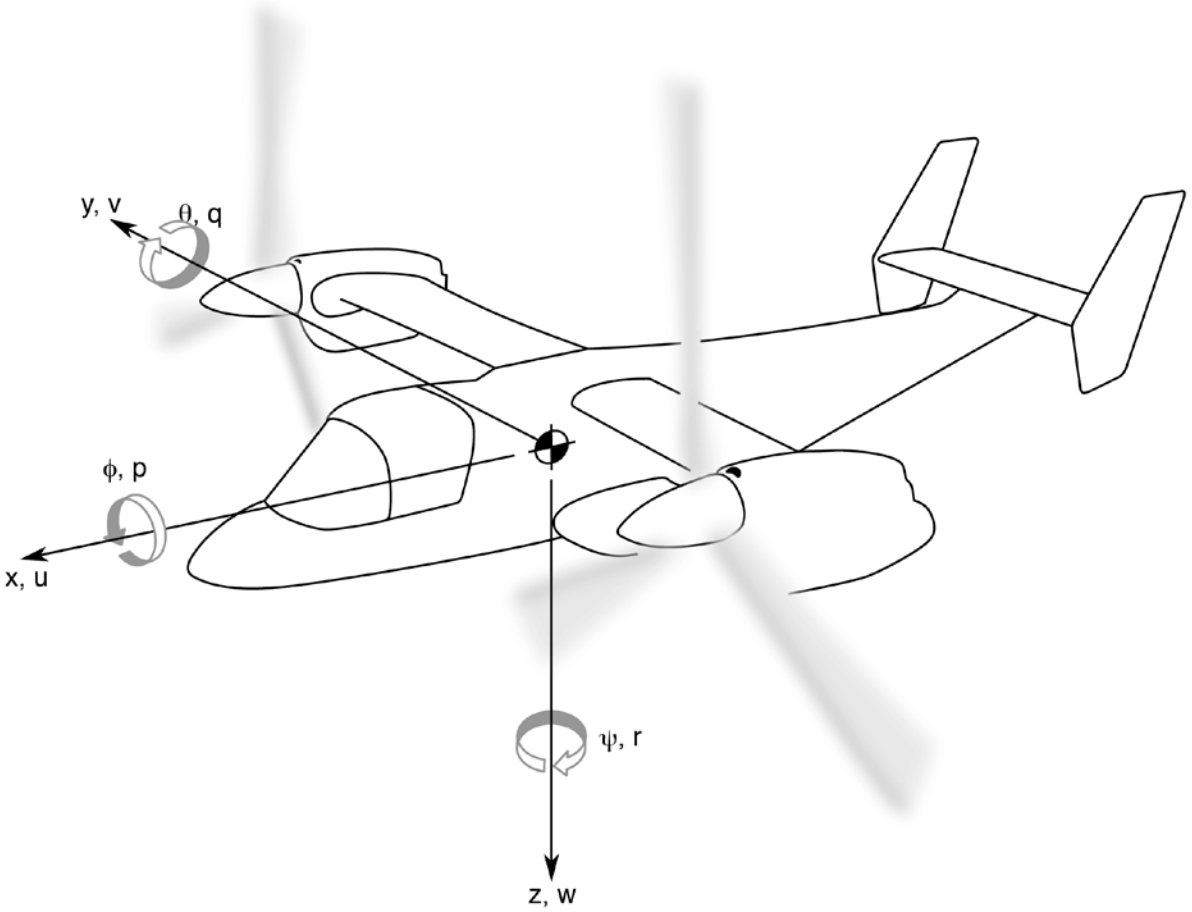


Figure 28.- Perturbation displacements (x, y, z), rotations (θ, φ, ψ), and velocities (u, v, w, p, q, r) comprising the state variables used to form the rigid-body state-space equations of the XV-15.

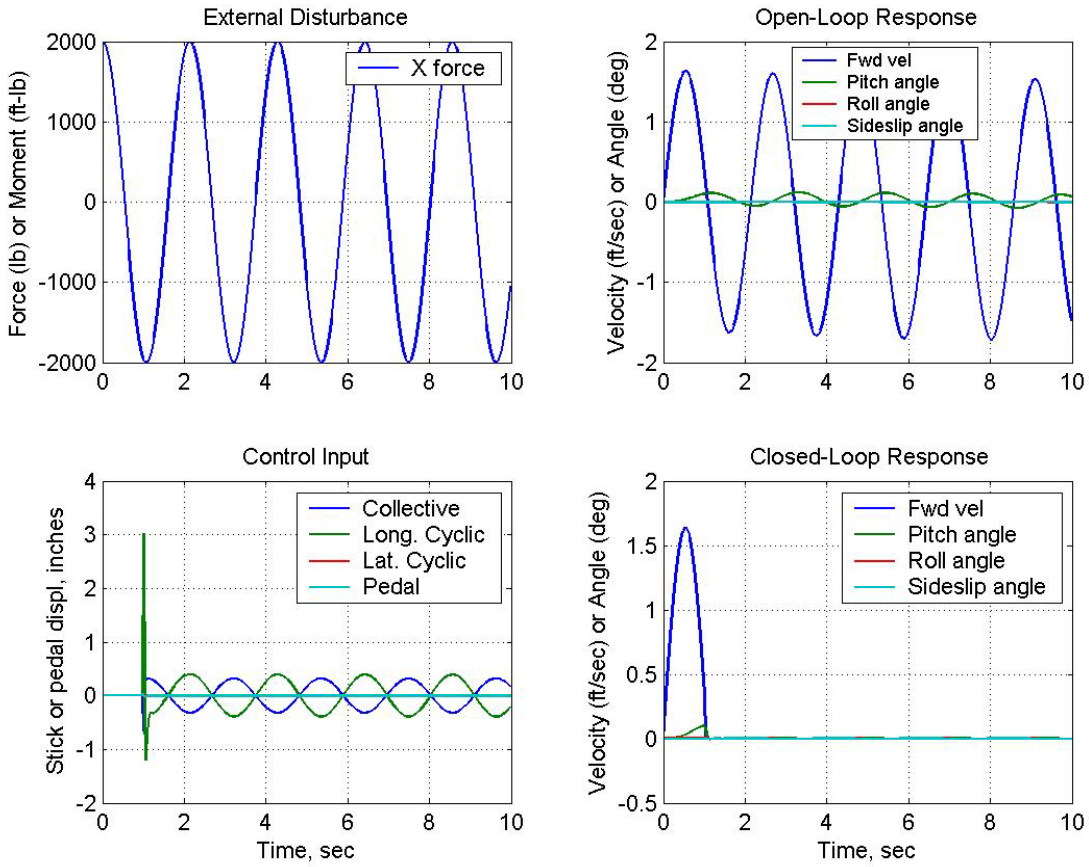


Figure 29.- Regulation of XV-15 subjected to a sinusoidal axial force disturbance at 0.46734 Hz.

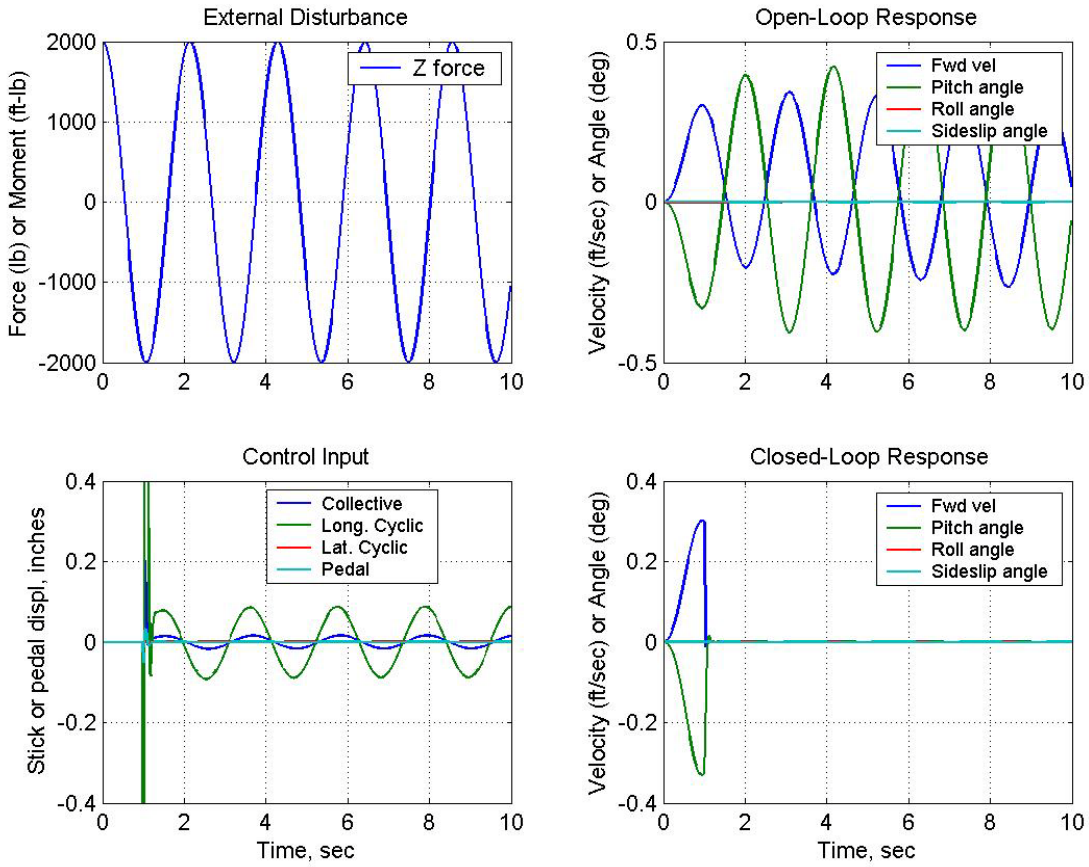


Figure 30.- Regulation of XV-15 subjected to a sinusoidal vertical force disturbance at 0.46734 Hz.

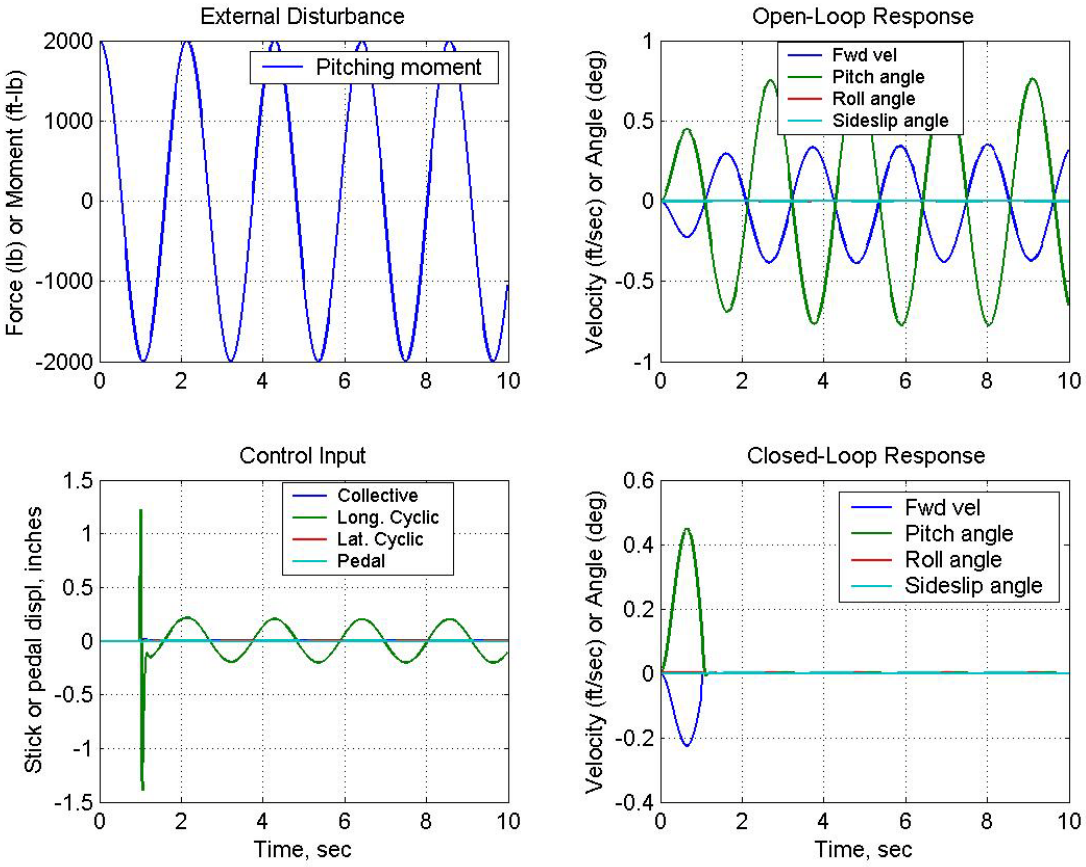


Figure 31.- Regulation of XV-15 subjected to a sinusoidal pitching moment disturbance at 0.46734 Hz.

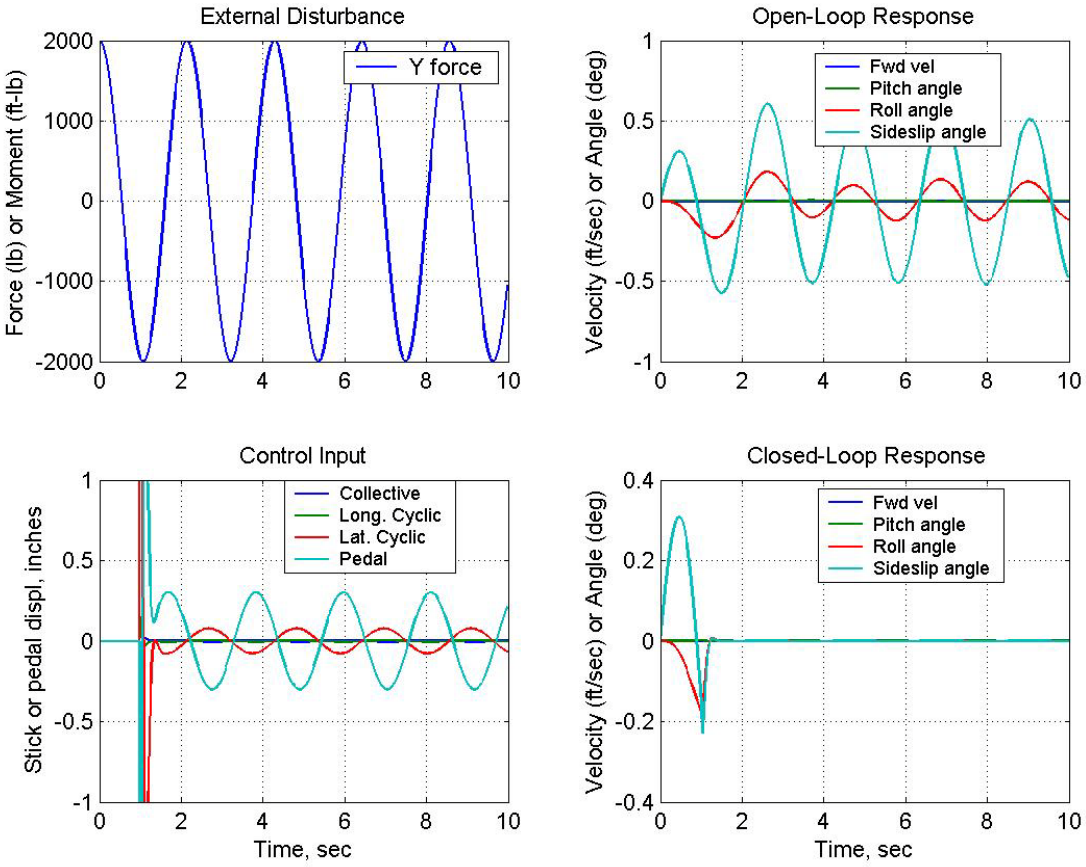


Figure 32.- Regulation of XV-15 subjected to a sinusoidal side force disturbance at 0.46734 Hz.

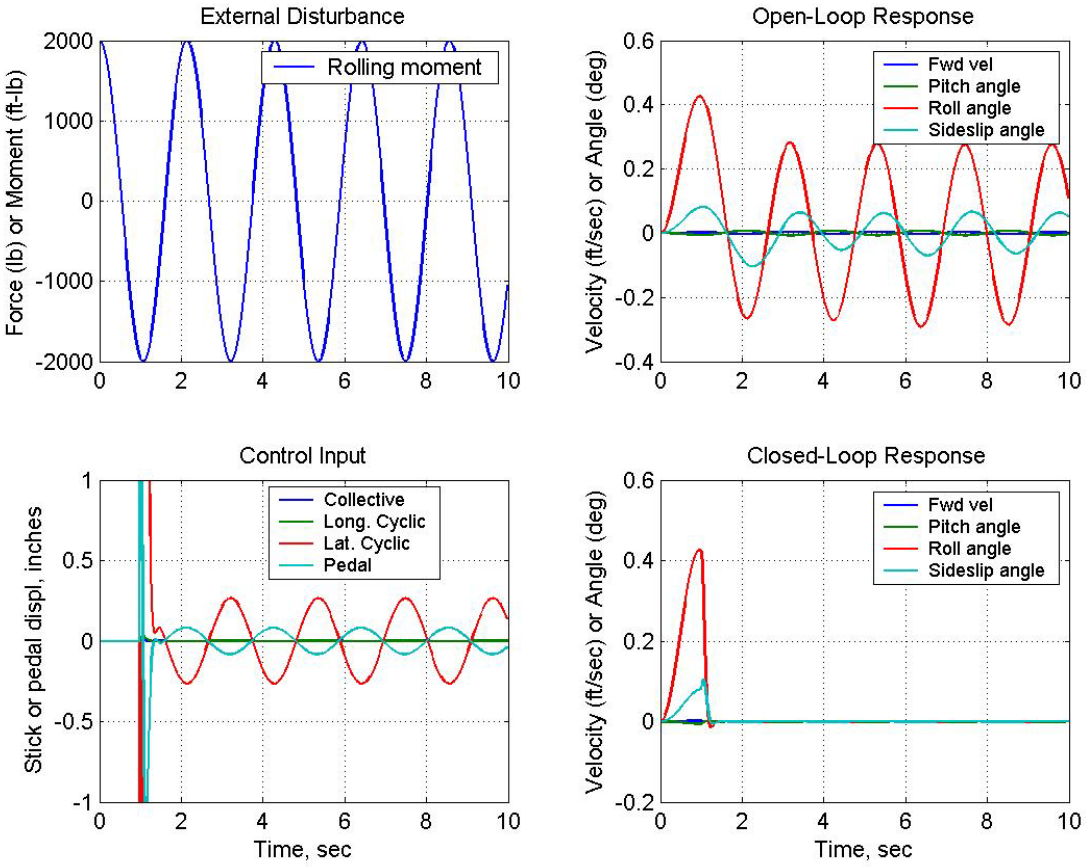


Figure 33.- Regulation of XV-15 subjected to a sinusoidal rolling moment disturbance at 0.46734 Hz.

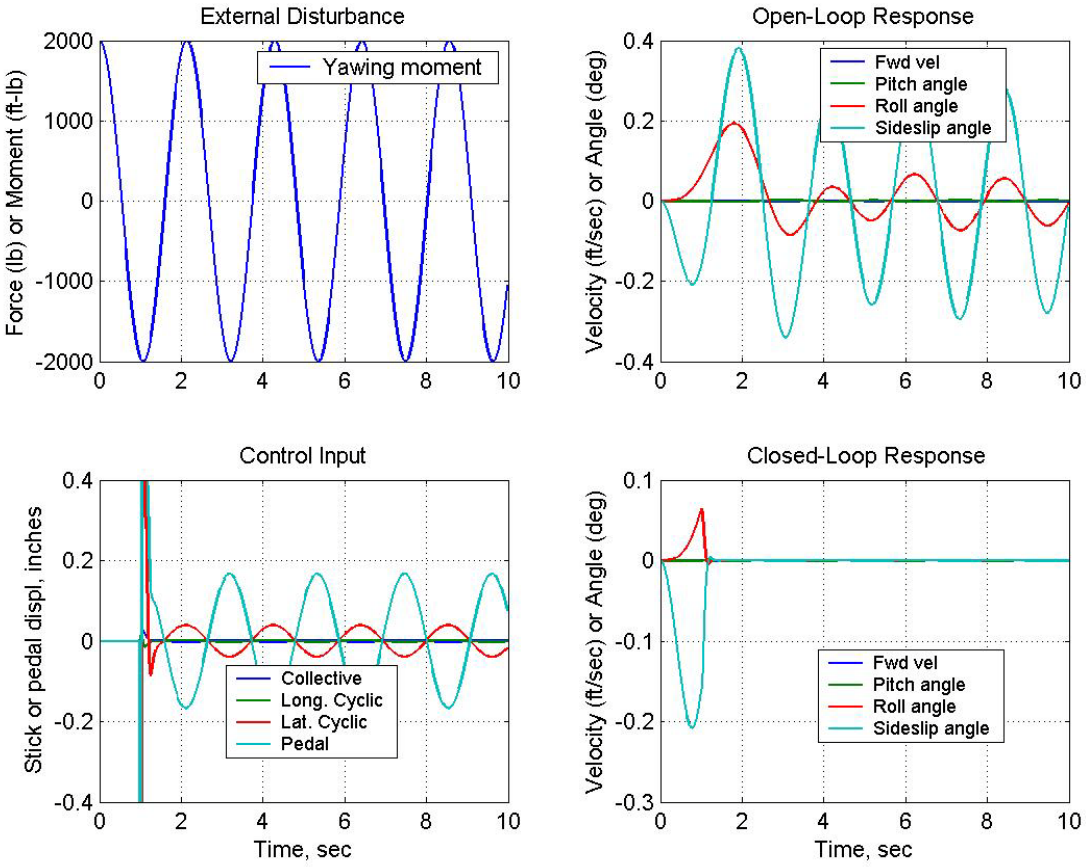


Figure 34.- Regulation of XV-15 subjected to a sinusoidal yawing moment disturbance at 0.46734 Hz.

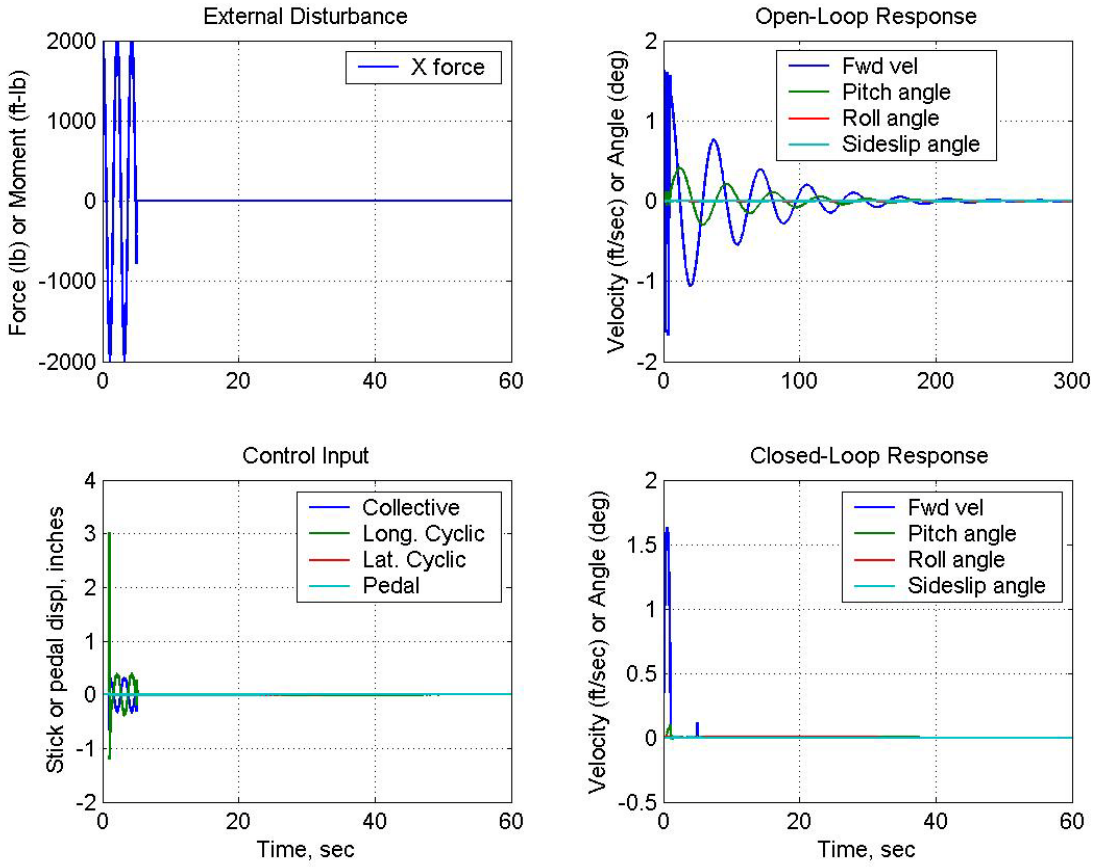


Figure 35.- Regulation of XV-15 subjected to a 2¼-cycle sine-pulse axial force disturbance.

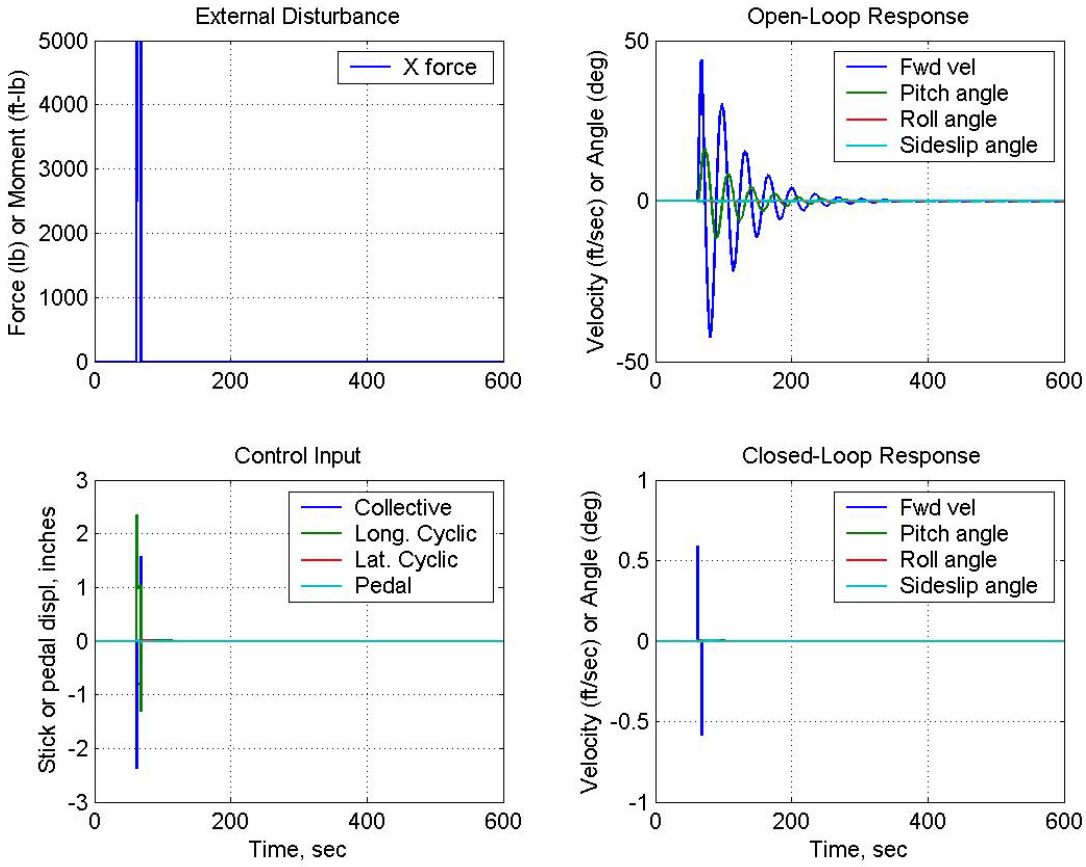


Figure 36.- Regulation of XV-15 subjected to a 5-sec rectangular pulse axial disturbance.

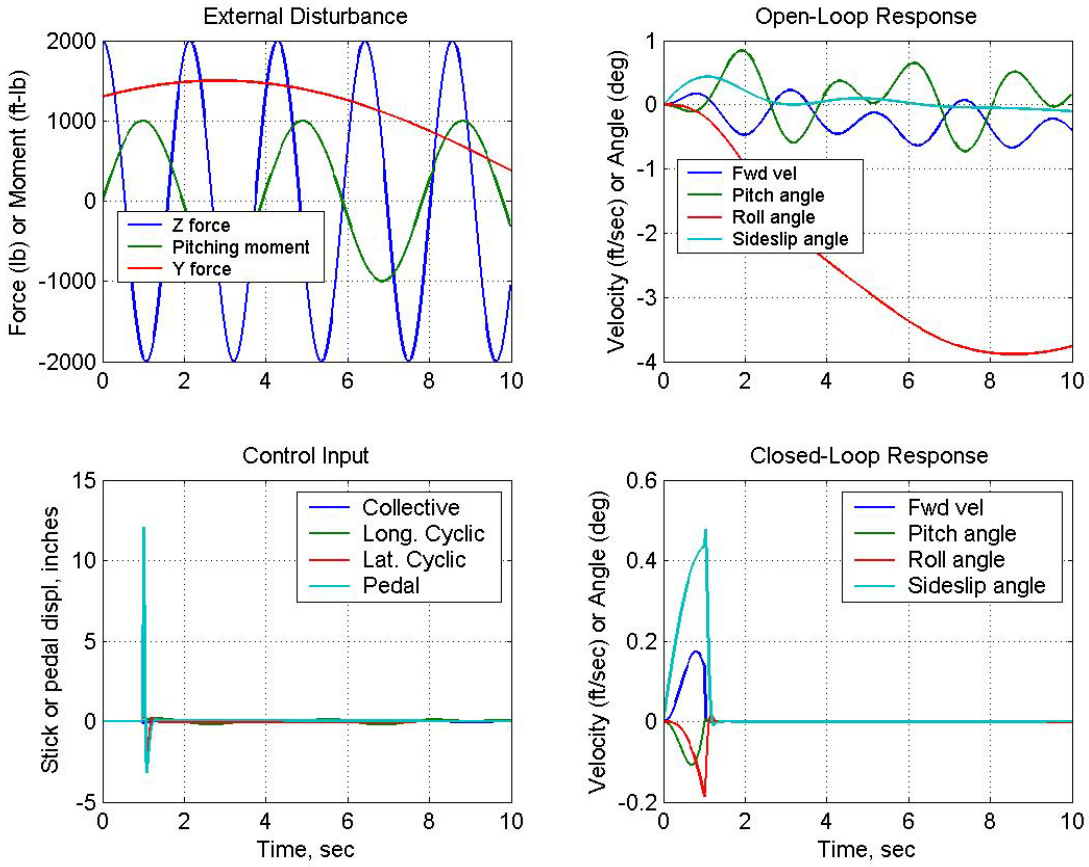


Figure 37.- Regulation of XV-15 subjected to Z, PM, and Y sinusoidal disturbances at frequencies of the short period (0.46734 Hz), Dutch roll (0.25556 Hz), and phugoid (0.029291 Hz) modes, respectively.

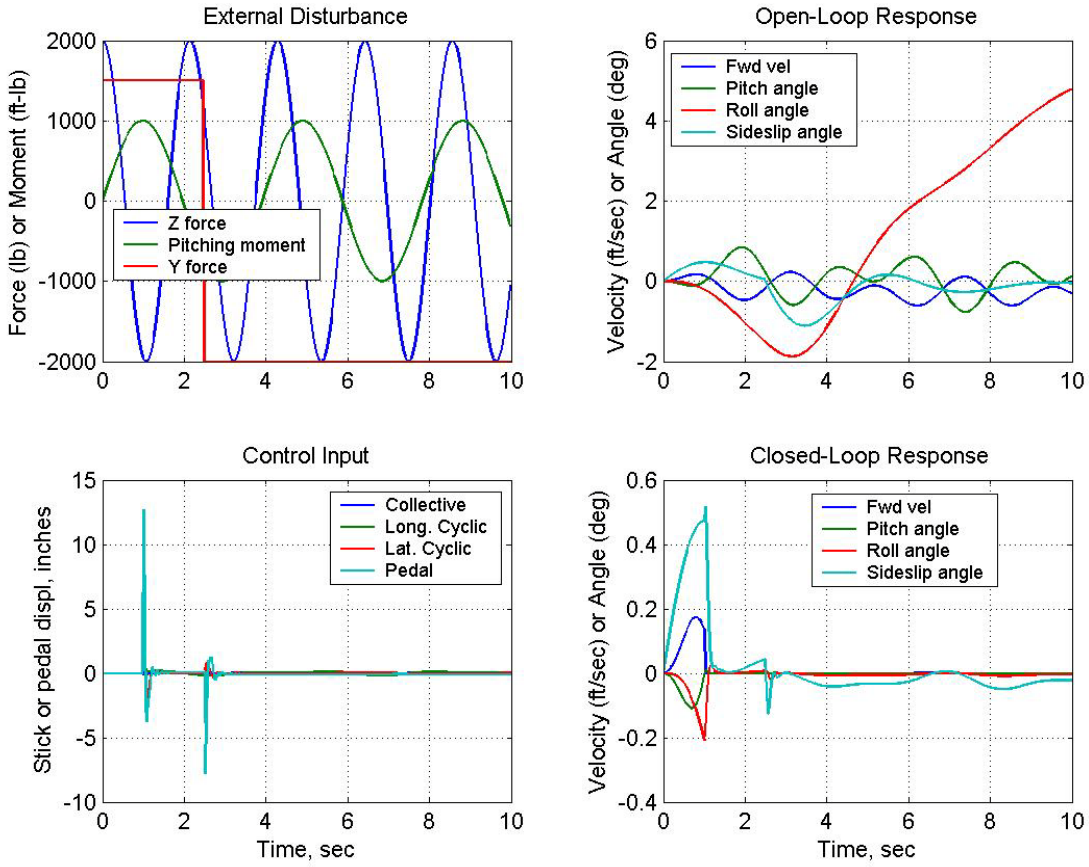


Figure 38.- Regulation of XV-15 subjected to disturbances Z = a 0.46734 Hz sinusoid, PM = a 0.25556 Hz sinusoid, and Y = a step function.

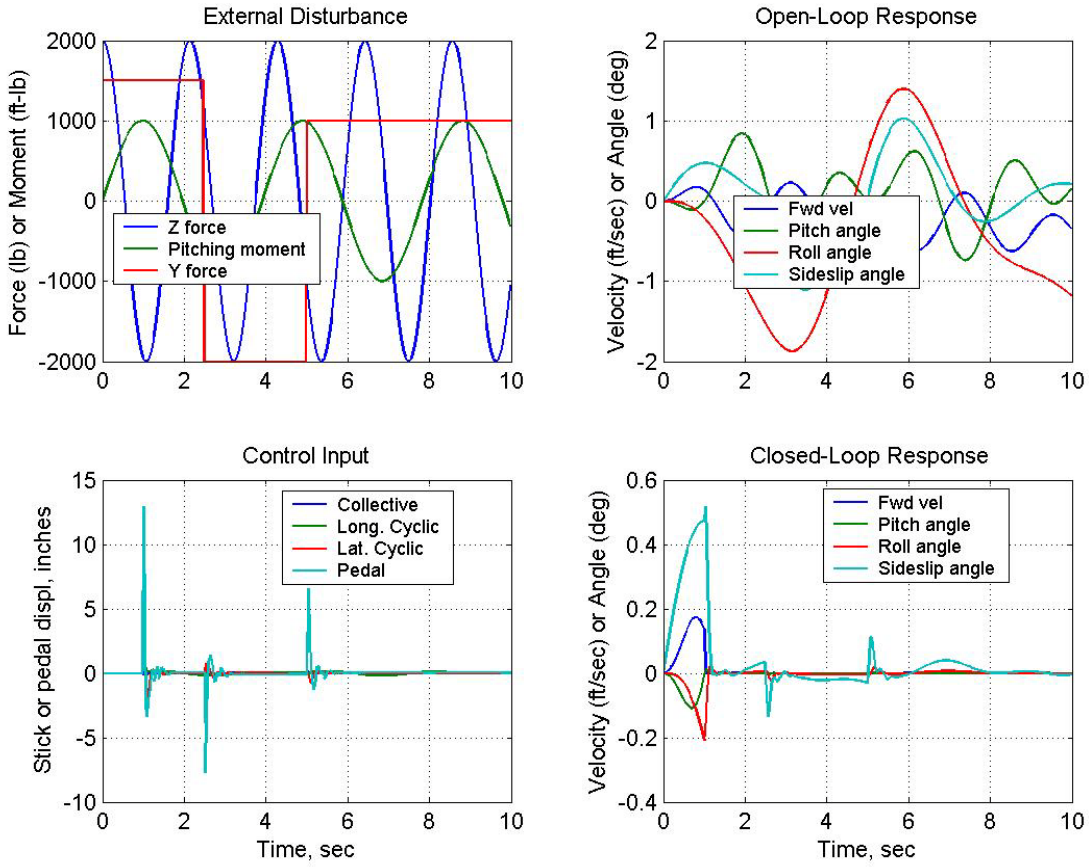


Figure 39.- Regulation of XV-15 with disturbances Z = a 0.46734 Hz sinusoid, PM = a 0.25556 Hz sinusoid, and Y = a 2-step step function.

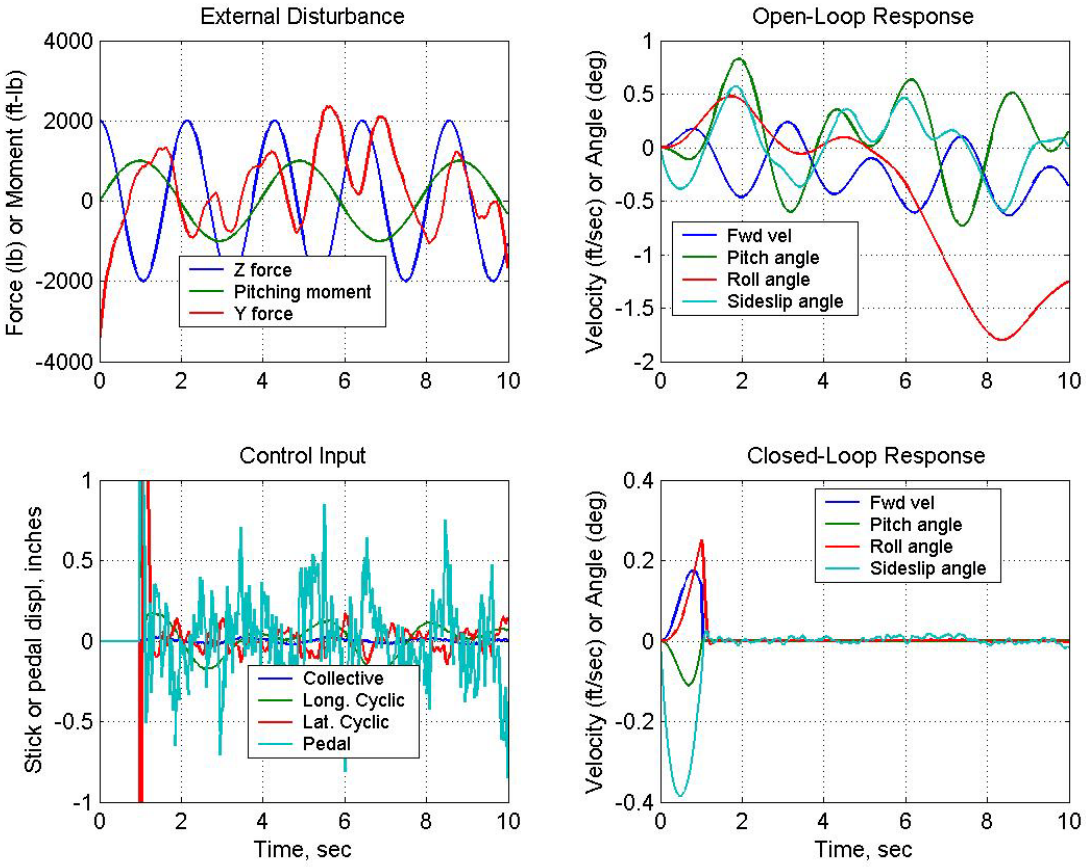


Figure 40.- Regulation of XV-15 where disturbances X, PM, and Y are all random functions.

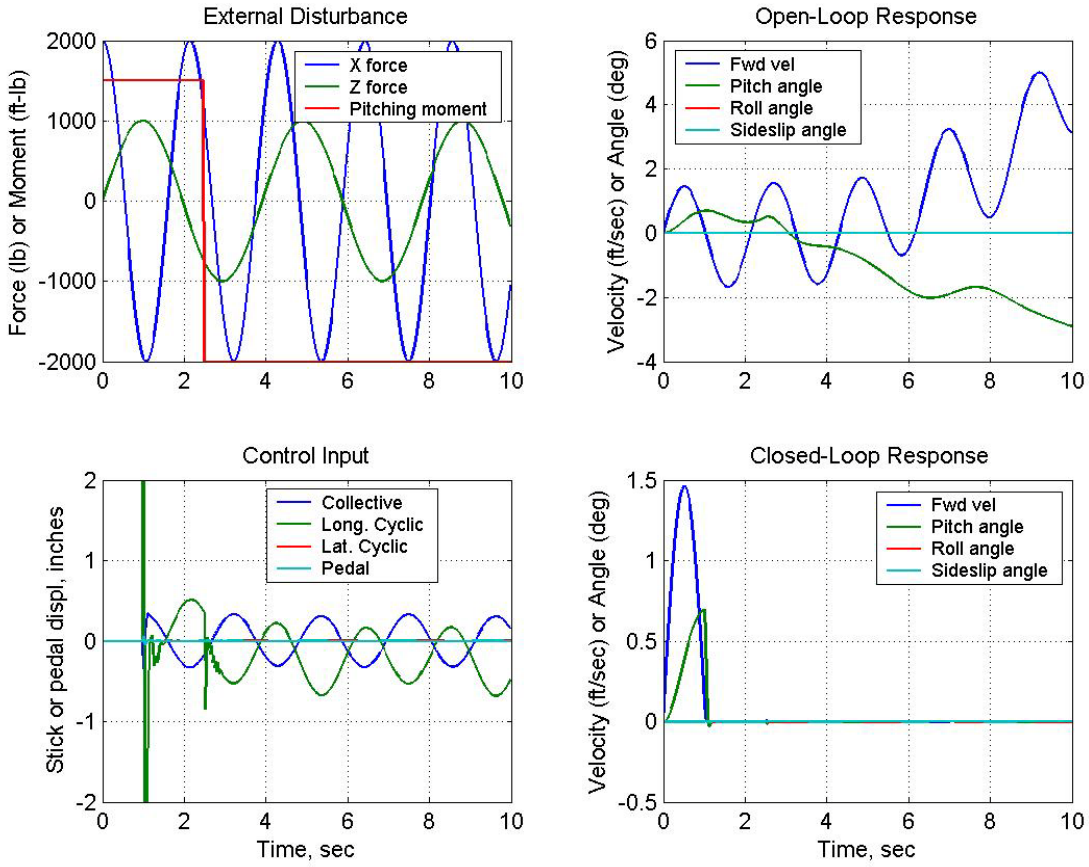


Figure 41.- Regulation of XV-15 subjected to longitudinal disturbances X = a 0.46734 Hz sinusoid, Z = a 0.25556 Hz sinusoid, and PM = a one-step step function.

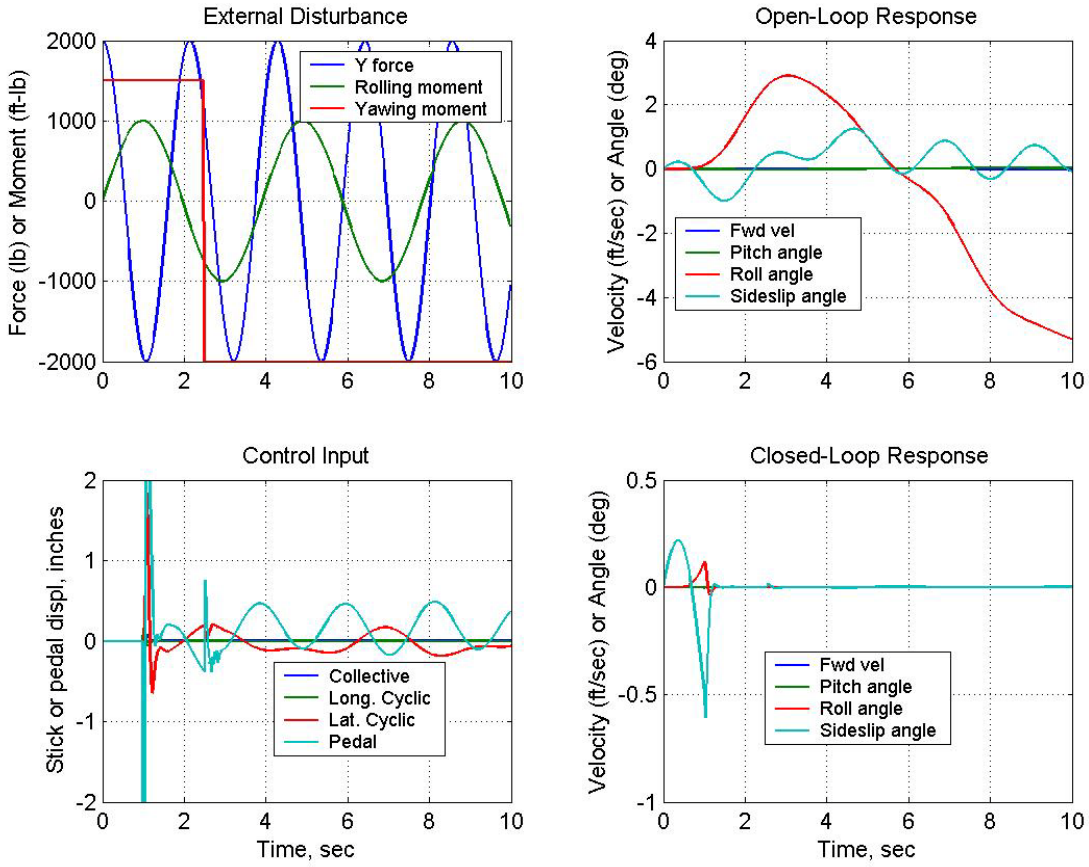


Figure 42.- Regulation of XV-15 subjected to lateral disturbances Y = a 0.46734 Hz sinusoid, RM = a 0.25556 Hz sinusoid, and YM = a one-step step function.

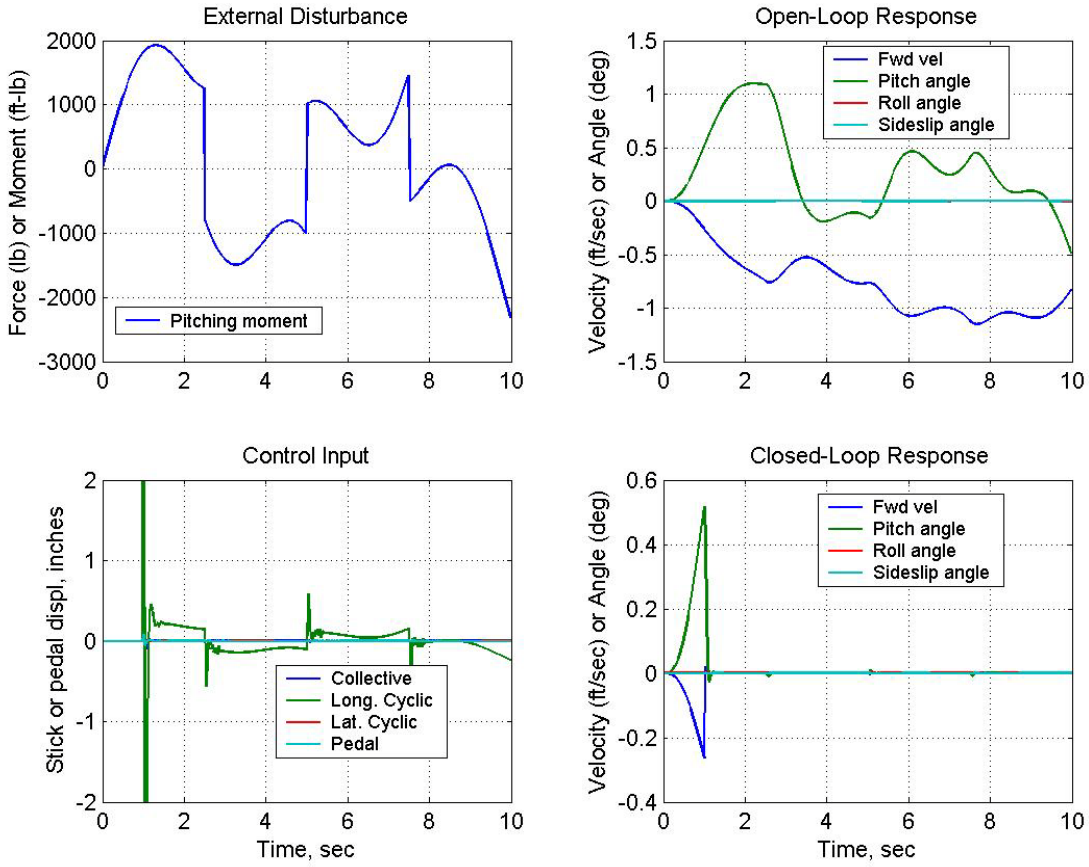


Figure 43.- Regulation of XV-15 subjected to a convoluted pitch disturbance.

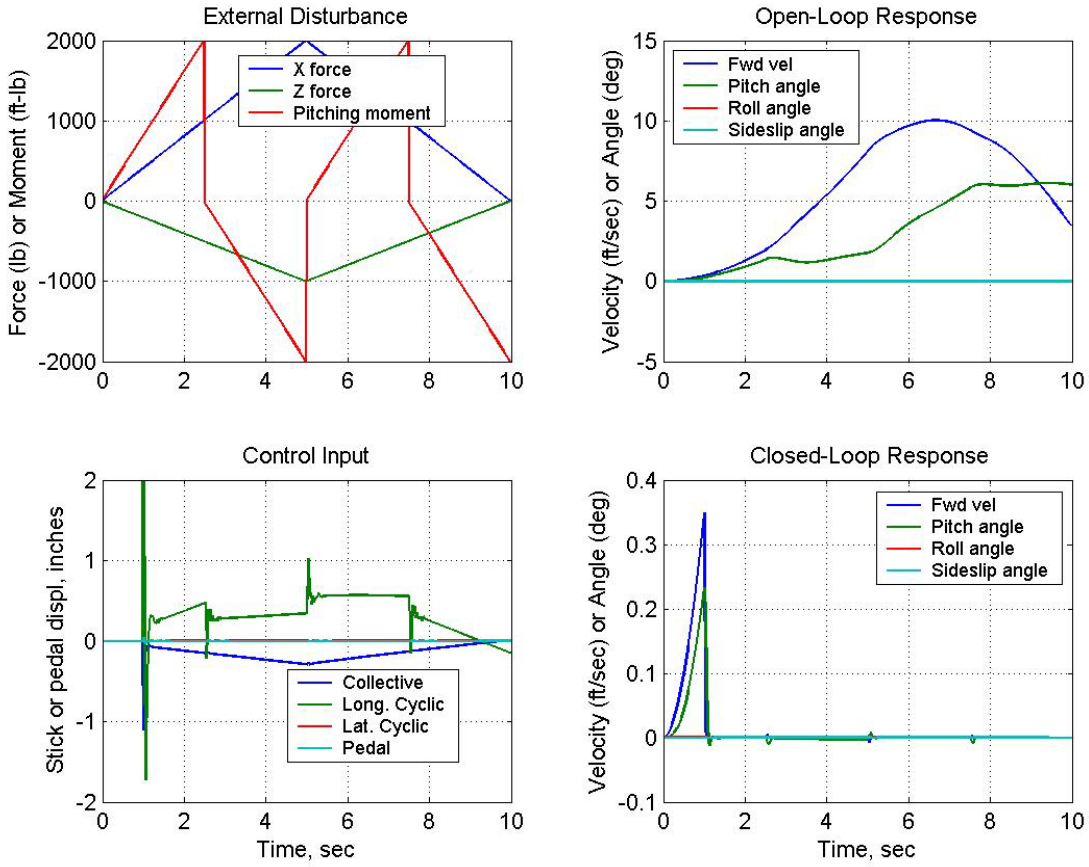


Figure 44.- Regulation of XV-15 subjected to X, Z, and PM disturbances formed from triangular waveforms.

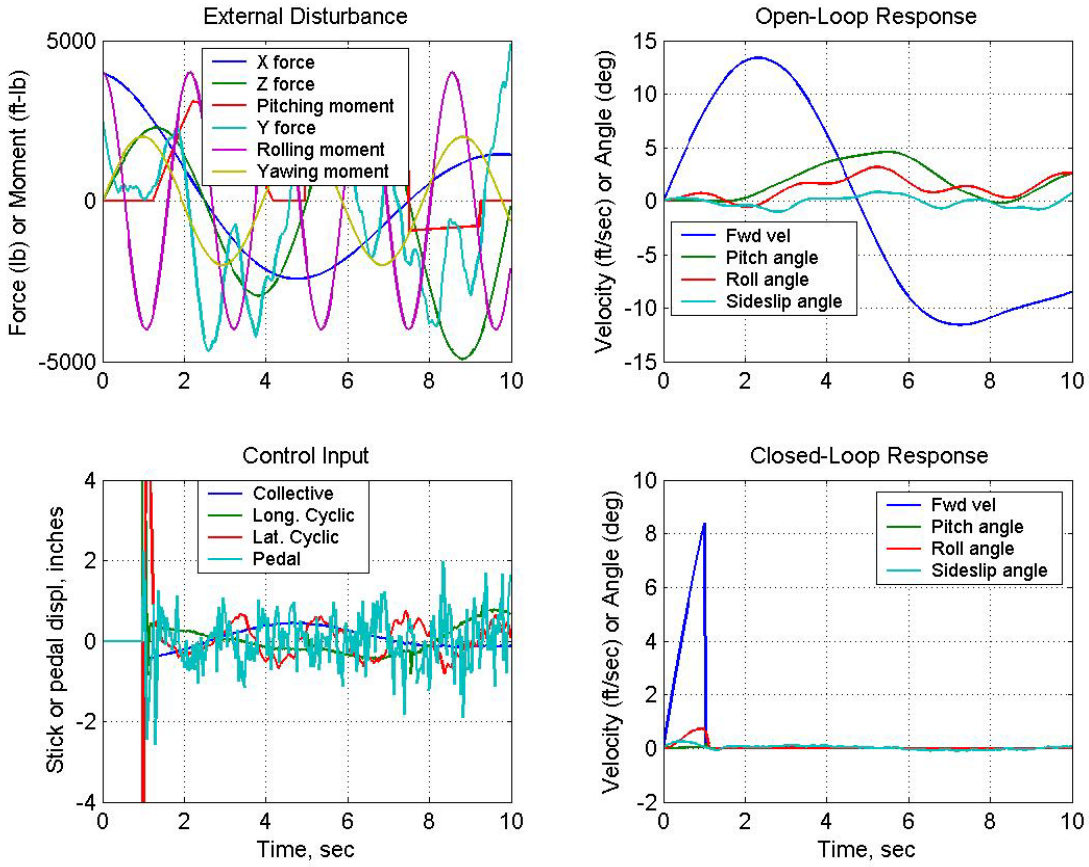


Figure 45.- Regulation of XV-15 subjected to a full complement of different disturbances.

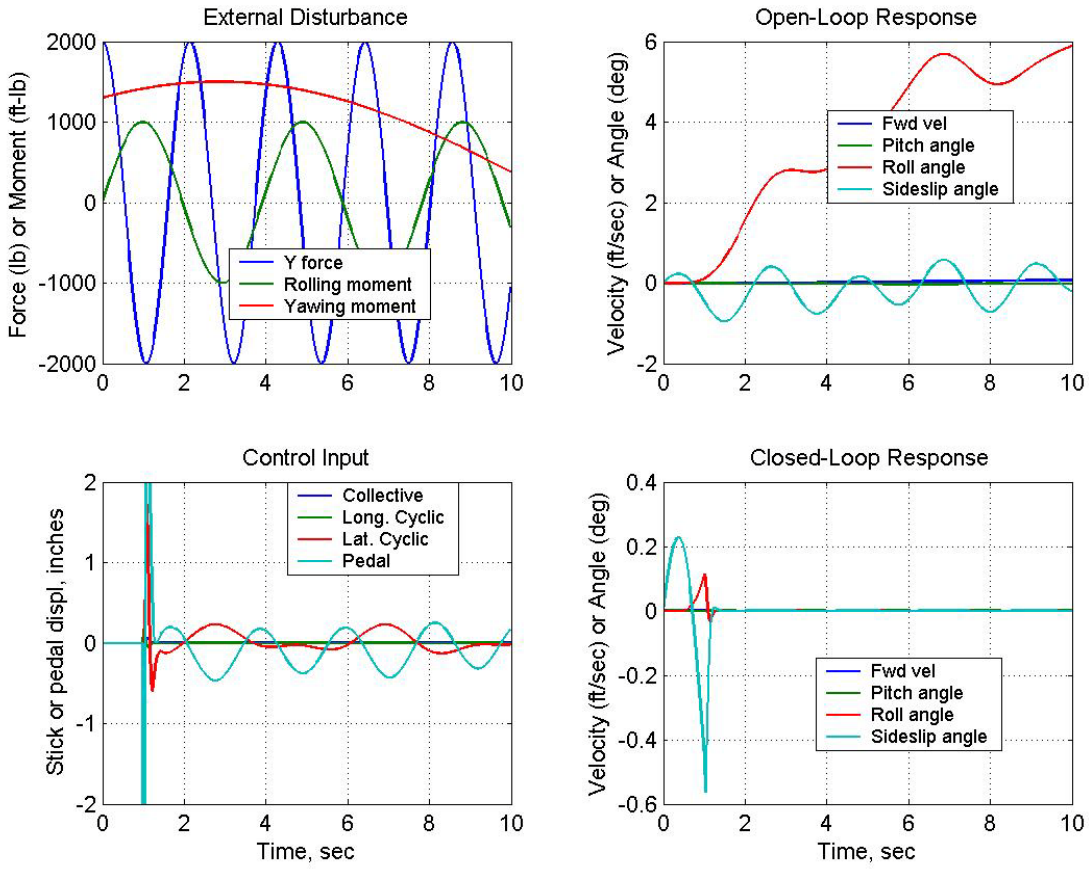


Figure 46.- Regulation of XV-15 subjected to disturbances Y = a 0.46734 Hz sinusoid, RM = a 0.25556 Hz sinusoid, and YM = a 0.029291 sinusoid.

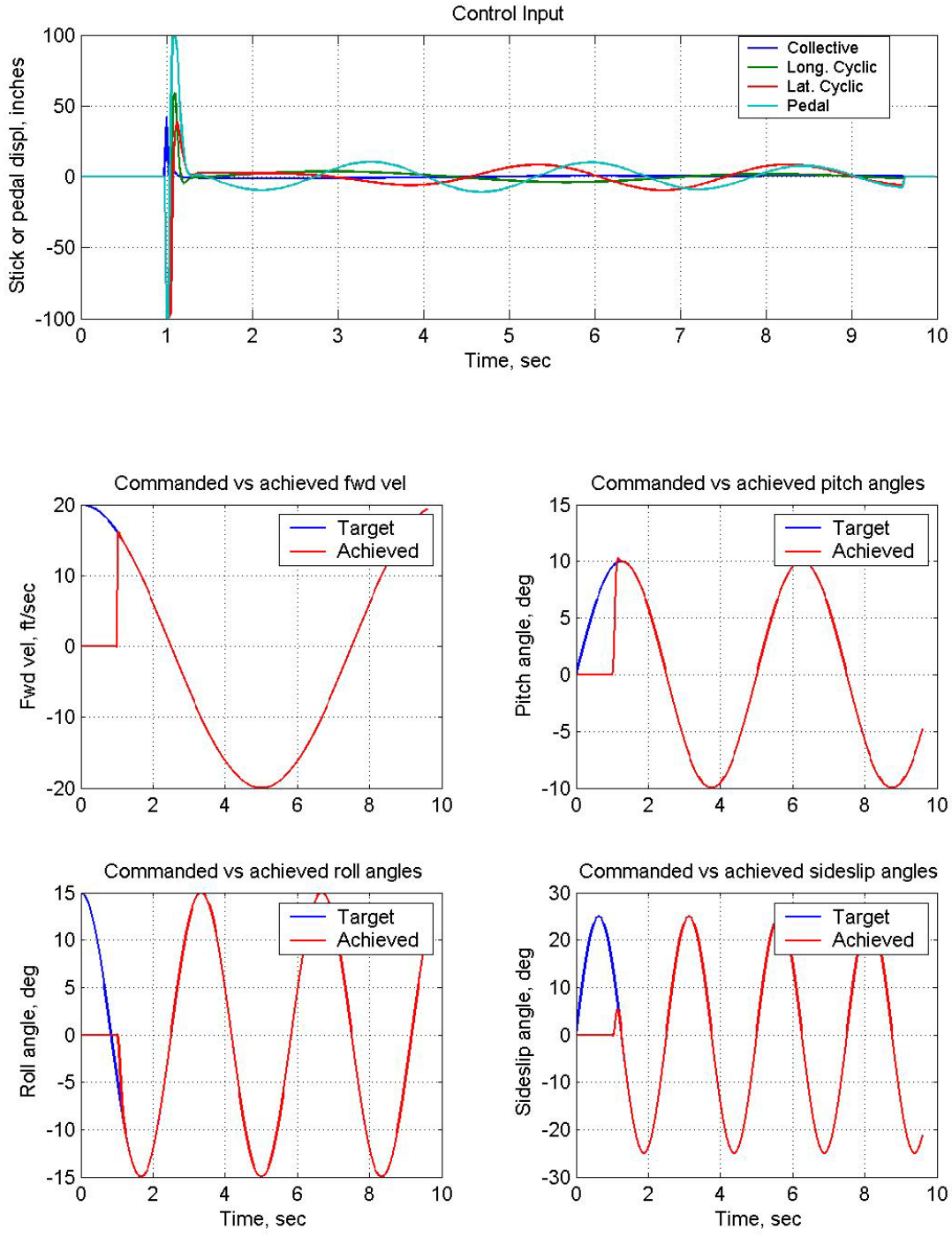


Figure 47.- Tracking of undisturbed XV-15 with targets yt1 = a 0.1 Hz sinusoid, yt2 = a 0.2 Hz sinusoid, yt3 = a 0.3 Hz sinusoid, and yt4 = a 0.4 Hz sinusoid.

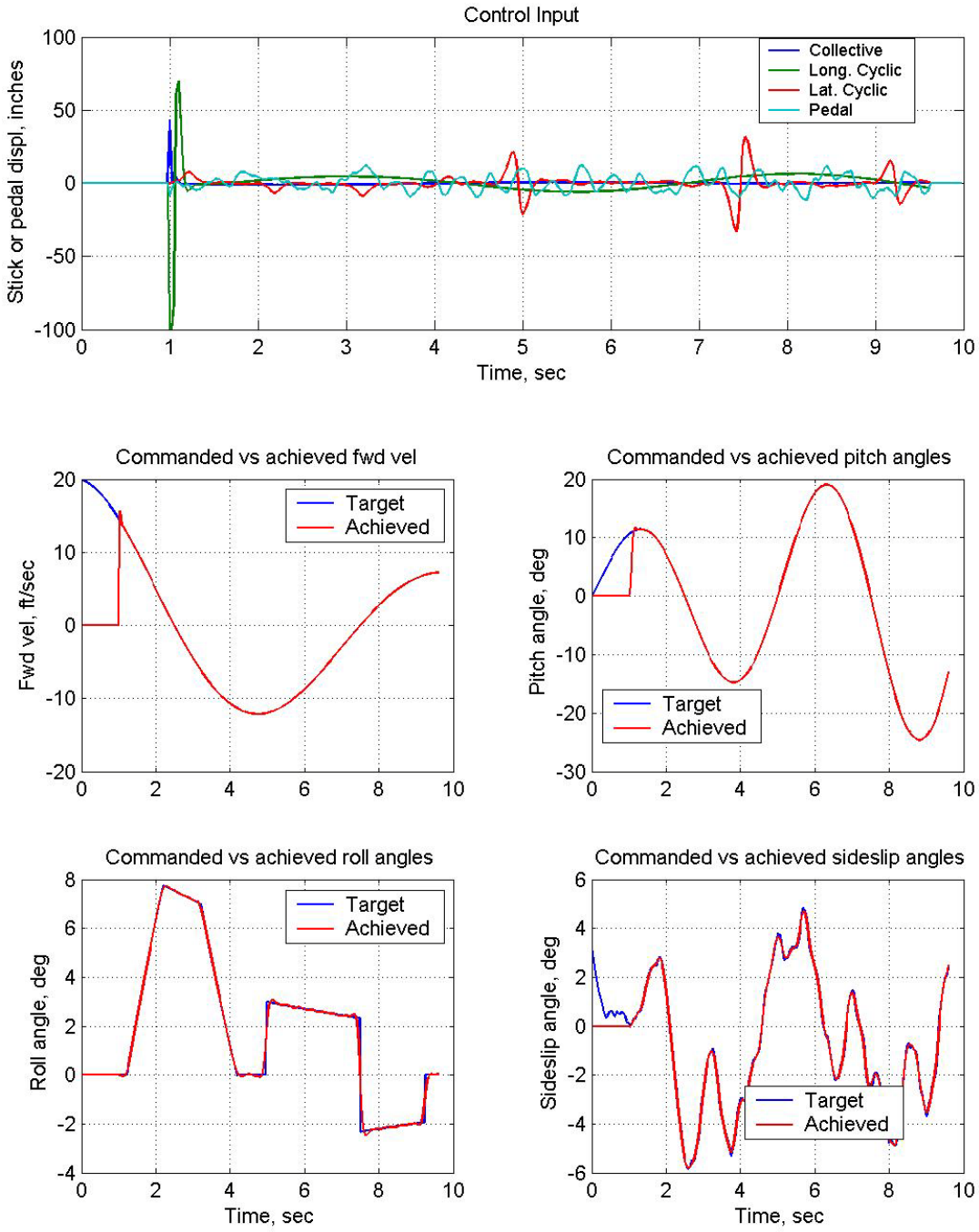


Figure 48.- Tracking of undisturbed XV-15 with targets yt1 = an exponentially decreasing sinusoid, yt2 =an exponentially increasing sinusoid, yt3 = a non-uniform saw-tooth-type wave, and yt4 = an exponentially diverging random function.

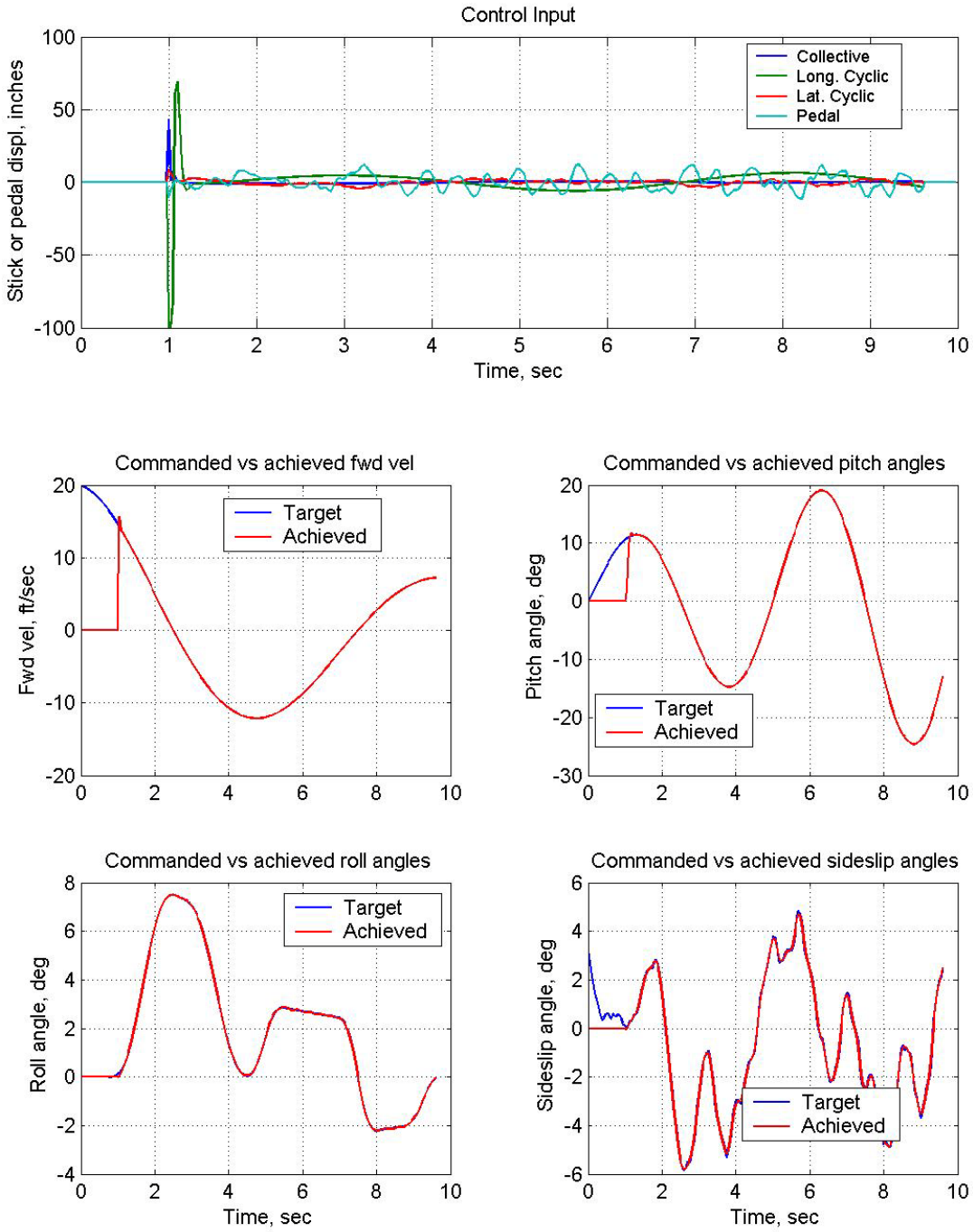


Figure 49.- Repeat of figure 48 but with a filtered roll target.

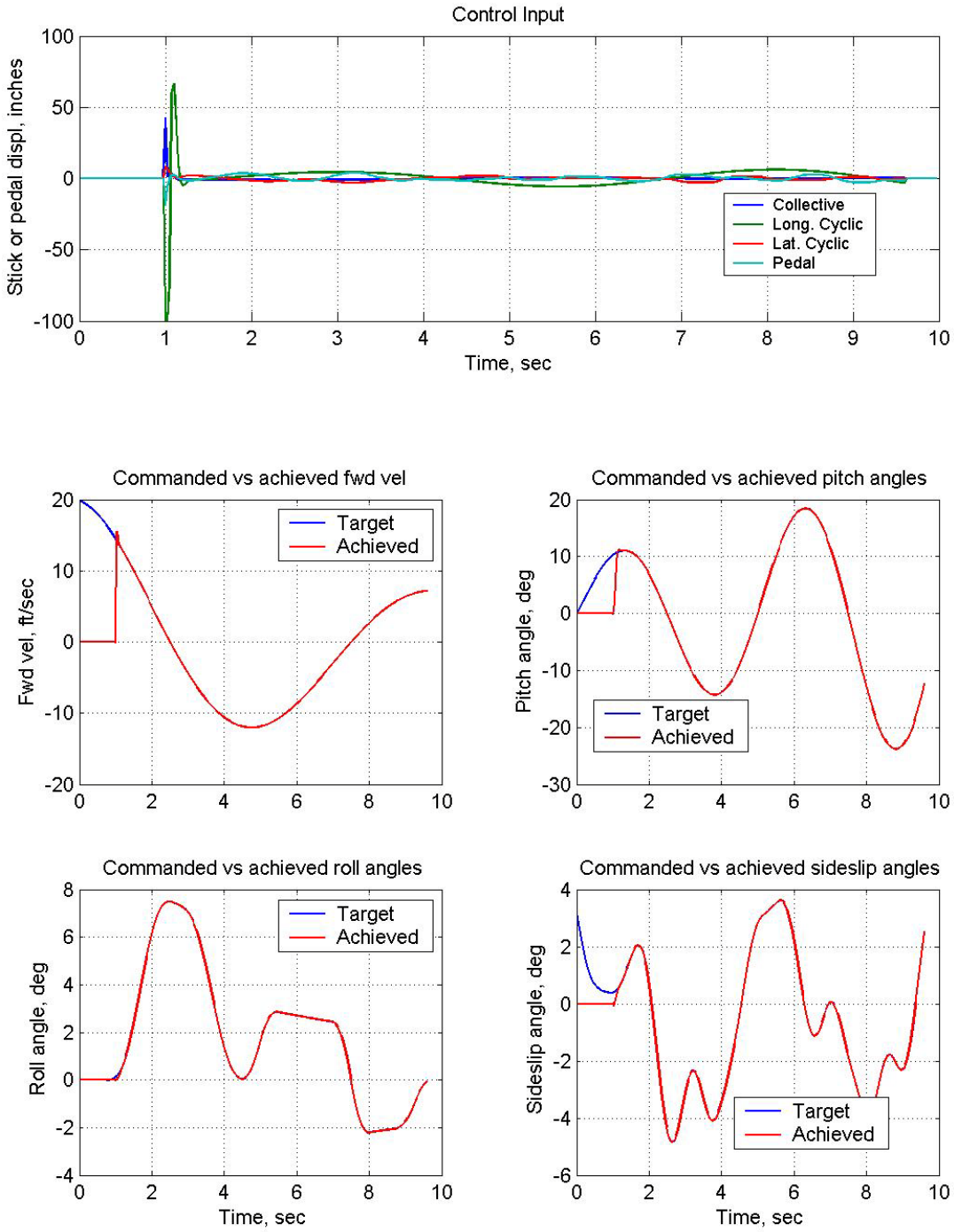


Figure 50.- Repeat of figure 48 but with filtered roll and sideslip targets.

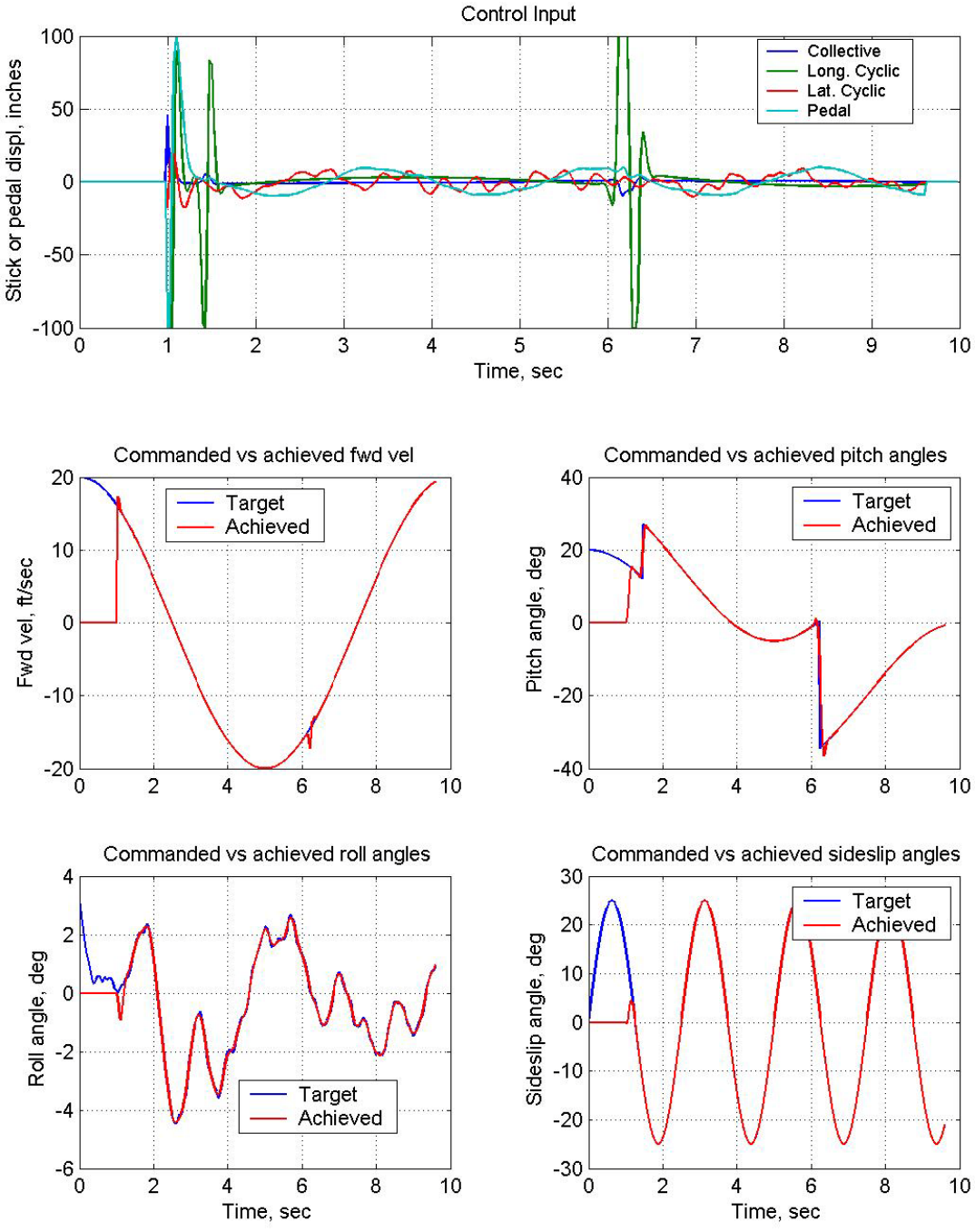


Figure 51.- Tracking of undisturbed XV-15 using a variety of target waveforms.

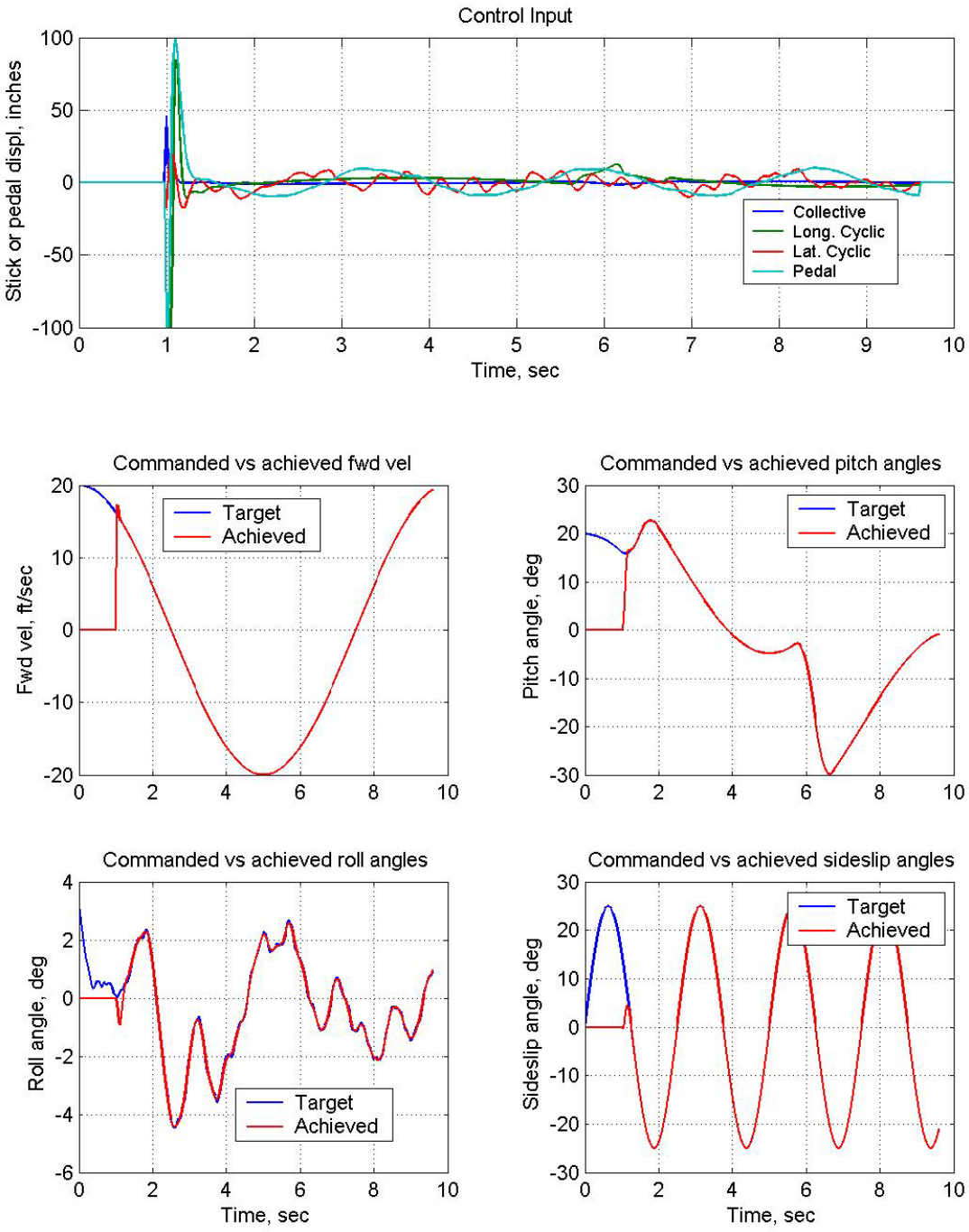


Figure 52.- Repeat of figure 51 but with filtered pitch target.

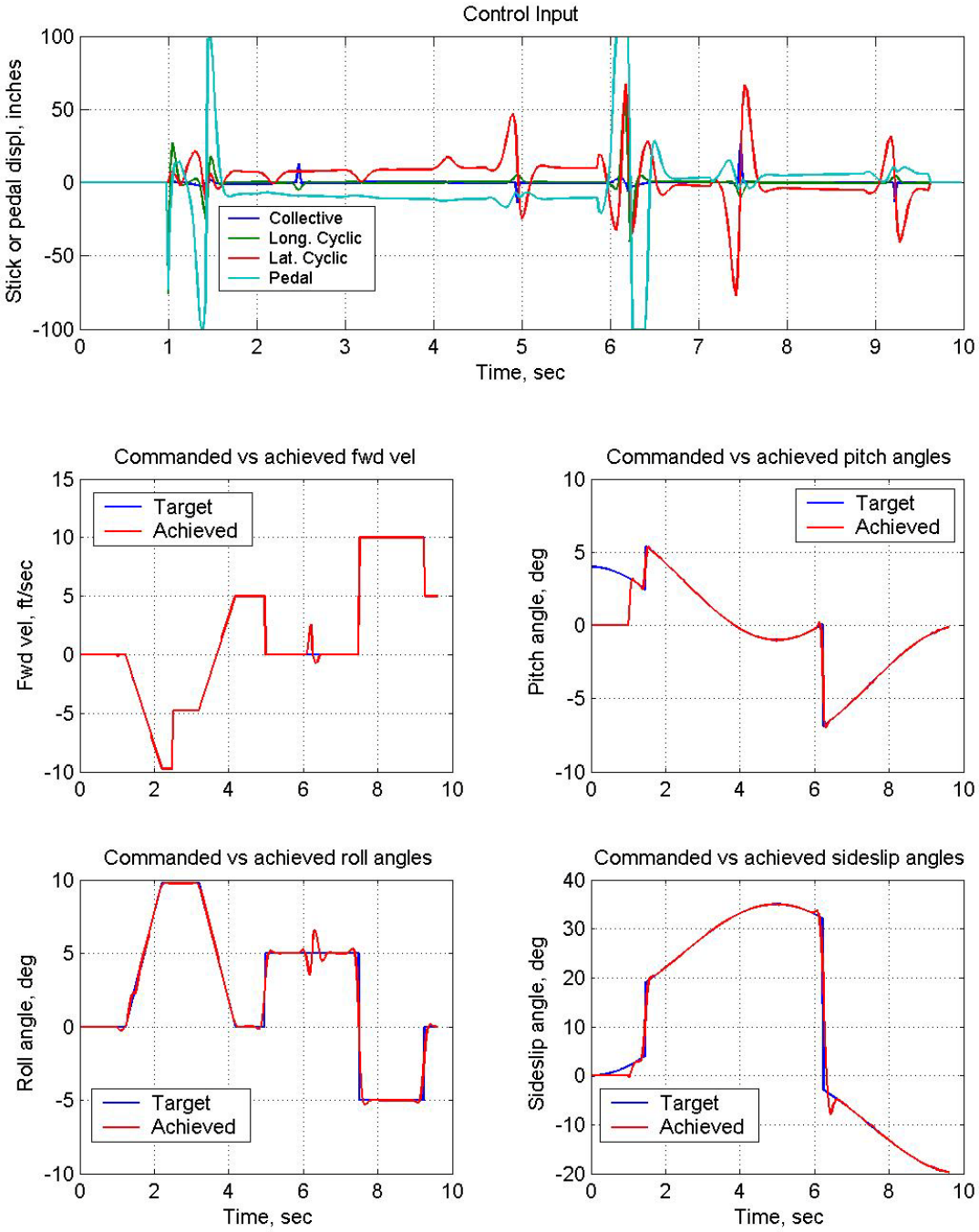


Figure 53.- Tracking of undisturbed XV-15 using a variety of target waveforms.

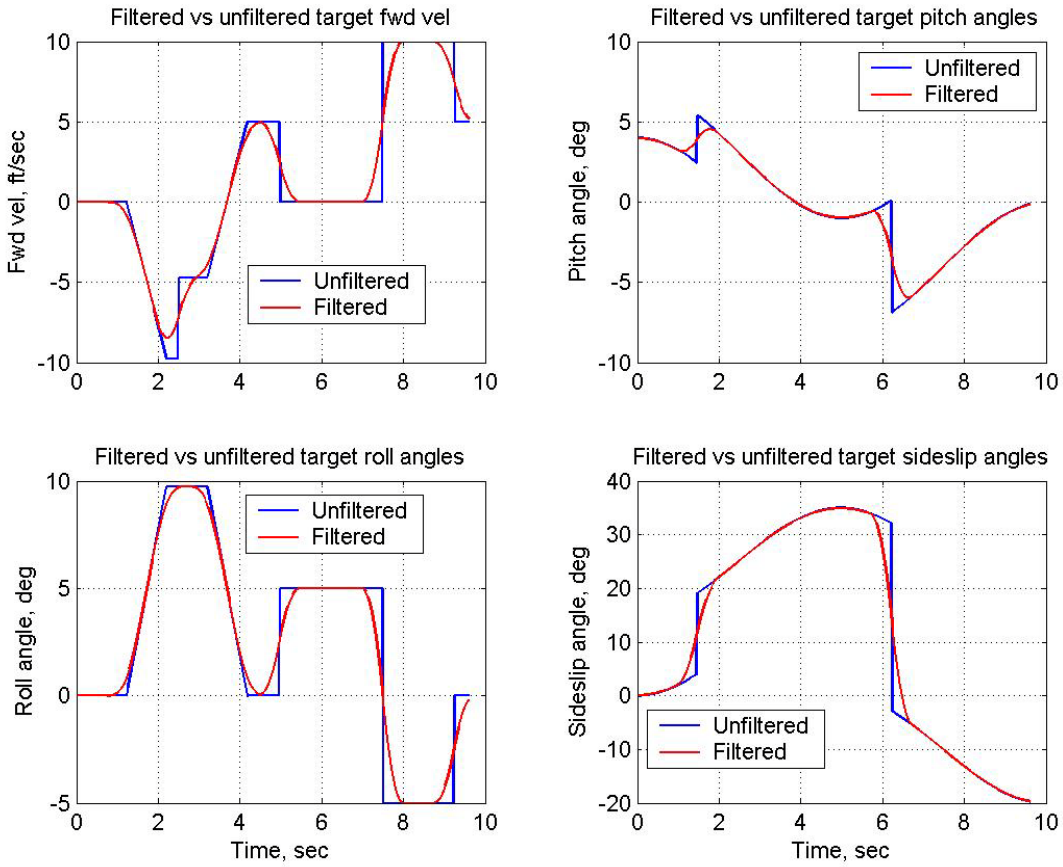


Figure 54.- Comparison of filtered and unfiltered targets for figure 53

.

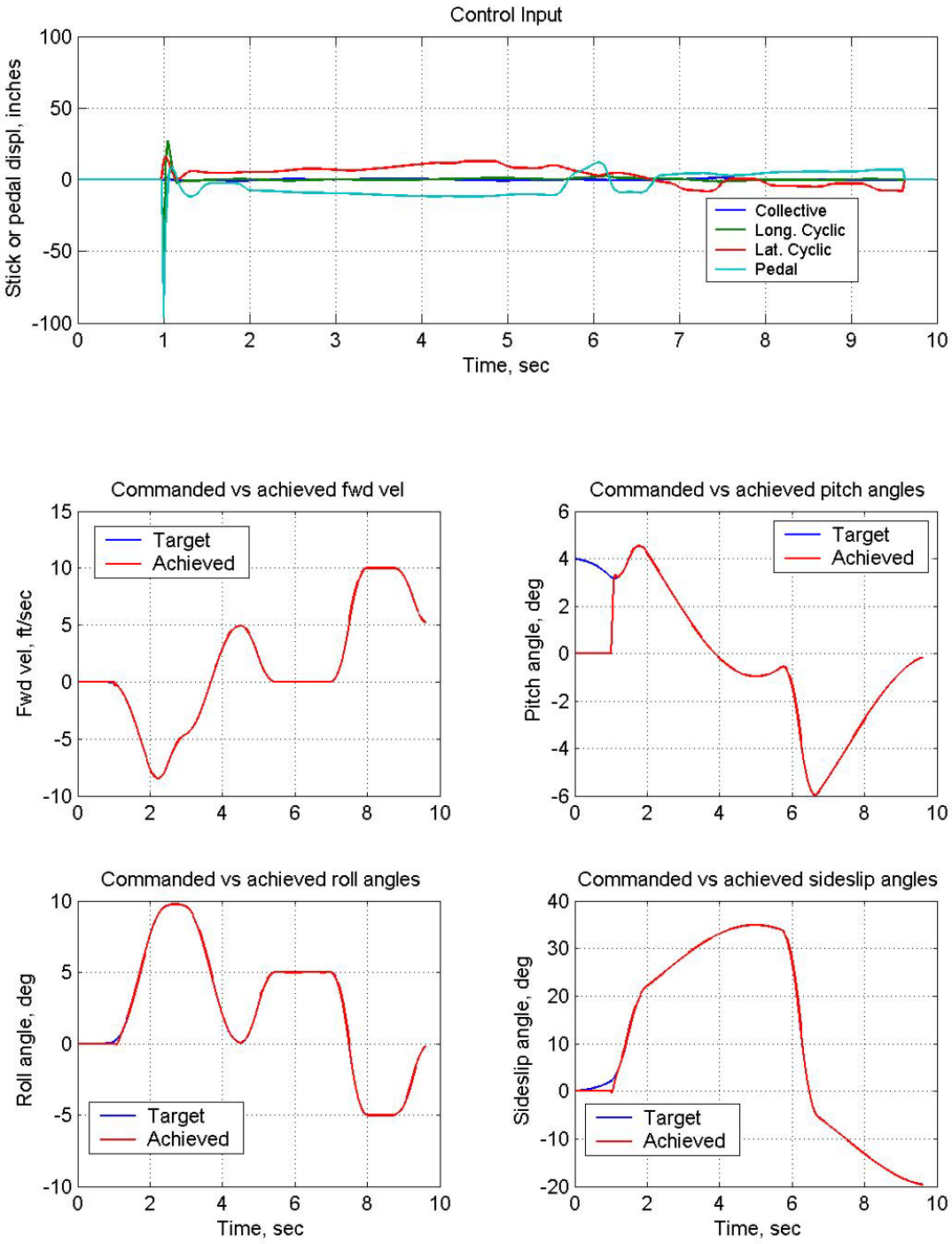


Figure 55.- Repeat of figure 53 but with all targets filtered.

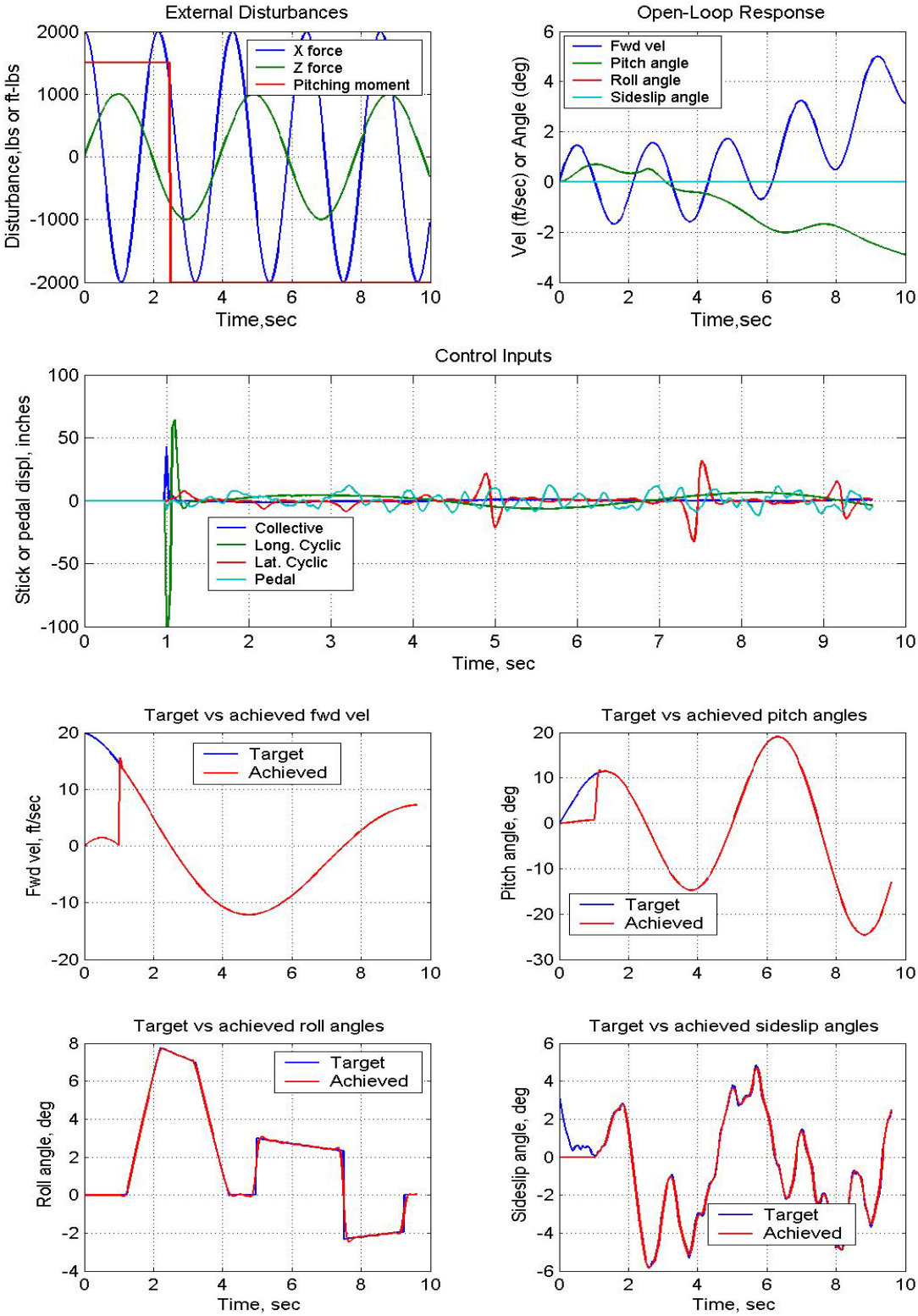


Figure 56.- Tracking of disturbed XV-15 using the same targets as in figure 48.

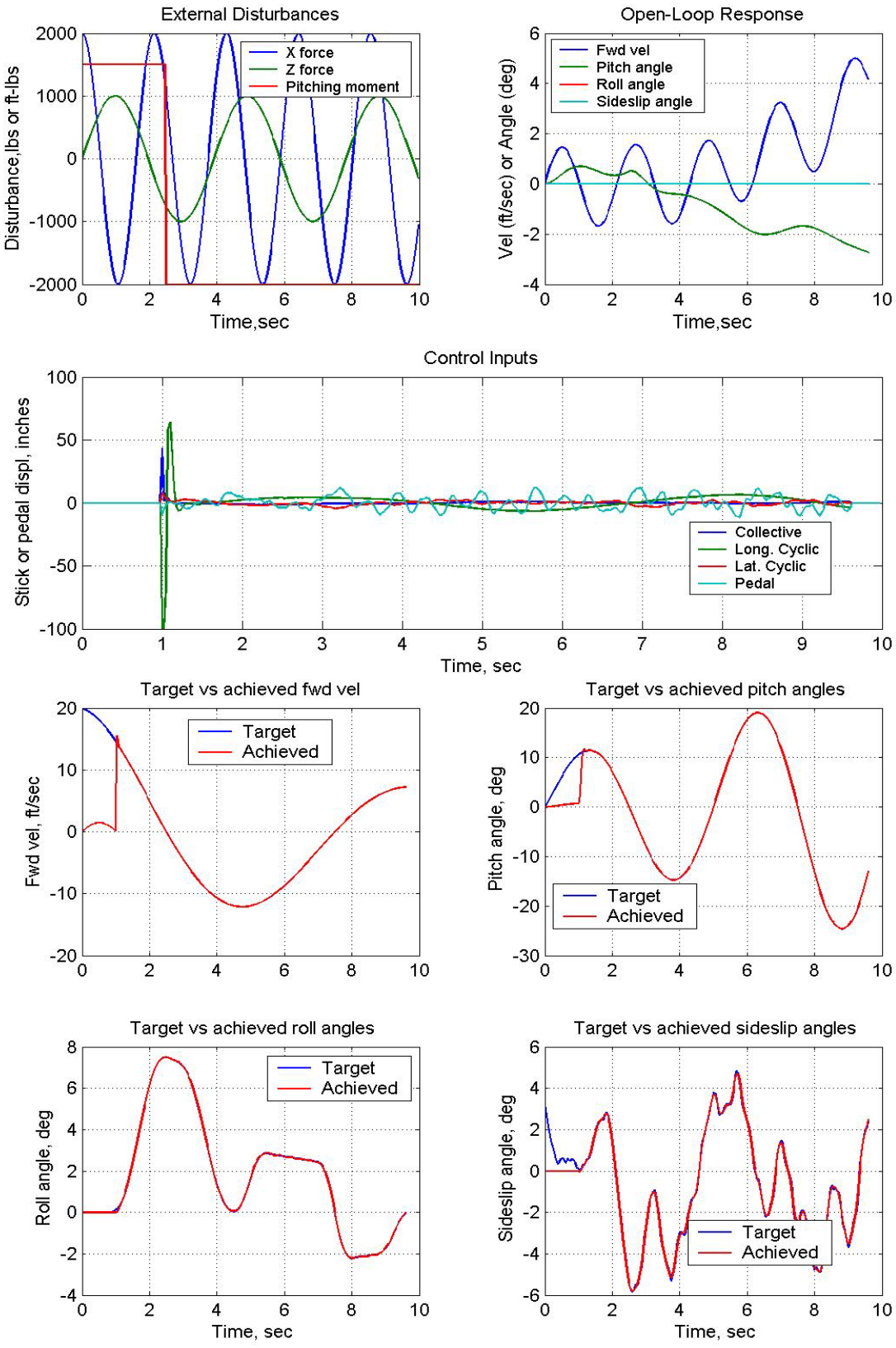


Figure 57.- Repeat of figure 56 but with filtered roll target.

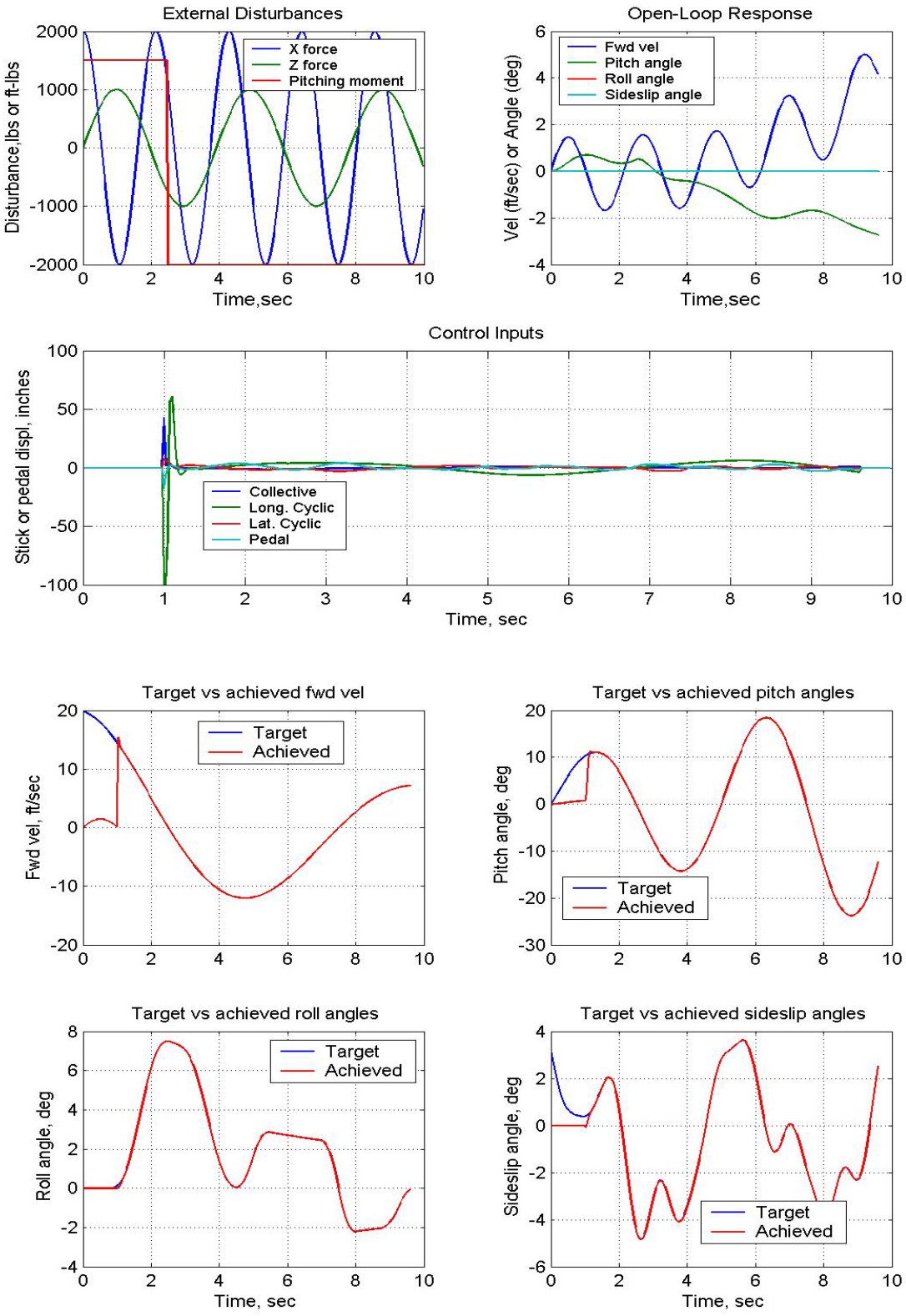


Figure 58.- Repeat of figure 56 but with filtered roll and sideslip targets.

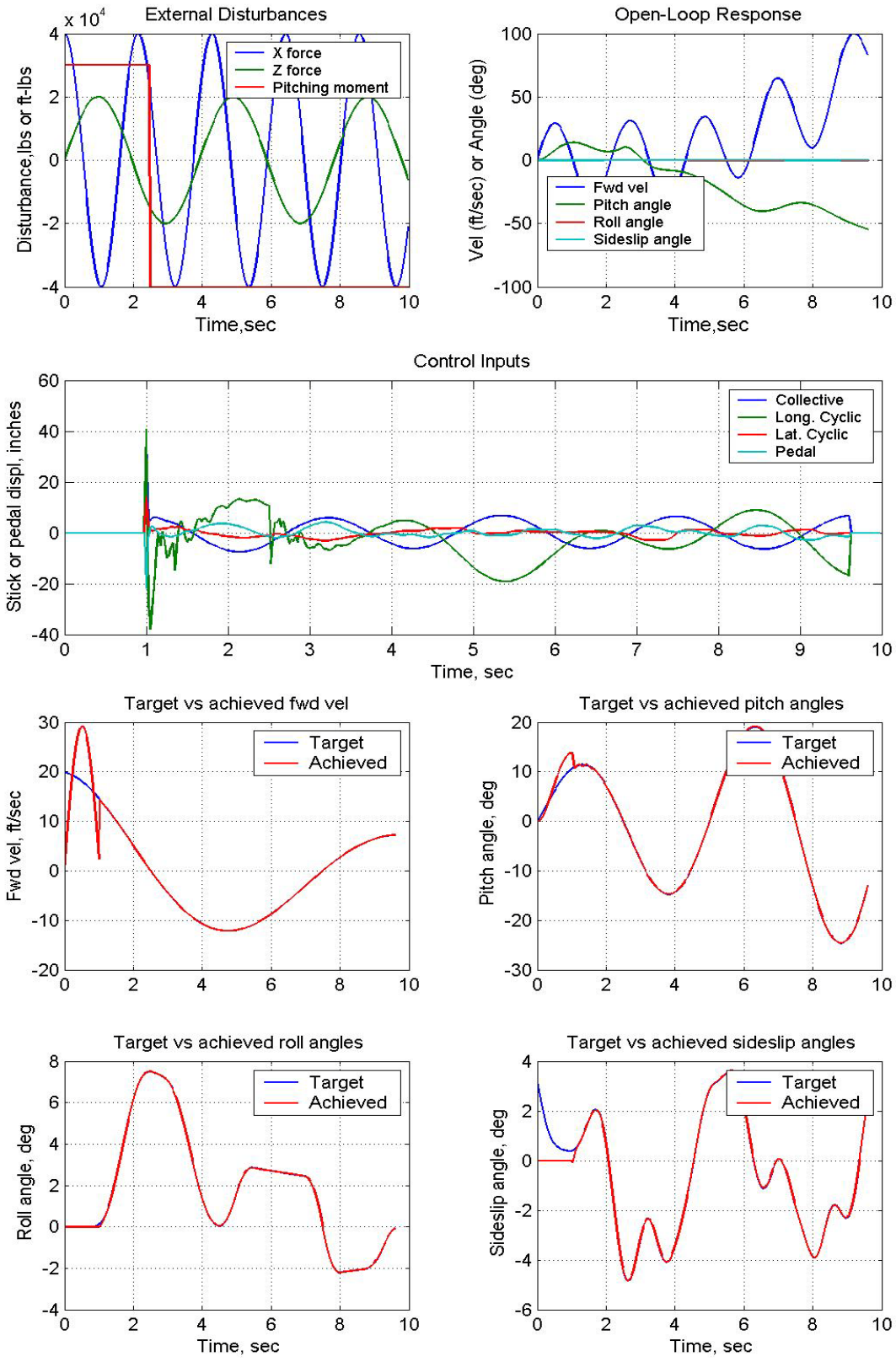


Figure 59.- Repeat of figure 58 but with disturbances that are a factor of 20 larger.

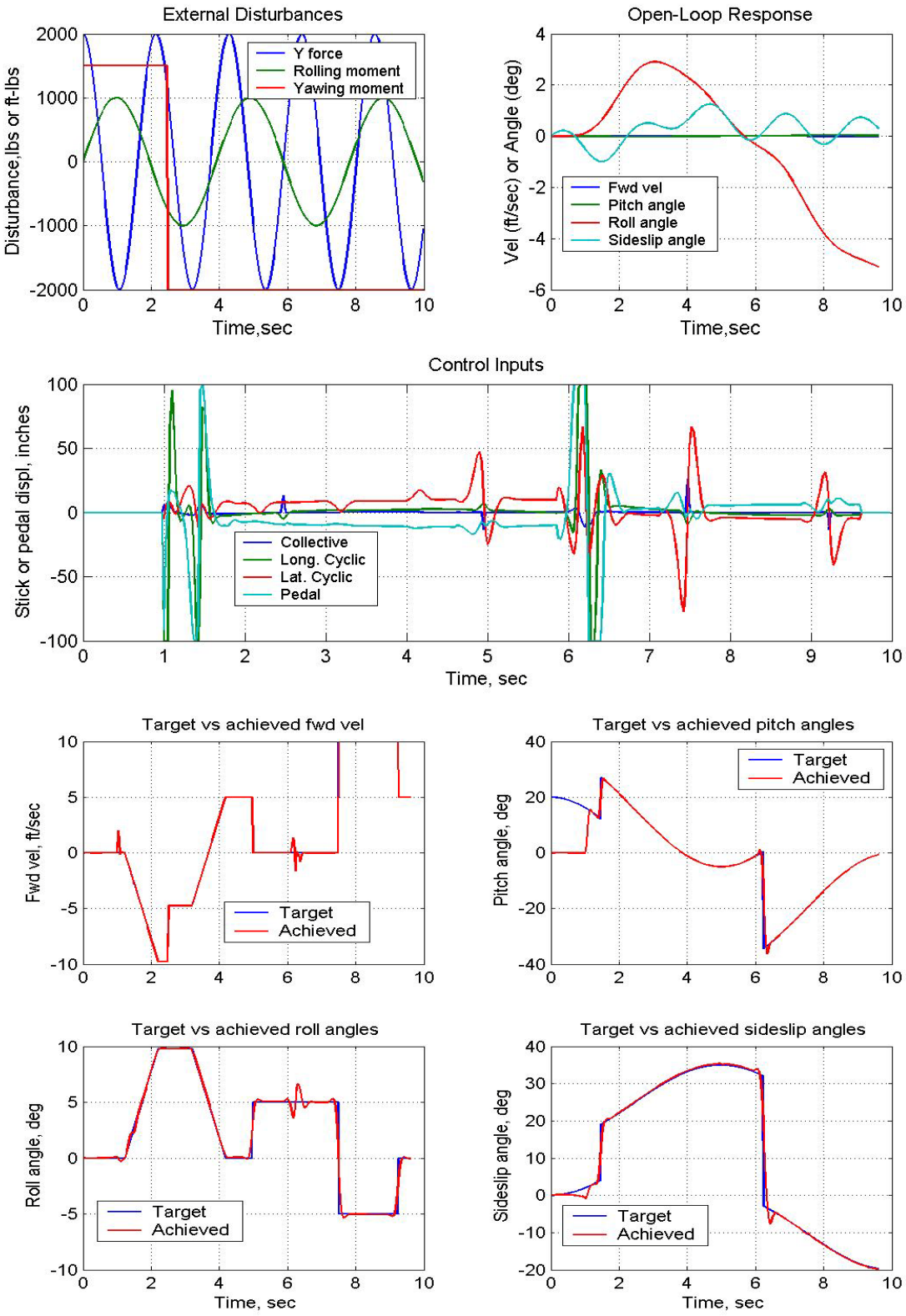


Figure 60.- Tracking of disturbed XV-15 subjected to various target responses.

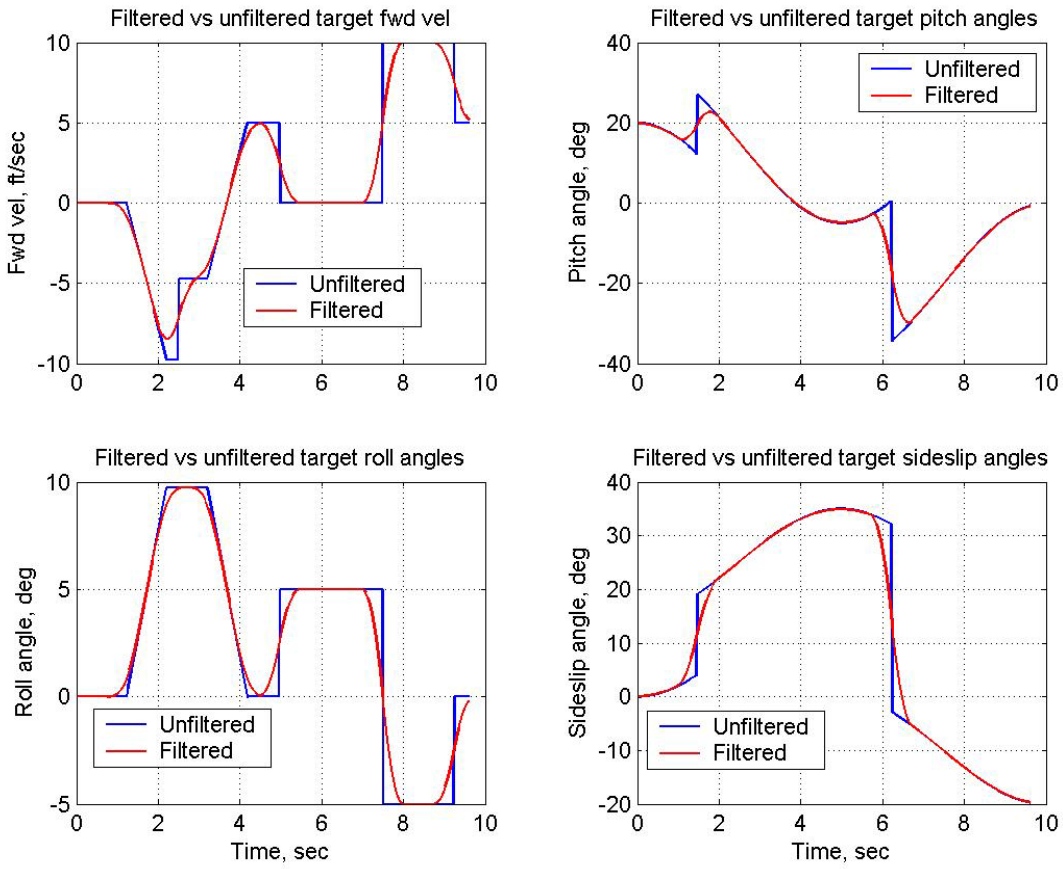


Figure 61.- Comparison of filtered and unfiltered targets for figure 60.

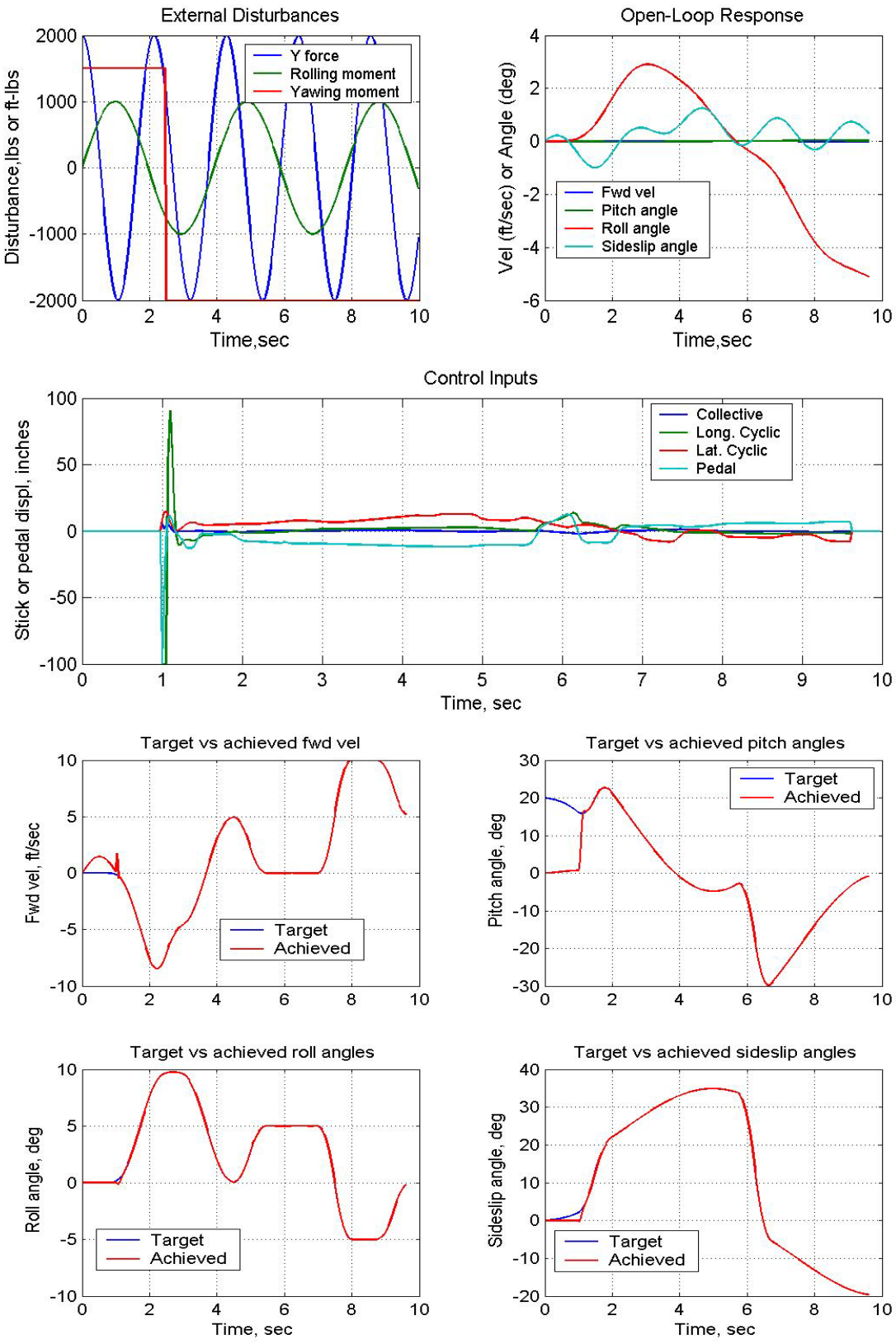


Figure 62.- Repeat of figure 60 but with filtered targets.

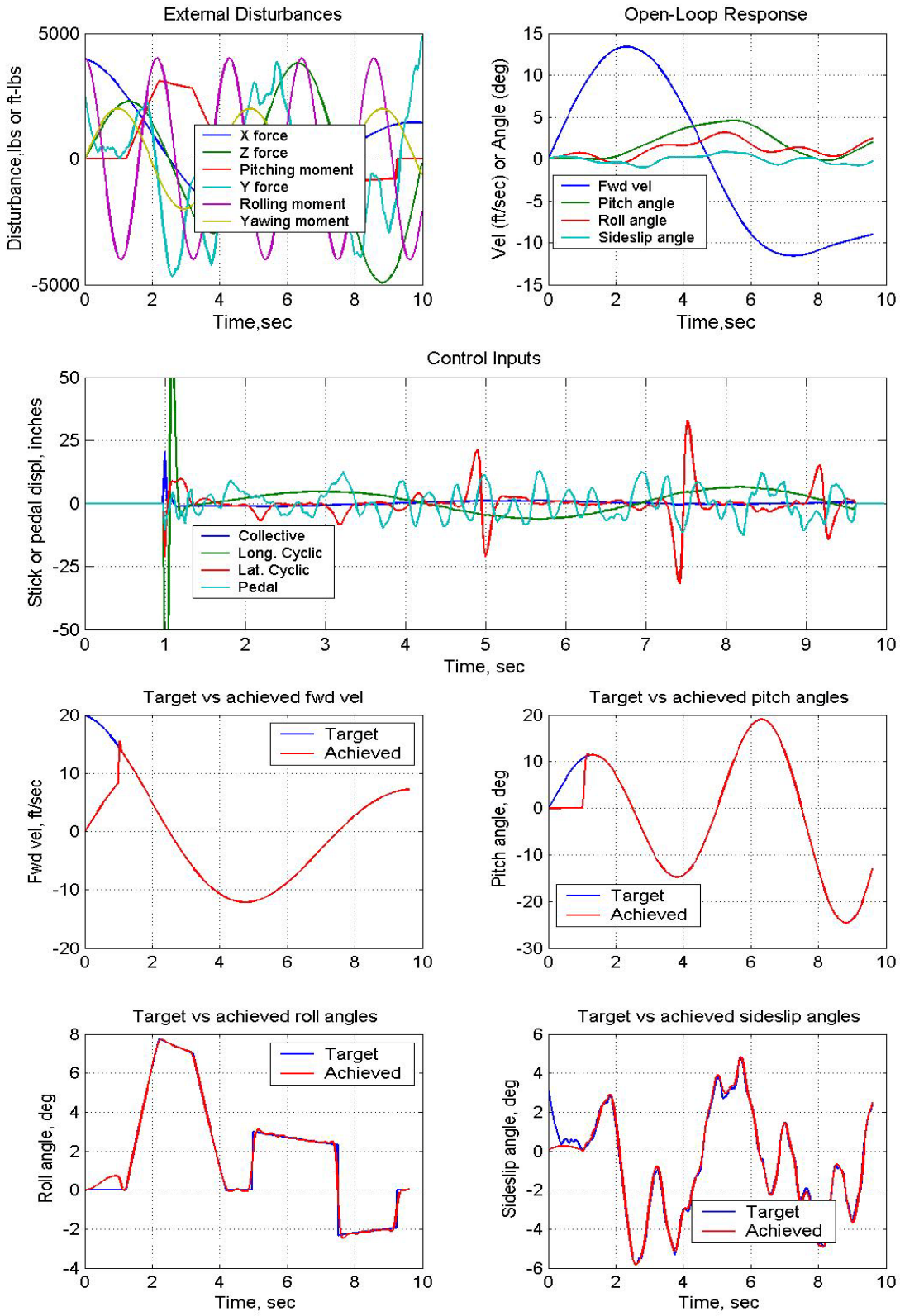


Figure 63.- Tracking of XV-15 subjected to a full complement of disturbances and using the same unfiltered targets as in figure 56.

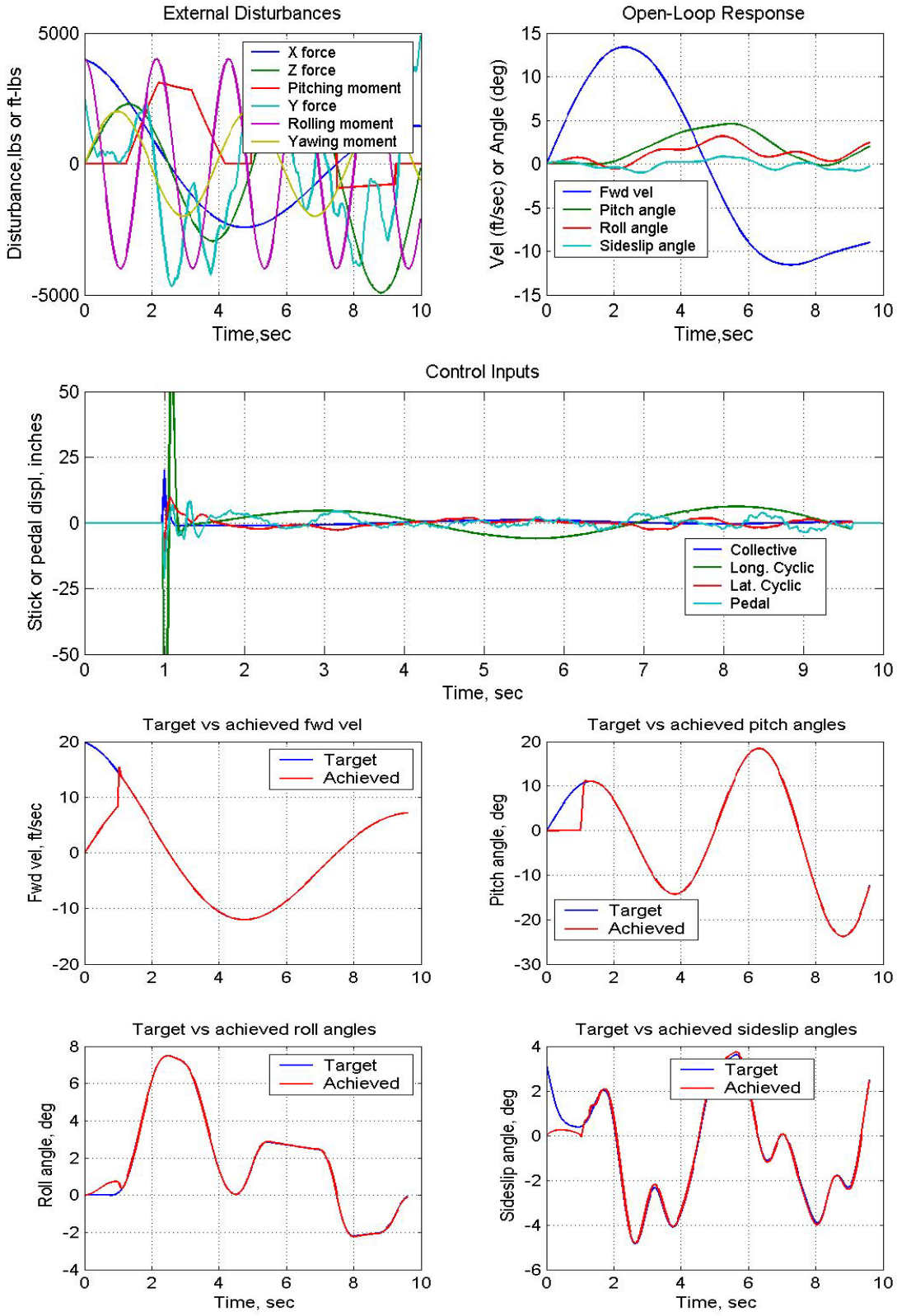


Figure 64.- Repeat of figure 63 but with filtered roll and sideslip targets.

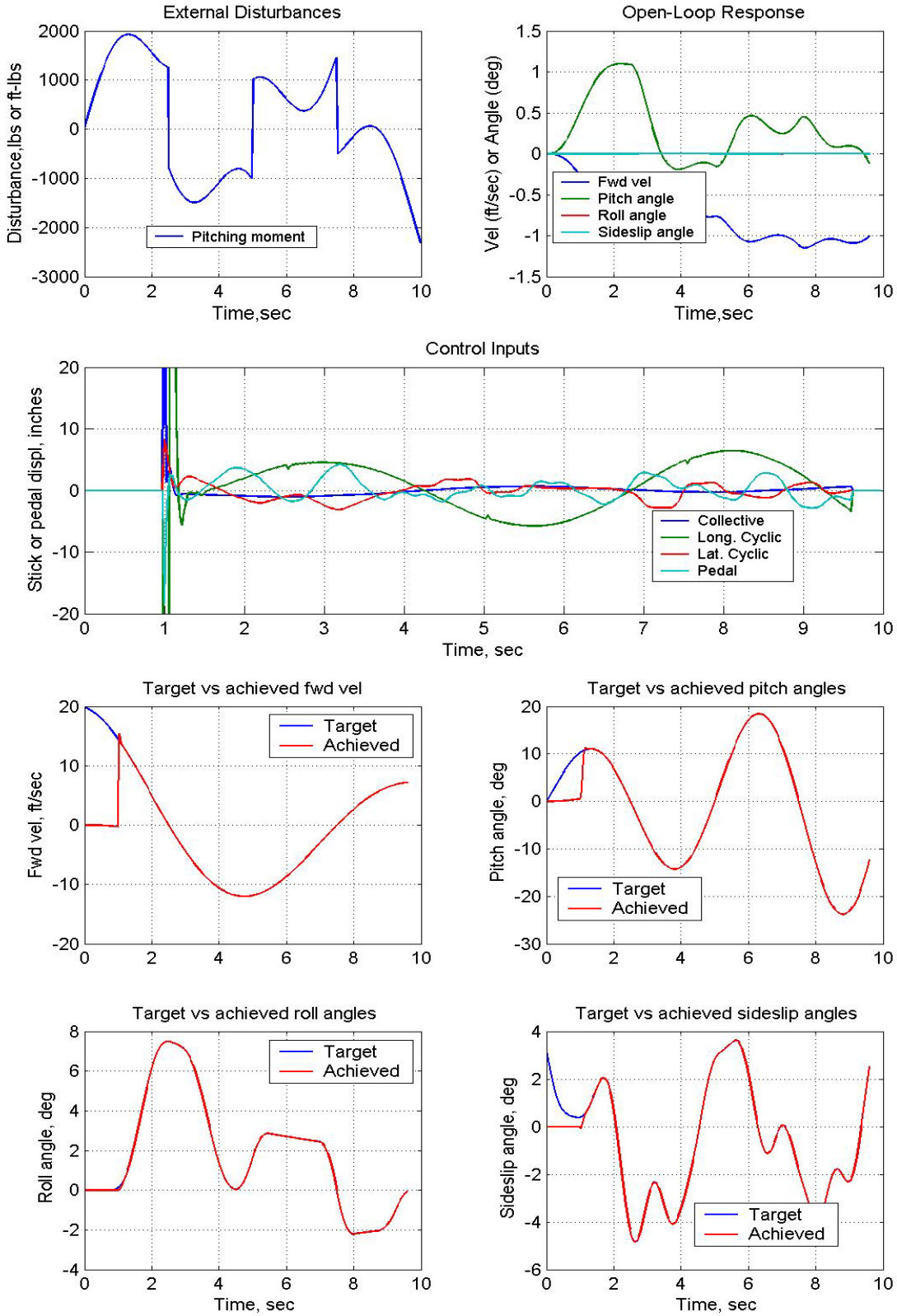


Figure 65.- Tracking of XV-15 subjected to a convoluted pitching moment disturbance and using the same targets as in figure 64.

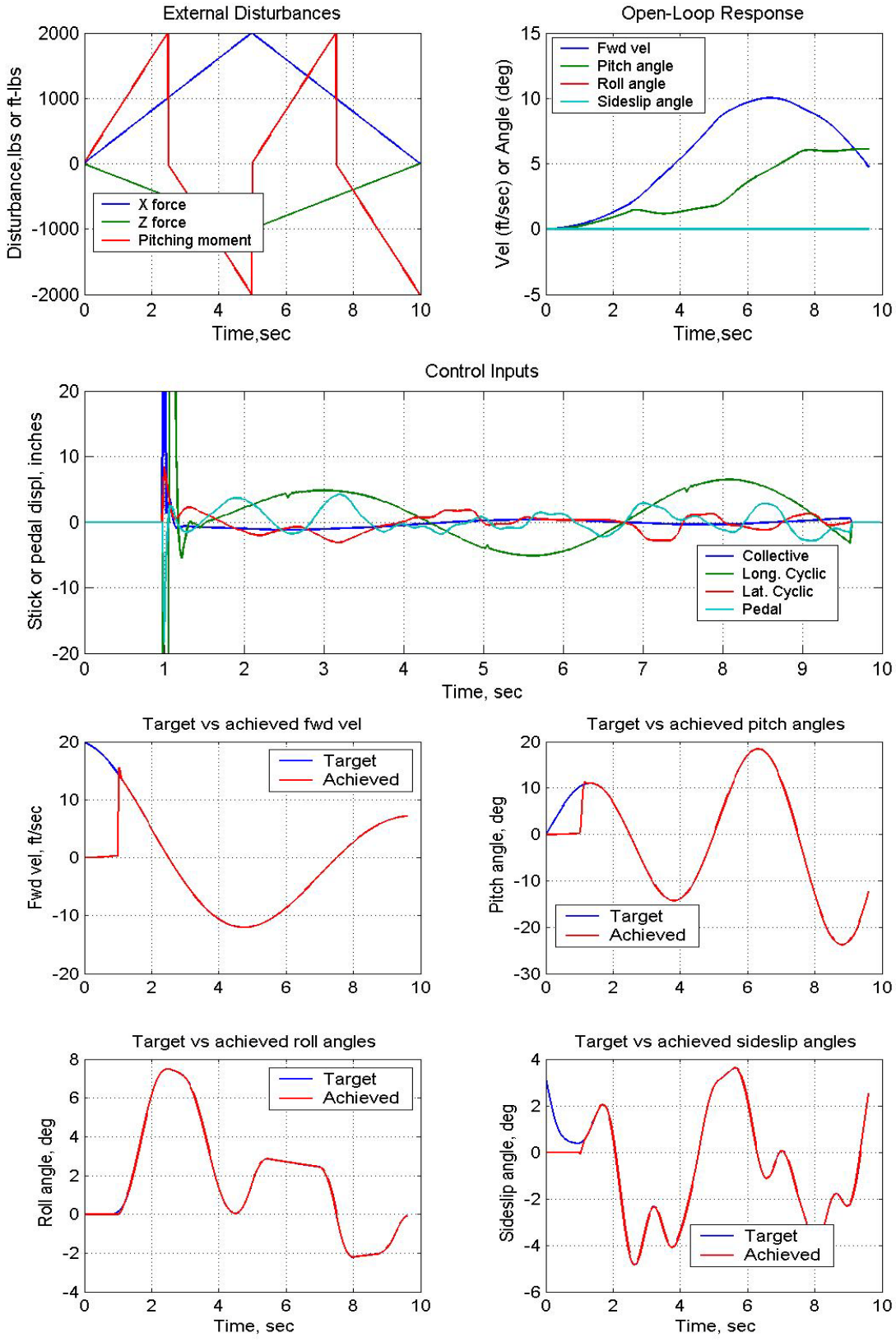


Figure 66.- Tracking of XV-15 subjected to triangular longitudinal disturbances and using the same targets as in figure 65.

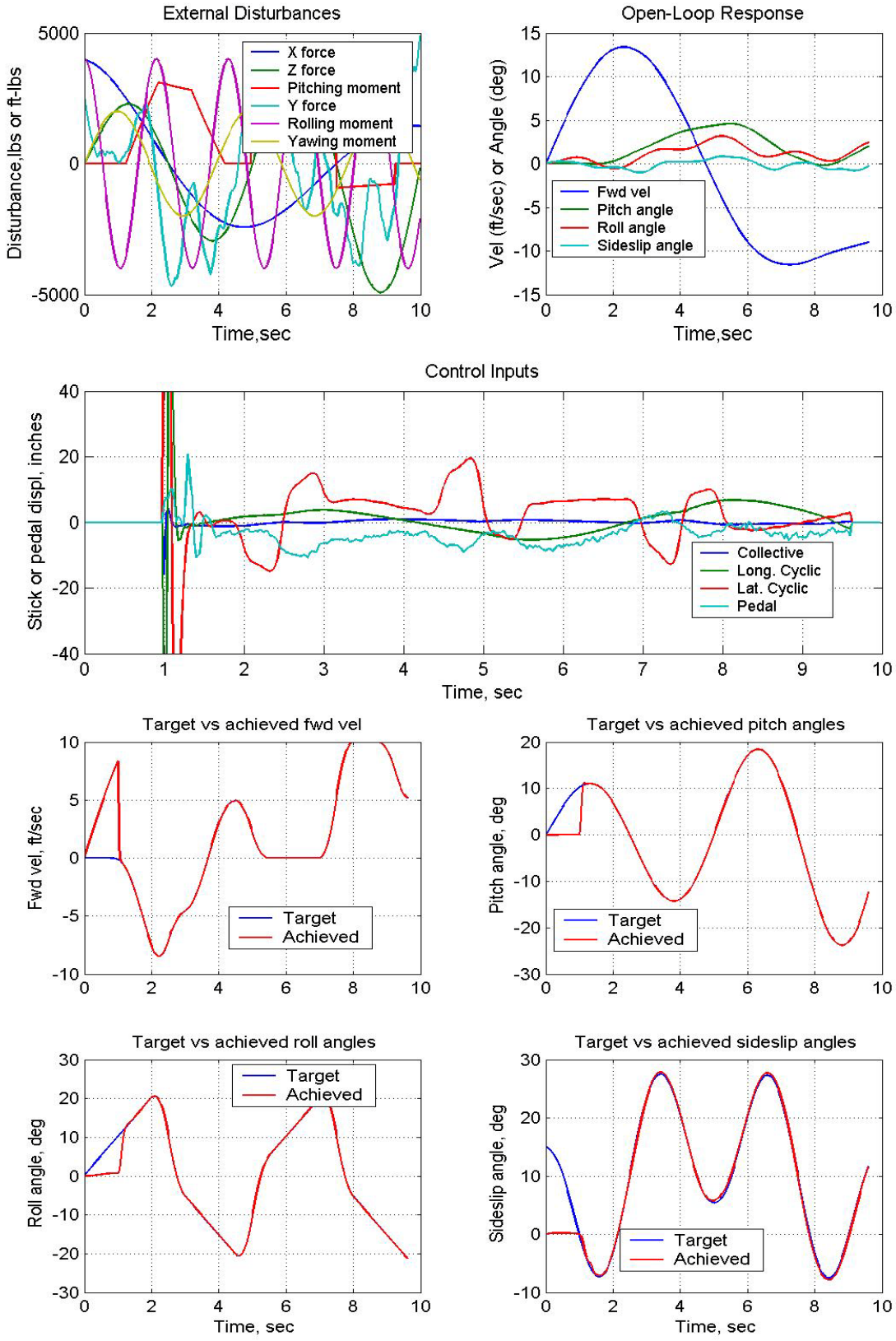


Figure 67.- Tracking of XV-15 subjected to the same full set of disturbances used in figure 64 and a variety of filtered targets.

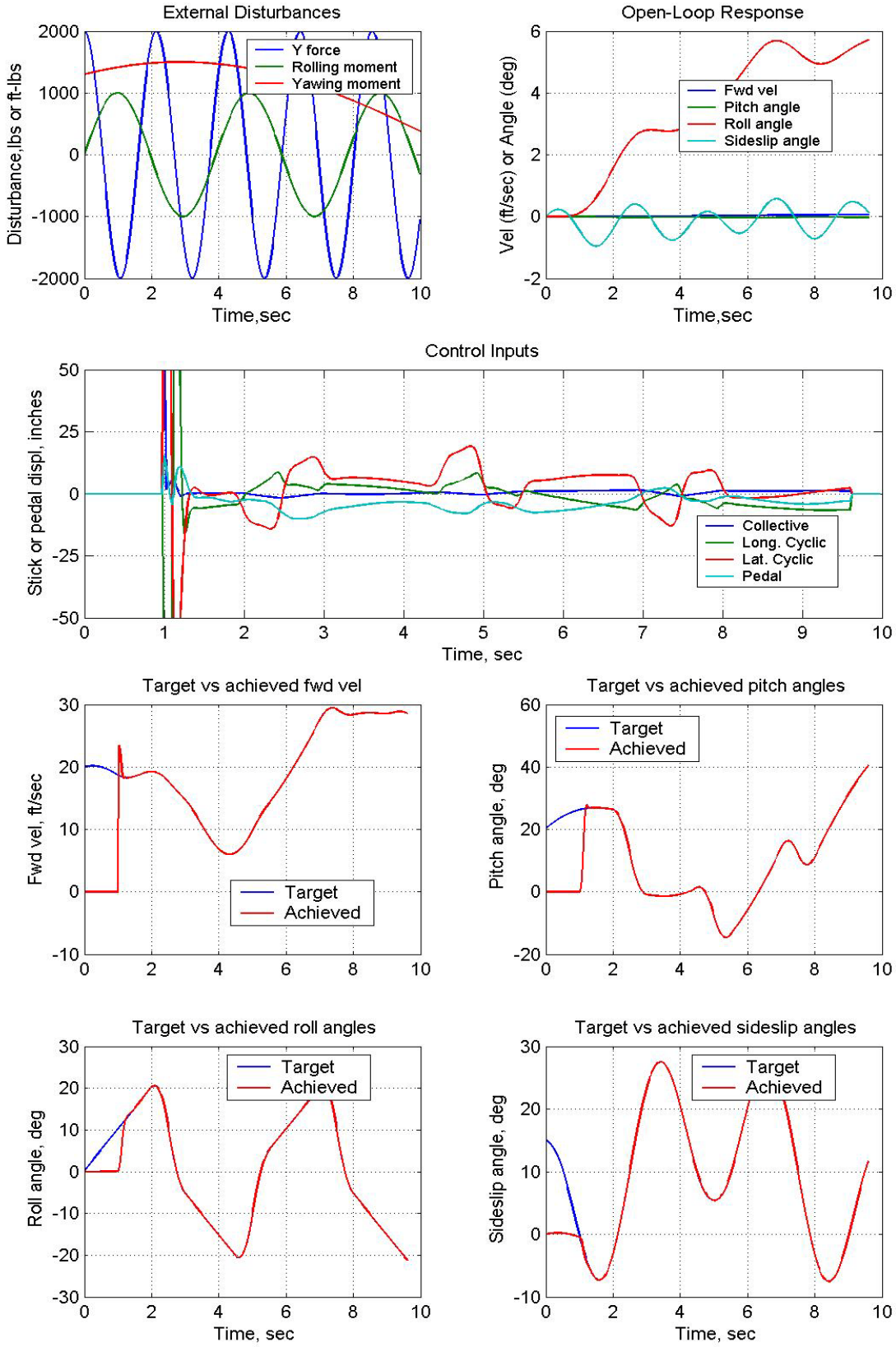


Figure 68.- Tracking of XV-15 subjected to lateral sinusoidal disturbances and using the same targets as in figure 67.

# REPORT DOCUMENTATION PAGE

*Form Approved*
*OMB No. 0704-0188*



| 1. REPORT DATE *(DD-MM-YYYY)* | 2. REPORT TYPE | 3. DATES COVERED *(From - To)* |
|---|---|---|
| 01- 04 - 2013 | Technical Memorandum | May 2009 - July 2011 |

**4. TITLE AND SUBTITLE**

Generalized Predictive Control of Dynamic Systems with Rigid-Body Modes

**5a. CONTRACT NUMBER**

**5b. GRANT NUMBER**

**5c. PROGRAM ELEMENT NUMBER**

**6. AUTHOR(S)**

Kvaternik, Raymond G.

**5d. PROJECT NUMBER**

**5e. TASK NUMBER**

**5f. WORK UNIT NUMBER**

432938.11.01.07.43.40.08

**7. PERFORMING ORGANIZATION NAME(S) AND ADDRESS(ES)**

NASA Langley Research Center
Hampton, VA 23681-2199

**8. PERFORMING ORGANIZATION REPORT NUMBER**

L-20211

**9. SPONSORING/MONITORING AGENCY NAME(S) AND ADDRESS(ES)**

National Aeronautics and Space Administration
Washington, DC 20546-0001

**10. SPONSOR/MONITOR'S ACRONYM(S)**

NASA

**11. SPONSOR/MONITOR'S REPORT NUMBER(S)**

NASA/TM-2013-217976

**12. DISTRIBUTION/AVAILABILITY STATEMENT**

Unclassified - Unlimited
Subject Category 08
Availability: NASA CASI (443) 757-5802

**13. SUPPLEMENTARY NOTES**

Author is a Distinguished Research Associate at NASA Langley Research Center.

**14. ABSTRACT**

Numerical simulations to assess the effectiveness of Generalized Predictive Control (GPC) for active control of dynamic systems having rigid-body modes are presented. GPC is a linear, time-invariant, multi-input/multi-output predictive control method that uses an ARX model to characterize the system and to design the controller. Although the method can accommodate both embedded (implicit) and explicit feedforward paths for incorporation of disturbance effects, only the case of embedded feedforward in which the disturbances are assumed to be unknown is considered here. Results from numerical simulations using mathematical models of both a free-free three-degree-of-freedom mass-spring-dashpot system and the XV-15 tiltrotor research aircraft are presented. In regulation mode operation, which calls for zero system response in the presence of disturbances, the simulations showed reductions of nearly 100%. In tracking mode operations, where the system is commanded to follow a specified path, the GPC controllers produced the desired responses, even in the presence of disturbances.

**15. SUBJECT TERMS**

Active control; GPC; Generalized predictive control; Regulation and tracking control; Rigid-body dynamic control

| 16. SECURITY CLASSIFICATION OF: | | | 17. LIMITATION OF ABSTRACT | 18. NUMBER OF PAGES | 19a. NAME OF RESPONSIBLE PERSON |
|---|---|---|---|---|---|
| a. REPORT | b. ABSTRACT | c. THIS PAGE | | | STI Help Desk (email: help@sti.nasa.gov) |
| | | | | | 19b. TELEPHONE NUMBER *(Include area code)* |
| U | U | U | UU | 110 | (443) 757-5802 |